Aus der Klinik für Nuklearmedizin, AB Klinische Nuklearmedizin,
der Medizinischen Fakultät Charité – Universitätsmedizin Berlin

DISSERTATION

Optimierte semi-quantitative Analyse der Dopamintransporter-SPECT zur Unterstützung der visuellen Bildinterpretation in der Diagnostik von Parkinsonsyndromen

--

Optimized semi-quantitative analysis of dopamine transporter SPECT to support visual image interpretation in the diagnosis of parkinsonian syndromes

zur Erlangung des akademischen Grades
Doctor rerum medicinalium (Dr. rer. medic.)

vorgelegt der Medizinischen Fakultät
Charité – Universitätsmedizin Berlin

von
Catharina Lange
aus Leipzig

Datum der Promotion: 04.03.2022

Inhaltsverzeichnis

1. Abkürzungsverzeichnis

AC	engl. *attenuation correction*
AUC	engl. *area under the curve*
CT	Computertomographie
DAT	Dopamintransporter
FBP	engl. *filtered backprojection*
FP-CIT	N-ω-fluoropropyl-2β-carbomethoxy-3β-(4-123I-iodophenyl)nortropane
HV	engl. *hottest voxels*
IQR	engl. *interquartile range*
IR	Iterative Rekonstruktion
KI	Konfidenzintervall
Ln	Natürlicher Logarithmus
MNI	Montreal Neurological Institute
MRT	Magnetresonanztomographie
NDB	Normaldatenbank
PPMI	Parkinson's Progression Markers Initiative
PS	Parkinsonsyndrom
ROC	engl. *receiver operating characteristic*
ROI	engl. *region of interest*
SBR	engl. *specific binding ratio*
SPECT	engl. *single-photon emission computed tomography*
SPM	Statistical Parametric Mapping
SUSI	engl. *specific uptake size index*
SWEDD	engl. *subjects without evidence of dopaminergic deficit*

2. Zusammenfassung

Zur Differenzierung von neurodegenerativen und nicht-neurodegenerativen Ursachen eines klinisch unklaren Parkinsonsyndroms wird die Dopamintransporter-SPECT (DAT-SPECT) eingesetzt. Neben der visuellen Bildinterpretation unterstützt die semi-quantitative Analyse der striatalen Dopamintransporter-Verfügbarkeit die Befundung. Die vorliegende Dissertationsschrift fasst drei Studien zusammen, die klinisch relevante Parameter der Bildentstehung und Bildverarbeitung in der semi-quantitativen Analyse der DAT-SPECT identifizierten, optimierten und hinsichtlich ihrer diagnostischen Genauigkeit untersuchten.

In der *ersten Studie* wurde eine vollautomatische Methode zur Abgrenzung der äußeren Kopfkontur als Teil der Schwächungskorrektur nach Chang implementiert und gegenüber einer klinisch etablierten halbautomatischen Methode validiert. Die Auswertung eines multizentrischen Datensatzes ergab, dass beide Methoden zur Kopfabgrenzung sowohl vergleichbare semi-quantitative Werte als auch eine vergleichbare diagnostische Genauigkeit lieferten. Damit kann die vollautomatische Methode für den Einsatz in der klinischen Versorgung empfohlen werden, da keine Interaktion durch den Nutzer erforderlich ist.

Die *zweite Studie* untersuchte zwei Methoden zur semi-quantitativen Abschätzung der Tracer-Bindung hinsichtlich ihrer diagnostischen Genauigkeit. Der auflösungsunabhängige *specific uptake size index* (SUSI) zeigte bei Datenerhebung an unterschiedlichen Kamerasystemen eine höhere diagnostische Genauigkeit als der Standardparameter, das sogenannte *specific binding ratio* (SBR). Dies ist besonders relevant für multizentrische Studien. Sobald jedoch nur ein Kamerasystem eingesetzt wurde, ist der Standardparameter SBR dem SUSI vorzuziehen, da dieser bei vergleichbarer diagnostischer Performance weniger anfällig gegenüber einer fehlerhaften Abschätzung der nicht-spezifischen Tracer-Bindung in der Referenzregion ist.

Ziel der *dritten Studie* war die Untersuchung des Einflusses der Größe der Normaldatenbank (NDB) auf die diagnostische Genauigkeit einer semi-quantitativen Auswertung der DAT-SPECT. Dabei erfolgte eine Simulation von unterschiedlichen Größen der NDB (n=5, 10, 15, …, 50) durch zufälliges Ziehen aus dem Pool an Kontrollen und Validierung der jeweiligen NDB in der Gesamtkohorte anhand von Klassifizierungsgenauigkeit, Sensitivität und Spezifität. Die Analyse ergab, dass ein Mindestumfang von 25 bis 30 DAT-SPECT-Datensätzen zur Bildung einer NDB notwendig ist. Eine Vergrößerung der NDB über 40 Fälle hinaus führt hingegen zu keiner weiteren relevanten Steigerung der diagnostischen Genauigkeit.

3. Abstract

Dopamine transporter SPECT (DAT-SPECT) is an established method to differentiate neurodegenerative and non-neurodegenerative causes in clinically uncertain parkinsonian syndromes. Besides visual image interpretation, semi-quantitative analysis of the striatal dopamine transporter availability is used to support medical diagnosis. The present doctoral thesis summarizes three studies that identified, optimized and validated clinically relevant, semi-quantitative parameters of DAT-SPECT image acquisition and processing with reference to their diagnostic accuracy.

The *first study* proposed a fully automatic segmentation method of the outer head contour as a part of attenuation correction according to Chang and validated this method to a well-established semi-automatic method. Both methods for head delineation showed comparable semi-quantitative properties as well as comparable diagnostic accuracy based on multi-center patient data. For this reason, we suggest to use the fully automatic method in clinical patient care since no user interaction is required.

A direct comparison of two semi-quantitative methods for estimation of tracer binding in reference to diagnostic accuracy was the aim of the *second study*. The spatial resolution independent *specific uptake size index* (SUSI) provided a higher diagnostic accuracy compared to the commonly used parameter, the *specific binding ratio* (SBR), when image acquisition is performed at various camera systems. This is highly relevant for multi-center image acquisition. However, in single-camera/mono-center settings SBR should be favored over SUSI, since SBR seemed to be less sensitive towards errors of the estimate of non-specific tracer uptake in the reference region with comparable diagnostic performance to SUSI.

Rationale of the *third study* was to evaluate the impact of the size of the normal database (NDB) on the diagnostic performance of semi-quantitative analysis in DAT-SPECT. For it, simulation of NDB with different sizes (n=5, 10, 15, …, 50) by randomly selecting subjects from the subcohort of normal controls was implemented and validation of each particular NDB based on the overall cohort was done concerning diagnostic accuracy, sensitivity and specificity as performance measures. The study results suggested that 25 to 30 DAT-SPECT data sets should be the minimum size of NDB. Increasing the size of NDB beyond 40 data sets provided only very small further improvement in diagnostic accuracy.

4. Einleitung und Zielstellung

Morbus Parkinson ist durch den Untergang von Zellen in der Substantia Nigra gekennzeichnet, der zur Reduktion der dopaminergen Innervierung und damit der Dichte präsynaptischer Dopamintransporter (DAT) im Striatum führt (Bernheimer et al. 1973). Zur in-vivo Evaluation des nigrostriatalen DAT-Status bei klinisch unklaren Parkinsonsyndromen (PS) wird die Einzelphotonen-Emissionscomputertomographie (SPECT, engl. *single-photon emission computed tomography*) mit dem Tracer N-ω-fluoropropyl-2β-carbomethoxy-3β-(4-123I-iodophenyl)nortropane (FP-CIT) eingesetzt (Booij et al. 2001). Die Interpretation der DAT-SPECT beruht primär auf der visuellen Beurteilung der SPECT-Bilder, die gemäß aktueller Leitlinien durch eine semi-quantitative Analyse der striatalen DAT-Verfügbarkeit unterstützt werden sollte (Morbelli et al. 2020).

Die diagnostische Genauigkeit der DAT-SPECT hinsichtlich der Differenzierung von neurodegenerativen und nicht-neurodegenerativen Ursachen des PS wird von diversen Parametern beeinflusst, die sich sowohl auf die visuelle als auch auf die semi-quantitative Beurteilung der Bilddaten auswirken. Dazu zählen physikalische Faktoren im Rahmen der Bildakquisition und -rekonstruktion, bildverarbeitungsbezogene Prozeduren sowie die Methodik zur semi-quantitativen Analyse der striatalen DAT-Dichte (Tatsch et al. 2012, Tossici-Bolt et al. 2017).

In der DAT-SPECT führt Photonenschwächung zur Unterschätzung der Tracer-Aufnahme in tiefen Strukturen des Gehirns (z.B. Striatum) relativ zum zerebralen Kortex, welcher im Rahmen der semi-quantitativen Analyse häufig als Referenzregion verwendet wird. Der Grad der Unterschätzung hängt von Kopfgröße, -form und der Dicke des Schädelknochens ab. Eine Korrektur der Photonenschwächung (AC, engl. *attenuation correction*) kann auf Basis einer low-dose Computertomographie (CT) erfolgen, welche die individuelle Verteilung der Schwächungskoeffizienten misst. In Kombination mit Korrekturen für Photonenstreuung und die limitierte räumliche Auflösung des SPECT-Systems liefert diese AC die genauste Abschätzung der DAT-Dichte (Soret et al. 2003). Alternativ stehen vereinfachte rechnerische Methoden zur Verfügung, die kein low-dose CT benötigen. Die klinisch etablierte Methode nach Chang nimmt eine homogene Schwächung innerhalb des Schädels an (Chang 1978). In einer Vorarbeit konnten wir zeigen, dass die DAT-SPECT mit AC nach Chang eine vergleichbare diagnostische Performance zu der CT-basierten AC aufweist (Lange et al. 2014). Letztere ist im Rahmen der klinischen Patientenversorgung nicht notwendig, da sie mit einer zusätzlichen Strahlenexposition verbunden ist. Eine entscheidende Limitation der rechnerischen Methode nach Chang ist die Abgrenzung der äußeren Kopfkontur auf Grundlage der SPECT-Aufnahme, sowohl für halb- als auch vollautomatische Verfahren. Da es sich bei FP-CIT um einen hoch-spezifischen Tracer handelt und die Tracer-Retention in der Kopfhaut interindividuell stark variiert, bedarf es im klinischen Einsatz einer manuellen Nachbearbeitung der Kontur durch den Anwender, die potentielle Fehlerquellen mit sich bringt und sehr zeitintensiv sein kann.

Vor diesem Hintergrund wurde in der *ersten Studie* eine vollautomatische Methode zur Abgrenzung der Kopfkontur unter Einsatz von stereotaktischer Normalisierung des individuellen

Scans auf ein Standard-Template implementiert und gegen eine halbautomatische, schwellwertbasierte Methode getestet.

Neben der Verwendung geeigneter Rekonstruktionsalgorithmen und Bildkorrekturen setzt die Quantifizierung eines biologischen Parameters wie der DAT-Dichte eine dynamische Bildakquisition, kinetische Modellierung (engl. *tracer kinetic modeling*) anhand von Zeitaktivitätskurven und eine Bestimmung der Aktivitätskonzentration im arteriellen Blut voraus (Mintun et al. 1984). Da dieses Prozedere im klinischen Einsatz nicht praktikabel ist, wurden vereinfachte Methoden zur semi-quantitativen Abschätzung der Tracer-Bindung auf Basis von statischen Spätaufnahmen vorgeschlagen, wobei das Signal der Zielregion auf das einer Referenzregion skaliert wird (Booij et al. 1999). Ein klinisch etablierter Surrogatmarker für die DAT-Dichte ist das sogenannte *specific binding ratio* (SBR) (Tossici-Bolt et al. 2006). Aufgrund der limitierten räumlichen Auflösung der SPECT-Bildgebung und des kleinen Volumens der Zielstruktur wird die Tracer-Anreicherung im Striatum um bis zu 50% unterschätzt (Lange et al. 2014). Variabilität striataler Atrophie zwischen Patienten führt dabei zu einer zusätzlichen Variabilität der mittels SPECT gemessenen DAT-Dichte, welche die Differenzierung von neurodegenerativen und nicht-neurodegenerativen PS erschwert. Diese Partialvolumeneffekte können auf Basis einer strukturellen Bildmodalität, idealerweise einer hochaufgelösten Magnetresonanztomographie (MRT), korrigiert werden. Da in der klinischen Routine nicht für jeden Patienten geeignete Bildaufnahmen vorliegen, wurde ein weiteres semi-quantitatives Maß eingeführt, der *specific uptake size index* (SUSI) (Fleming et al. 2004). Dieser ist gegenüber variierenden Auflösungseigenschaften einzelner SPECT-Kamerasysteme unempfindlich (Goethals et al. 2007).

Das Ziel der *zweiten Studie* bestand darin, die diagnostische Genauigkeit auf Basis einer semi-quantitativen Abschätzung der DAT-Dichte mittels SBR und SUSI zu vergleichen. Dies beinhaltete zunächst die Überprüfung an einer multizentrischen Patientenkohorte, gefolgt von einer Untersuchung an einem monozentrischen Patientenkollektiv.

Die Empfindlichkeit semi-quantitativer Parameter der striatalen DAT-Verfügbarkeit gegenüber zentrum- und kameraabhängigen Einflussfaktoren erschwert den Einsatz einer zentralen Normaldatenbank (NDB) mit Etablierung eines abgeleiteten Schwellwertes zur Differenzierung von pathologischer versus normaler Tracer-Bindung (Dickson et al. 2017). In multizentrischen Studien erfolgt daher eine strikte Harmonisierung der Akquisitionsbedingungen und eine zentralisierte Bildrekonstruktion und -verarbeitung (Tossici-Bolt et al. 2011). In der klinischen Patientenversorgung, bei der in manchen Einrichtungen zum Teil verschiedene Kamerasysteme zum Einsatz kommen, hat sich hingegen das Anlegen von kameraspezifischen Datenbanken etabliert. Dieses Vorgehen ist nicht nur bei einer prospektiven Erhebung von Kontrolldaten aufwändig, sondern auch bei einer retrospektiven Zusammenstellung von visuell unauffälligen DAT-SPECT-Aufnahmen. Beim letzteren Ansatz sollten nur Patienten eingeschlossen werden, die nach der SPECT-Untersuchung einen klinisch unauffälligen Verlauf aufweisen, wobei die Frage nach der notwendigen Mindestanzahl von Patienten in einer NDB häufig diskutiert wird.

In der *dritten Studie* wurde deshalb der Einfluss der Größe der NDB auf die diagnostische Genauigkeit der DAT-SPECT zum Nachweis / Ausschluss einer nigrostriatalen Degeneration in

Abhängigkeit von unterschiedlichen Rekonstruktionsalgorithmen, semi-quantitativen Methoden zur Abschätzung der DAT-Dichte und zwei unabhängigen Patientenkollektiven untersucht.

5. Methodik

In den drei Studien erfolgte die Bildverarbeitung standardisiert und vollautomatisiert mithilfe von in *MATLAB* (The Mathworks Inc., Version 2013b) implementierten Pipelines und unter Einbindung von Routinen der frei verfügbaren Software *Statistical Parametric Mapping* (SPM, https://www.fil.ion.ucl.ac.uk/spm/).

Zunächst wurde die individuelle Aufnahme eines jeden Patienten durch stereotaktische Normalisierung in den standardisierten, anatomischen Referenzraum des Montreal Neurological Institutes (MNI) transformiert, um darin vordefinierte Masken (ROIs, engl. *regions of interest*) der Ziel- und Referenzregion verwenden zu können. Zur Abschätzung der DAT-Verfügbarkeit im Striatum und dessen Unterregionen, Nucleus Caudatus und Putamen, kamen entsprechend der Fragestellung der Studie die folgenden semi-quantitativen Methoden zum Einsatz:

(M1) die konventionelle Definition des *specific binding ratio* SBR = (C−CR) / CR unter Nutzung von anatomischen ROIs,

(M2) die Definition des *specific uptake size index* SUSI = (T−V·CR) / CR unter Verwendung von über die anatomischen Grenzen hinausgehenden ROIs, um das gesamte striatale Signal zu berücksichtigen (Fleming et al. 2004), und

(M3) eine adaptierte Variante des SBR unter Einsatz von ausgedehnten ROIs und der Berücksichtigung eines fest definierten Volumens der heißesten striatalen Voxelintensitäten (HV, engl. *hottest voxels*) anstelle aller Voxelintensitäten (Kupitz et al. 2014).

Zur Berechnung des SUSI wurde die gemittelte Voxelintensität C durch die Summe aller Voxelintensitäten T im Striatum ersetzt und eine Skalierung anhand des Volumens V der striatalen ROI vorgenommen. Als Referenzregion diente das gesamte Großhirn ausgenommen Strukturen mit einer nicht vernachlässigbaren DAT-Verfügbarkeit (Kupitz et al. 2014). Zur Abschätzung der nicht-spezifischen Tracer-Bindung in der Referenzregion CR diente das 75. Perzentil der Voxelintensitäten (Kupitz et al. 2014).

In allen Studien diente die Genauigkeit der Unterscheidung von neurodegenerativen und nicht-neurodegenerativen PS im Vergleich zum jeweiligen Goldstandard als Güteparameter. Die Ergebnisse wurden auf das Putamen der jeweils stärker betroffenen Hemisphäre beschränkt, da der striatale DAT-Verlust beim Morbus Parkinson in der Regel im posterioren Putamen beginnt und meist eine deutliche Seitenasymmetrie aufweist (Kaasinen et al. 2017).

Publikation 1

Patientenkollektiv

Es wurden FP-CIT SPECT-Datensätze von insgesamt 62 konsekutiv untersuchten Patienten mit klinisch unklarem PS eingeschlossen. Die Datenerhebung erfolgte an drei Zentren, unter

harmonisierten Akquisitionsbedingungen und unter Einhaltung der damaligen Leitlinienempfehlungen (Darcourt et al. 2010, Djang et al. 2012). Die Bildrekonstruktion und -verarbeitung erfolgte zentralisiert in unserer Arbeitsgruppe an der Charité – Universitätsmedizin Berlin.

Datenevaluation und Statistik

Die schwellwertbasierte, halbautomatische Methode zur Kopfabgrenzung wurde mithilfe einer kommerziellen Rekonstruktionssoftware unter Standardeinstellungen ausgeführt. Dabei waren manuelle Korrekturen nicht ausgeschlossen. Die vollautomatische Abgrenzung der Kopfkontur wurde mithilfe stereotaktischer Normalisierung der individuellen Patienten-SPECT auf ein FP-CIT Template im anatomischen Referenzraum des MNI ausgeführt. Durch Invertierung der ermittelten Normalisierungsparameter erfolgte die Rücktransformation einer im Referenzraum vordefinierten Kopfmaske auf den Kopf des individuellen Patienten. Es wurden keine manuellen Korrekturen durch den Benutzer vorgenommen. Für beide Methoden der Kopfabgrenzung erfolgte die Schwächungskorrektur nach Chang unter Verwendung eines homogenen Schwächungskoeffizienten von μ=0,148 cm^{-1} (Chang 1978).

Die diagnostische Genauigkeit der semi-quantitativen DAT-Verfügbarkeit für beide Methoden wurde mittels der Quantifizierungsmethode M3 (adaptierte Variante des SBR mit HV) untersucht. Darüber hinaus erfolgte eine visuelle Bewertung des DAT-Status durch sechs unabhängige Reader und pro Zentrum (5-Punkte-Skala, nachträgliche Dichotomisierung in neurodegeneratives / nicht-neurodegeneratives PS, Konsensentscheidung bei abweichender Befundung innerhalb eines Zentrums). Dabei diente die Fläche unter der *receiver operating characteristic* (ROC) Kurve (AUC, engl. *area under the curve*) bzw. die prozentuale Übereinstimmung zum Referenzstandard als Gütemaß. Als Referenzstandard wurde der Befund in der Patientenakte verwendet. Das Signifikanzniveau lag bei $p<0,05$.

Publikation 2

Patientenkollektiv

In die Analyse wurde zum einen eine monozentrische Kohorte von insgesamt 122 Patienten mit klinisch unklarem PS eingeschlossen. Es erfolgte eine dichotome Aufteilung in die entsprechende Diagnosegruppe anhand von klinischen Verlaufsdaten (neurodegeneratives PS, n=84, nicht-neurodegeneratives PS, n=38). Die Bildakquisition erfolgte bei allen Patienten mit derselben SPECT-Kamera und unter Berücksichtigung der damaligen Leitlinienempfehlungen (Darcourt et al. 2010, Djang et al. 2012). Für eine einheitliche Bildqualität wurden alle Rohdaten retrospektiv erneut rekonstruiert (iterative Rekonstruktion, IR, Schwächungskorrektur nach Chang).

Zum anderen wurden insgesamt 645 Patienten einer multizentrischen Kohorte der *Parkinson's Progression Markers Initiative* (PPMI) Datenbank (www.ppmi-info.org) eingeschlossen, darunter 438 Patienten mit Morbus Parkinson und 207 gesunde Kontrollen (Marek et al. 2011). Die rekrutierenden Zentren durchliefen einen aufwändigen Prozess zur Harmonisierung der Bildakquisition. Des Weiteren wurde eine zentralisierte Bildrekonstruktion (IR, AC nach Chang)

sowie eine einheitliche Bildverarbeitung durch das Imaging Core Lab durchgeführt. Es waren ausschließlich vorverarbeitete SPECT-Daten im MNI-Referenzraum, und nicht im nativen Patientenraum, verfügbar (Marek et al. 2018).

Datenevaluation und Statistik

Die semi-quantitative Auswertung erfolgte nach Methode M1 (klassische Definition des SBR), wobei das Putamen als Zielstruktur zusätzlich in einen anterioren und posterioren Anteil unterteilt wurde, und nach Methode M2 (SUSI). Zur Testung der Primärhypothese, dass der SUSI dem SBR im multizentrischen Setting überlegen ist, dienten sowohl die AUC unter der ROC Kurve als auch die diagnostische Genauigkeit unter Verwendung des Youden-Kriteriums als Vergleichsmaß (Youden 1950).

Die ursprüngliche Definition des SUSI basiert auf ROI-Analysen im Patientenraum, das heißt das individuelle anatomische Volumen des Striatums in Relation zur Größe der angewendeten striatalen ROI beeinflusst den absoluten Wert des SUSI. Diese Fehlerquelle kann durch stereotaktische Normalisierung und einer nachfolgenden Bestimmung des SUSI im Referenzraum minimiert werden. Deshalb wurde als Sekundärhypothese getestet, ob die Berechnung des SUSI im Referenz- verglichen zum Patientenraum zu einer verbesserten diagnostischen Genauigkeit führt. Letztere Auswertung beschränkte sich auf das monozentrische Kollektiv. Das putaminale Volumen wurde auf Basis von Rücktransformation der anatomischen ROI abgeschätzt und zwischen richtig positiven, richtig negativen, falsch positiven und falsch negativen Fällen verglichen (univariate Varianzanalyse).

Eine Vorarbeit zeigte, dass der SUSI im Vergleich zum SBR empfindlicher gegenüber Messfehlern der nicht-spezifischen Tracer-Bindung in der Referenzregion ist (Buchert et al. 2016). Daher wurde als weitere Sekundärhypothese geprüft, ob sich die Fehlerempfindlichkeit und die damit einhergehende Beeinträchtigung der diagnostischen Genauigkeit des SUSI gegenüber des SBR bestätigt. Als Maß der Messunsicherheit diente der relative Interquartilsabstand (IQR, engl. *interquartile range*) der Voxelintensitäten der Referenzregion, normiert auf das 75. Perzentil der Voxelintensitäten der Referenzregion. Es erfolgte ein Vergleich des relativen IQR zwischen korrekt und nicht-korrekt klassifizierten Fällen (Zweistichproben-t-Test, unverbunden). SUSI und SBR wurden außerdem unter Berücksichtigung des relativen IQR auf Unterschiede zwischen korrekt und nicht-korrekt klassifizierten Fällen getestet (univariate Varianzanalyse mit Diagnose-Referenzstandard und diagnostischer Genauigkeit des SUSI bzw. SBR als feste Effekte). Bei allen statistischen Tests lag das Signifikanzniveau bei $p<0,05$.

Publikation 3

Patientenkollektiv

In dieser Studie wurde dasselbe harmonisierte multizentrische Patientenkollektiv des PPMI-Konsortiums mit insgesamt 645 DAT-SPECT-Datensätzen wie in Publikation 2 eingeschlossen (438 Patienten mit idiopathischem PS und 207 Kontrollen). Der Datenpool wurde um 372 Datensätze aus der klinischen Patientenversorgung ergänzt, da die PPMI-Datenbank

ausschließlich vorverarbeitete Daten zum Download zur Verfügung stellt (IR, AC nach Chang unter Einsatz eines Studienzentrum-spezifischen Schwächungskoeffizienten, keine Korrektur für Streuung) (Marek et al. 2018).

Das klinische Patientenkollektiv umfasste insgesamt 372 Patienten mit klinisch unklarem PS, wobei die Datenerhebung an zwei SPECT-Kamerasystemen und unter Berücksichtigung der damaligen Leitlinien erfolgte (Darcourt et al. 2010, Djang et al. 2012). Die klinische Diagnose wurde der Patientenakte des Neurologen entnommen und diente als Referenzstandard. Die Diagnose der Gruppe neurodegenerativer PS (n=186) wurde durch einen klinischen Verlauf von mindestens 12 Monaten gesichert. Dasselbe galt für 44 Patienten der Gruppe von nicht-neurodegenerativen PS, wobei diese Gruppe um weitere Patienten mit kürzeren Verlaufszeiten ergänzt wurde, um ein ausbalanciertes Verhältnis hinsichtlich der Gruppengrößen zu erzielen (neurodegeneratives PS, n=186, nicht-neurodegeneratives PS, n=186). Die SPECT-Rohdaten wurden retrospektiv rekonstruiert. Dabei wurden zwei Settings implementiert, die sich vom PPMI-Datensatz unterschieden, um ein möglichst großes Spektrum hinsichtlich der Bildqualität zu realisieren: (i) gefilterte Rückprojektion (FBP, engl. *filtered backprojection*) mit AC nach Chang und Schwächungskoeffizient von μ=0,12 cm^{-1}, keine Korrektur für Streuung, und (ii) IR mit AC nach Chang und μ=0,146 cm^{-1}, Korrektur für Streuung und Auflösungsrückgewinnung (sog. *resolution recovery*).

Datenevaluation und Statistik

Es erfolgte eine semi-quantitative Auswertung auf Basis der Definition des SBR, wobei Methode M1 (klassische SBR-Definition unter Einsatz einer anatomischen ROI) und Methode M3 (SBR beruhend auf den heißesten Voxeln in einer ausgedehnten ROI) zum Einsatz kamen.

Um den Zusammenhang von Größenumfang der Normaldatenbank und diagnostischer Genauigkeit der semi-quantitativen DAT-SPECT-Auswertung zu untersuchen, wurden Simulationen für jeden der Datensätze (PPMI und klinische Kohorte), für die unterschiedlichen Rekonstruktionsalgorithmen (FBP und IR der klinischen Kohorte) und für beide Methoden der semi-quantitativen Analyse (SBR-klassisch und SBR-HV) durchgeführt. Dabei kam das nachfolgend beschriebene Simulationsschema zum Einsatz:

(1) Durch zufälliges Ziehen ohne Zurücklegen aus dem Pool von Kontrollen (PPMI) bzw. nicht-neurodegenerativer PS (klinisches Patientenkollektiv) wurde eine NDB definiert. Es wurden unterschiedliche NDB-Größenumfänge simuliert, indem es jeweils zum Einschluss von 5, 10, 15, 20, …, 50 Personen kam.

(2) Als Testsample wurde die gesamte Kohorte (PPMI: n=645, klinisches Kollektiv: n=372) definiert, unabhängig vom jeweiligen Umfang der NDB. Zur Evaluation der jeweiligen NDB wurde für jede Person die individuelle Abweichung des SBR zur SBR-Verteilung der NDB ermittelt. Die Abweichung wurde als z-Wert ausgedrückt:

z-Wert = (individuelles SBR−Mittelwert SBR in NDB) / Standardabweichung SBR in NDB.

Die automatische Klassifizierung einer jeden Testperson in die Kategorie einer normalen (PPMI: Kontrollen, klinisches Kollektiv: nicht-neurodegenerative PS) bzw. reduzierten

DAT-Verfügbarkeit (PPMI: idiopathisches PS, klinisches Kollektiv: neurodegenerative PS) erfolgte anhand eines festen z-Wert-Schwellwertes von -2,5 (entspricht einer 2,5-fachen Standardabweichung). Als Maß der diagnostischen Performance dienten Klassifizierungsgenauigkeit, Sensitivität und Spezifität.

(3) Das Prozedere erfolgte mit 10.000 Wiederholungen. Als Benchmark-Performance diente das Setting, in dem alle Kontrollen (n=207) bzw. nicht-neurodegenerativen PS Fälle (n=186) in die NDB eingeschlossen wurden. Dabei erfolgte die Berechnung des Verlusts der Detektionsgenauigkeit in Relation zur Benchmark-Performance und unter Angabe des mittleren sowie des „maximalen“ (5. Perzentil) relativen Verlusts über die 10.000 Realisierungen. Das Signifikanzniveau lag bei allen statistischen Tests bei $p<0,05$.

6. Ergebnisse

Publikation 1

Semi-quantitative Auswertung

Zwischen der voll- und halbautomatischen Methode zur Kopfabgrenzung ergab sich keine signifikante Differenz hinsichtlich des putaminalen SBR (relative Differenz: 0,69±5,50%; p=0,276; Einstichproben-t-Test). Des Weiteren lieferten beide Methoden eine vergleichbare diagnostische Performance hinsichtlich der Differenzierung von neurodegenerativen und nicht-neurodegenerativen PS: die AUC für die automatische und halbautomatische, schwellwertbasierte Methode betrug 0,935 und 0,938 (p=0,808; Test nach DeLong).

Visuelle Auswertung

Die Übereinstimmung der visuellen Beurteilung bei den beiden Varianten zur Kopfabgrenzung war höher für die dichotome Bewertung der DAT-Verfügbarkeit im Vergleich zur 5-Punkte-Skala (88,2±4,8% versus 78,2±2,8%; Mittelwert über Reader) und konnte durch Bildung einer Konsens-Bewertung verbessert werden (89,8±4,1% versus 81,7±3,7%; Mittelwert über Zentren).

Beim Vergleich zum Referenzstandard zeigten beide Methoden zur Kopfabgrenzung keinen relevanten Unterschied bezüglich der diagnostischen Genauigkeit, sowohl für die 5-Punkte-Skala (vollautomatisch versus halbautomatisch: 79,6±3,3% versus 79,6±1,7%; Mittelwert über Reader) als auch für die dichotome Bewertung (82,3±3,2% versus 79,6±2,5%; Mittelwert über Zentren).

Publikation 2

Monozentrisches Setting

Die höchste AUC wurde für das SBR des posterioren Anteils des Putamens ermittelt (AUC=0,981), gefolgt vom SBR des gesamten Putamens (0,976), SUSI berechnet im Referenzraum (0,969) bzw. im Patientenraum (0,961). Dabei ergab sich ein statistisch

signifikanter Unterschied zwischen SUSI im Patientenraum und den SBR-Ergebnissen (p<0,050; DeLong Test) sowie ein Trend zwischen beiden SUSI-Ergebnissen (p=0,129).

Beim Vergleich des SUSI, berechnet im Patientenraum, und des SBR gab es sieben diskordante Fälle (5,7%; bezogen auf das gesamte Putamen), die ausschließlich der neurodegenerativen Diagnosegruppe zugehörig waren. Eine nachträgliche visuelle Beurteilung der Fälle ergab, dass es sich um grenzwertige Befunde handelte. In sechs Fällen erfolgte die Klassifizierung auf Basis des SUSI falsch negativ und für das SBR richtig positiv. Im verbleibenden Fall führte der SUSI zu einem richtig positiven und das SBR zu einem falsch negativen Befund.

Bei Betrachtung der Klassifizierung auf Basis des SUSI im Patientenraum konnte ein kleineres putaminales Volumen für die beiden falsch positiven im Vergleich zu den 36 richtig negativen Fällen ermittelt werden. Für die zehn falsch negativen Fälle ergab sich wiederum ein größeres Volumen verglichen zu den 74 richtig positiven Fällen. Die Differenzen erreichten jedoch nicht das statistische Signifikanzlevel unter Berücksichtigung des „Diagnosegruppen-Referenzstandards“ (p=0,314) und der „diagnostischen Genauigkeit des SUSI“ (p=0,372) als feste Effekte in der univariaten Varianzanalyse (Interaktionseffekt „Diagnosegruppe*Genauigkeit des SUSI“: p=0,170).

Auf Basis des im Patientenraum berechneten SUSI zeigte der relative IQR der Voxelintensitäten der Referenzregion keinen signifikanten Unterschied zwischen den korrekt und nicht-korrekt klassifizierten Fällen (0,164±0,012 versus 0,173±0,024; p=0,199; unverbundener Zweistichproben-t-Test).

Multizentrisches Setting

Auch in der multizentrischen Kohorte konnte die höchste AUC für das SBR des posterioren Putamens ermittelt werden (AUC=0,998), gefolgt vom SUSI (0,993) und dem SBR des gesamten Putamens (0,991), wobei sich für SUSI versus SBR des gesamten Putamens kein signifikanter Unterschied ergab (p=0,207; Test nach DeLong).

Beim Vergleich von richtig und falsch klassifizierten Patienten wurden sowohl für den SUSI als auch für das SBR statistisch signifikante Unterschiede hinsichtlich des relativen IQR der Voxelintensitäten in der Referenzregion gefunden (SUSI: 0,157±0,031 versus 0,144±0,023; p=0,007; unverbundener Zweistichproben-t-Test; SBR: 0,155±0,026 versus 0,144±0,023; p=0,012).

Bei der Gegenüberstellung der Klassifizierungsergebnisse beider semi-quantitativer Parameter ergaben sich 23 diskordante Fälle (3,6%; bezogen auf das gesamte Putamen), wobei der relative IQR für die diskordanten Fälle höher ausfiel im Vergleich zu den verbleibenden 622 konkordanten Fällen (0,154±0,028 versus 0,144±0,023; p=0,044). Dabei zeigte sich, dass die Differenz des relativen IQR zwischen von SUSI korrekt und falsch kategorisierten Fällen für die durch das SBR korrekt klassifizierten Fälle größer (0,157±0,037 mit n=8 versus 0,144±0,023 mit n=607) als für die durch das SBR inkorrekt klassifizierten Fälle war (0,157±0,029 mit n=15 versus 0,152±0,024 mit n=15). Diese Differenz war nicht statistisch signifikant (Interaktionseffekt „Genauigkeit der SUSI*Genauigkeit des SBR“: p=0,482).

SUSI versus SBR im multi- versus monozentrischen Setting

Für das monozentrische Patientenkollektiv lieferte der putaminale SUSI eine leicht niedrigere AUC als das putaminale SBR (0,969 versus 0,976; p=0,259), jedoch ergab sich für den SUSI eine leicht höhere AUC im Vergleich zum SBR im multizentrischen Setting (0,993 versus 0,991; p=0,207).

Publikation 3

Klassifizierungsgenauigkeit, Sensitivität, Spezifität

Mit zunehmender Größe der NDB ergab sich ein monotoner Anstieg aller Performance-Parameter (mittlere Klassifizierungsgenauigkeit, Sensitivität und Spezifität) an das Niveau der Benchmark-Performance. Parallel kam es zur Reduktion der Varianz (5. Perzentil) der einzelnen Parameter mit steigender Größe der NDB. Absolut gesehen war die Spezifität höher als die Sensitivität, unabhängig vom Patientenkollektiv, dem Rekonstruktionsalgorithmus und der SBR-Methode. Der absolute Wert der Klassifizierungsgenauigkeit war im PPMI-Datensatz am höchsten.

Relativer Verlust der Klassifizierungsgenauigkeit

Der mittlere Verlust der Klassifizierungsgenauigkeit in Relation zur Benchmark-Performance fiel mit zunehmendem Umfang der NDB, wobei der mittlere Verlust für alle simulierten Settings (Patientenkohorte, Rekonstruktionsalgorithmus, SBR-Definition) unter einem Wert von 1% lag, wenn mindestens 15 Fälle für die Erstellung der NDB eingeschlossen worden sind. Der „maximale“ Verlust der Klassifizierungsgenauigkeit (ausgedrückt durch das 5. Perzentil über 10.000 Wiederholungen) unterschritt einen Wert von 5% ab dem Erreichen einer NDB-Größe von 25 bis 30 Personen, unabhängig von der getesteten Patientenkohorte, dem Rekonstruktionsalgorithmus und der SBR-Methode.

Verteilung der SBR-Werte

Es ergab sich eine Abhängigkeit zwischen den absoluten SBR-Werten und den angewendeten Rekonstruktionsalgorithmen (IR und FBP) sowie den Methoden zur Abschätzung der DAT-Verfügbarkeit (SBR-klassisch und SBR-HV). Dabei waren die SBR-Werte auf Basis der IR in der klinischen Kohorte im Mittel höher als bei FBP. Das SBR-HV wies im Vergleich zum SBR-klassisch eine geringere Streubreite auf, unabhängig von der Patientenkohorte.

Darüber hinaus konnte eine Asymmetrie in der Verteilung der SBR-Werte auf Basis der Kontrollen bzw. Patienten mit nicht-neurodegenerativen PS beobachtet werden. Die Rechtsschiefe war am deutlichsten in der klinischen Kohorte mit IR ausgeprägt (Schiefe=0,877 bzw. 0,908 für SBR-klassisch und SBR-HV) und fiel am geringsten in der selbigen Kohorte auf Basis einer Rekonstruktion mittels FBP aus (Schiefe=0,560 bzw. 0,455). Die SBR-Werte wurden daraufhin unter Anwendung des natürlichen Logarithmus transformiert („Ln-Transformation“) und erst danach erfolgte die Berechnung des individuellen z-Wertes. Die Ln-Transformation führte zur

Steigerung der mittleren Klassifizierungsgenauigkeit, Sensitivität und Spezifität und zur Minimierung der Varianz (5. Perzentil über alle Realisierungen).

7. Diskussion

Publikation 1

Die in dieser Studie untersuchten Methoden zur Bestimmung der Kopfkontur für die AC in der DAT-SPECT hatten keinen signifikanten Einfluss auf das semi-quantitative Maß der DAT-Verfügbarkeit im Putamen. Auch hinsichtlich des klinisch relevanten Outcome-Parameters, der diagnostischen Genauigkeit zur Unterscheidung von neurodegenerativen und nicht-neurodegenerativen PS, ergaben sich keine Unterschiede. Die in diesem multizentrischen Datensatz ermittelte diagnostische Performance lag in der Größenordnung der in der Literatur beschriebenen Werte (Suwijn et al. 2015, Buchert et al. 2019).

Die Auswertung des visuellen Ratings bestätigte die Ergebnisse der semi-quantitativen Analyse. Beim direkten Vergleich beider Methoden zur Kopfabgrenzung ergaben sich in knapp 10% der Fälle diskordante Ergebnisse (dichotomes Rating des DAT-Status), welche bei retrospektiver Sichtung als visuell nicht unterscheidbar bewertet worden sind. Diese Diskrepanzen sind demnach am ehesten durch die Intrarater-Variabilität bedingt.

Als Limitation der Studie ist der Referenzstandard zur Bewertung des DAT-Status hervorzuheben. Hier fand der Befund aus der Patientenakte Berücksichtigung, der maßgeblich durch das Ergebnis der DAT-SPECT bestimmt wird. Die dadurch bedingte Zirkularität beeinflusst jedoch nur den absoluten, nicht aber den relativen Wert der diagnostischen Genauigkeit. Letzterer war in dieser Studie relevant, da zwei Methoden zur Bestimmung der Kopfkontur verglichen worden sind. Der direkte Vergleich des putaminalen SBR und die Übereinstimmung des visuellen Ratings wurden davon nicht verzerrt.

Fazit

Die in dieser Studie eingeführte vollautomatische Kopfabgrenzung durch stereotaktische Normalisierung lieferte vergleichbare Ergebnisse wie das schwellwertbasierte, halbautomatische Verfahren. Da bei dem schwellwertbasierten Verfahren in vielen Fällen eine Interaktion durch den Nutzer erforderlich ist (z.B. ist die Tracer-Anreicherung in der Kopfhaut zwischen Patienten sehr variabel, sodass die über einen festen Schwellwert detektierten Kopfbegrenzungen in allen Schichten kontrolliert und ggf. korrigiert werden müssen), kann das neu eingeführte Verfahren für die Anwendung in der klinischen Patientenversorgung empfohlen werden. Es ist vollautomatisch, d.h. benötigt keinen Eingriff des Nutzers, und erzeugt robuste Ergebnisse, was durch eine retrospektive visuelle Überprüfung der individuellen Kopfbegrenzungen bestätigt wurde.

Publikation 2

Die Ausgangshypothese, dass der SUSI im multizentrischen Setting eine höhere diagnostische Genauigkeit zur Unterscheidung von neurodegenerativen und nicht-neurodegenerativen PS als

das SBR liefert, wurde bestätigt. Im monozentrischen Setting hingegen war der SUSI dem SBR leicht unterlegen. Diese Unterschiede waren trendsignifikant, was auf die grundlegend hohe Testgenauigkeit der DAT-SPECT von ≥90% zurückgeführt werden kann („Ceiling Effekt"). Dass die Überlegenheit des SUSI gegenüber dem SBR im multizentrischen Setting nicht eindeutiger ausfiel, kann durch die Harmonisierung der PPMI-Daten bedingt sein, das heißt die Variabilität der räumlichen Auflösung einzelner involvierter SPECT-Kamerasysteme wurde erfolgreich minimiert. Wir gehen davon aus, dass der SUSI im Vergleich zum SBR eine deutlich höhere diagnostische Genauigkeit liefert, wenn keine Harmonisierung innerhalb der Datenerhebung und -rekonstruktion vorgenommen wird.

Darüber hinaus konnte gezeigt werden, dass der relative Interquartilsabstand des Tracer-Uptakes in der Referenzregion, als Maß der Messunsicherheit des nicht-spezifischen Tracer-Uptakes, bei falsch klassifizierten DAT-SPECT größer ist als bei korrekt klassifizierten. Dies zeigte sich nicht nur für den SUSI, sondern auch für die klassische Berechnung des SBR, sodass beide Parameter von einer fehlerhaften Abschätzung der nicht-spezifischen Tracer-Bindung beeinflusst werden. Dabei ergab sich, dass der SUSI tendenziell stärker beeinträchtigt wird als das SBR, da der relative IQR für durch SUSI falsch versus richtig kategorisierte Fälle größer war, wenn der Vergleich separat für jene Fälle durchgeführt wird, die durch das SBR richtig bzw. falsch kategorisiert worden sind. Die berichtete Trendsignifikanz dieses Vergleichs kann auf die eingeschränkte statistische Power (n=8 versus 607 bzw. 15 versus 15) zurückgeführt werden.

Ein direkter statistischer Vergleich der Verteilung der AUC-Differenzen (AUC_{SUSI}–AUC_{SBR}) zwischen beiden Kohorten (mono- und multizentrisch) durch Anwendung von Bootstrapping mit 100.000 Wiederholungen bekräftigte, dass der SUSI im multizentrischen Setting bzw. bei Einsatz von mehr als nur einer SPECT-Kamera dem SBR vorzuziehen ist (p=0,073).

Im monozentrischen Setting zeigte der im nativen Patientenraum berechnete SUSI einen positiven Zusammenhang mit der individuellen Größe des Putamens, das heißt mit zunehmender Größe des Putamens tendiert der SUSI zur Überschätzung der putaminalen DAT-Verfügbarkeit. Da im klinischen Alltag nicht für jeden Patienten eine hochauflösende strukturelle Bildgebung zur Abschätzung des individuellen putaminalen Volumens verfügbar ist, empfehlen wir eine Berechnung des SUSI im Referenzraum. Letzterer zeigte eine bessere Performance als das Äquivalent, welches im Patientenraum berechnet wurde, da eine stereotaktische Normalisierung die interindividuelle Variabilität der Größe des Putamens minimierte. Der beobachtete Effekt war trendsignifikant, was am ehesten auf die limitierte statistische Power durch die geringe Anzahl von falsch klassifizierten Fällen zurückzuführen ist.

Goethals und Kollegen stellten einen direkten Vergleich des SUSI (Berechnung erfolgte im nativen Patientenraum) und SBR (Referenzraum) auf Basis von Daten an, die ausschließlich mit einem SPECT-Kamerasystem erhoben worden sind (Goethals et al. 2007). Von der Performance beider semi-quantitativen Parameter in Bezug auf die stärker betroffene Hemisphäre (unilaterale ROI des Putamens) wurde in der vorher benannten Arbeit nicht berichtet. Hingegen lieferte der SUSI unter Einbezug des gesamten Striatums die höchste Detektionsgenauigkeit mit einer AUC von 0,859 (95%-Konfidenzintervall, 95%-KI: 0,766-0,952). Für das SBR wurde das Minimum der bilateralen ROI von Caudatus und Putamen referiert (AUC=0,830, 95%-KI: 0,727-0,932). Die

Differenzen der absoluten AUC-Werte lassen sich am ehesten auf methodische Unterschiede bei der Berechnung des SBR zurückführen. Da sich die 95%-KI der oben genannten Ergebnisse überschnitten, konnten Goethals und Kollegen ebenfalls keine eindeutige Überlegenheit des SUSI gegenüber des SBR demonstrieren.

Es soll betont werden, dass sich die Patienten der in dieser Studie eingeschlossenen Kohorten stark unterschieden. Im klinischen Setting kam es neben dem Einschluss von Patienten mit idiopathischem PS auch zum Einschluss von Patienten mit atypischen PS, welche mit einer heterogenen DAT-Verfügbarkeit einhergehen. Im PPMI-Sample wurden Patienten ohne dopaminerges Defizit (SWEDD, engl. *subjects without evidence of dopaminergic deficit*) separat kategorisiert und somit von dieser Auswertung ausgeschlossen. Diese Kollektivunterschiede begründen in erster Linie, dass der absolute Wert der Detektionsgenauigkeit für die PPMI-Daten höher ausfiel als für die klinische Kohorte, unabhängig vom Einsatz der semi-quantitativen Methode (SUSI versus SBR).

Des Weiteren haben etliche Faktoren der Bildakquisition und -rekonstruktion nicht nur einen Einfluss auf den absoluten Wert der diagnostischen Performance von SUSI und SBR, sondern auch auf die relative Performance zwischen SUSI und SBR. Daher müssen die hier gefundenen Ergebnisse nicht zwangsläufig generalisierbar sein.

Fazit

Beim direkten Vergleich der Parameter SUSI und SBR zur semi-quantitativen Abschätzung der DAT-Verfügbarkeit konnte gezeigt werden, dass bei multizentrischer Datenerhebung der SUSI eine höhere diagnostische Treffsicherheit zur Differenzierung von Patienten mit nicht-neurodegenerativen und neurodegenerativen PS lieferte. Um den Effekt der interindividuellen Unterschiede der Größe der Basalganglien auf die diagnostische Performance des SUSI zu minimieren, empfiehlt es sich, eine stereotaktische Normalisierung durchzuführen und die semi-quantitative Analyse im Referenz- und nicht im nativen Patientenraum vorzunehmen. Da im monozentrischen Setting das SBR eine vergleichbare Performance zum SUSI aufwies, ist dieser dem SUSI hier vorzuziehen, da das SBR tendenziell weniger stark von Fehlern bei der Abschätzung der nicht-spezifischen Tracer-Bindung in der Referenzregion beeinträchtigt wird.

Publikation 3

Bereits bei Einschluss von mindestens 15 Fällen zur Erstellung einer NDB überstieg der Verlust der Detektionsgenauigkeit den Wert von 1% nicht mehr. Durch sukzessive Vergrößerung des Stichprobenumfangs der NDB konnte der maximale Verlust der Detektionsgenauigkeit reduziert werden, wobei dieser unter einem Wert von 5% lag, wenn insgesamt 25 bis 30 Fälle eine NDB bilden. Dabei stellte sich heraus, dass eine Erhöhung des Größenumfangs über 40 Personen hinaus zu keiner weiteren, signifikanten Reduktion des maximalen Verlusts der diagnostischen Treffsicherheit führte. Diese Zusammenhänge konnten in allen Settings reproduziert werden, das heißt für beide Patientenkohorten (harmonisierte multizentrische Kohorte der PPMI-Studie versus klinische Patientenkohorte), für die zwei getesteten Rekonstruktionsalgorithmen (FBP versus IR) und für die beiden untersuchten Methoden zur semi-quantitativen Abschätzung der DAT-Dichte

im Putamen (klassisches SBR in einer anatomischen ROI und SBR basierend auf den heißesten Voxeln in einer ausgedehnten, nicht-anatomischen ROI). Die Robustheit der Effekte deutet auf eine mögliche Generalisierbarkeit der Ergebnisse auf das breite Spektrum von DAT-SPECT Methoden in der klinischen Patientenversorgung hin.

Die nachweisliche Schiefe in der Verteilung der SBR-Werte der Kontrollen bzw. von Patienten mit nicht-neurodegenerativen PS konnte mittels Ln-Transformation reduziert werden. Es konnte gezeigt werden, dass eine Ln-Transformation vor Berechnung des z-Wertes zu einer Verbesserung der diagnostischen Genauigkeit inklusive Erhöhung der Sensitivität führte. Da es erwartungsgemäß beim Vorliegen einer schiefen Verteilung zur Überschätzung der Standardabweichung kommt, konnte durch die Anwendung einer Ln-Transformation sowohl eine Stabilisierung der diagnostischen Treffsicherheit als auch eine geringere Anfälligkeit bezüglich Ausreißern erzielt werden. Das deckt sich mit dem Ergebnis, dass der maximale Verlust an Detektionsgenauigkeit mit ansteigender Größe der NDB schneller minimiert werden konnte, wenn eine Ln-Transformation durchgeführt wurde.

Für alle Settings wurde eine im Vergleich zur Spezifität gering eingeschränkte Sensitivität ermittelt. Dies kann auf den konservativ angesetzten Schwellwert von z<-2,5 zur Einteilung in pathologische DAT-SPECT zurückgeführt werden. Dieser Schwellwert wurde bewusst gewählt, da bisher keine krankheitsverändernden Therapien für neurodegenerative PS zur Verfügung stehen. Es empfiehlt sich demnach, eine Optimierung der Test-Spezifität zu „Lasten“ der Sensitivität vorzunehmen. Der Schwellwert kann auch mittels einer ROC-Analyse festgelegt werden. Dieser Ansatz benötigt jedoch einen jeweils zweiten, unabhängigen Datensatz von Patienten mit neurodegenerativen und nicht-neurodegenerativen PS mit vergleichbaren Akquisitions- und Rekonstruktionsparametern und soll demnach Gegenstand künftiger Untersuchungen sein. Die absoluten Werte der diagnostischen Performance lagen in der Größenordnung der in der Literatur beschriebenen Werte (Suwijn et al. 2015, Buchert et al. 2019). Die leicht reduzierte Detektionsgenauigkeit in der klinischen Kohorte im Vergleich zum harmonisierten Studiensetting (PPMI) wurde durch falsch negative Klassifizierungsergebnisse getrieben. Eine retrospektive visuelle Beurteilung dieser Fälle ergab, dass es sich um Patienten ohne dopaminerges Defizit (sogenannte SWEDDs) handelte. Dies ist ein Hinweis auf Überdiagnostik neurodegenerativer PS im klinischen Setting.

Der Vergleich der zwei grundlegend verschiedenen Rekonstruktionsalgorithmen (FBP und IR) beschränkte sich auf die klinische Patientenkohorte, da die PPMI-Datenbank ausschließlich eine Variante der IR zum Download verfügbar macht. Es soll darauf hingewiesen werden, dass sich die Parameter der IR in beiden Kohorten unterscheiden, wobei der Einsatz eines Algorithmus zur Auflösungsrückgewinnung im klinischen Sample bewusst gewählt worden ist, um ein breites Spektrum an Rekonstruktionen und demnach an Bildqualitäten zu erzeugen.

Eine leichte überoptimistische Verzerrung hinsichtlich des absoluten Werts der Detektionsgenauigkeit wurde durch den Einschluss von Personen in das Testsample verursacht, die ebenfalls für die Erstellung der jeweiligen NDB verwendet wurden. Der Effekt kann jedoch als gering gewertet werden, da der zirkuläre Anteil maximal 13,5% der Gesamtkohorte ausmachte. Des Weiteren kam es zu einer Verzerrung der klinischen Diagnose, die der Patientenakte

entnommen und als Referenzstandard verwendet worden ist, da der Neurologe gegenüber dem Befund der DAT-SPECT nicht verblindet war. Dies führte zur Überschätzung der absoluten Werte der diagnostischen Performance-Parameter, jedoch beeinflusste dies nicht die Aussagen hinsichtlich der minimalen NDB-Größe zur semi-quantitativen Auswertung der putaminalen DAT-Verfügbarkeit.

Obwohl zunehmend Evidenz dafür vorliegt, dass die DAT-Verfügbarkeit mit steigendem Alter sinkt und bei Frauen höher ist als bei Männern, wurden Alter und Geschlecht in dieser Studie nicht berücksichtigt (Lavalaye et al. 2000, Karrer et al. 2017). Bisher liegen keine Studien vor, die eine eindeutige Überlegenheit der Korrektur von Alter und Geschlecht auf die diagnostische Performance des SBR als semi-quantitatives Maß der DAT-Verfügbarkeit zeigen konnten. Daher haben wir eine ausführliche Auswertung dieser Zusammenhänge in den oben beschriebenen Kohorten vorgenommen. Dabei ergab sich, dass die Korrektur beider Kovariaten keinen klinisch relevanten Einfluss auf die Genauigkeit zur Differenzierung von neurodegenerativen und nicht-neurodegenerativen PS hatte (Ergebnisse sind noch nicht publiziert). Der Anteil der interindividuellen Variabilität des SBR, der durch Alter und Geschlecht erklärt wird, liegt demnach deutlich unter der 50%-Schwelle des DAT-Verlusts für das Auftreten von Symptomen (Fearnley et al. 1991).

Fazit

Auf Basis dieser ausführlichen Analyse des Zusammenhangs von Größe der NDB für die semi-quantitative Einschätzung des DAT-Status und dessen diagnostische Genauigkeit empfiehlt sich ein Mindestumfang von 25 bis 30 DAT-SPECT-Datensätzen. Eine Vergrößerung der Normaldatenbank über 40 Fälle hinaus führt hingegen zu keiner weiteren relevanten Steigerung der diagnostischen Performance. Zur Stabilisierung der Klassifizierungsgenauigkeit empfiehlt sich eine Ln-Transformation der SBR-Werte, um die Empfindlichkeit gegenüber Ausreißern, vor allem in NDB mit kleinem Größenumfang, zu reduzieren.

8. Literaturverzeichnis

Bernheimer, H., Birkmayer, W., Hornykiewicz, O., Jellinger, K., Seitelberger, F. 1973. Brain dopamine and the syndromes of Parkinson and Huntington. Clinical, morphological and neurochemical correlations. *J Neurol Sci* 20(4): 415-455.

Booij, J., Hemelaar, J. T. G. M., Speelman, J. D., de Bruin, K., Janssen, A. G. M., van Royen, E. A. 1999. One-day protocol for imaging of the nigrostriatal dopaminergic pathway in Parkinson's disease by [I-123]FPCIT SPECT. *Journal of Nuclear Medicine* 40(5): 753-761.

Booij, J., Speelman, J. D., Horstink, M. W., Wolters, E. C. 2001. The clinical benefit of imaging striatal dopamine transporters with [123I]FP-CIT SPET in differentiating patients with presynaptic parkinsonism from those with other forms of parkinsonism. *Eur J Nucl Med* 28(3): 266-272.

Buchert, R., Buhmann, C., Apostolova, I., Meyer, P. T., Gallinat, J. 2019. Nuclear Imaging in the Diagnosis of Clinically Uncertain Parkinsonian Syndromes. *Dtsch Arztebl Int* 116(44): 747-754.

Buchert, R., Kluge, A., Tossici-Bolt, L., Dickson, J., Bronzel, M., Lange, C., Asenbaum, S., Booij, J., Atay Kapucu, L. O., Svarer, C., Koulibaly, P. M., Nobili, F., Pagani, M., Sabri, O., Sera, T., Tatsch, K., Vander Borght, T., Van Laere, K., Varrone, A., Iida, H. 2016. Reduction in camera-specific variability in [(123)I]FP-CIT SPECT outcome measures by image reconstruction optimized for multisite settings: impact on age-dependence of the specific binding ratio in the ENC-DAT database of healthy controls. *Eur J Nucl Med Mol Imaging* 43(7): 1323-1336.

Chang, L. T. 1978. Method for Attenuation Correction in Radionuclide Computed Tomography. *IEEE Transactions on Nuclear Science* 25(1): 638-643.

Darcourt, J., Booij, J., Tatsch, K., Varrone, A., Vander Borght, T., Kapucu, O. L., Nagren, K., Nobili, F., Walker, Z., Van Laere, K. 2010. EANM procedure guidelines for brain neurotransmission SPECT using (123)I-labelled dopamine transporter ligands, version 2. *Eur J Nucl Med Mol Imaging* 37(2): 443-450.

Dickson, J. C., Tossici-Bolt, L., Sera, T., Booij, J., Ziebell, M., Morbelli, S., Assenbaum-Nan, S., Borght, T. V., Pagani, M., Kapucu, O. L., Hesse, S., Van Laere, K., Darcourt, J., Varrone, A., Tatsch, K. 2017. The impact of reconstruction and scanner characterisation on the diagnostic capability of a normal database for [123I]FP-CIT SPECT imaging. *EJNMMI Res* 7(1): 10.

Djang, D. S., Janssen, M. J., Bohnen, N., Booij, J., Henderson, T. A., Herholz, K., Minoshima, S., Rowe, C. C., Sabri, O., Seibyl, J., Van Berckel, B. N., Wanner, M. 2012. SNM practice guideline for dopamine transporter imaging with 123I-ioflupane SPECT 1.0. *J Nucl Med* 53(1): 154-163.

Fearnley, J. M., Lees, A. J. 1991. Ageing and Parkinson's disease: substantia nigra regional selectivity. *Brain* 114 (Pt 5): 2283-2301.

Fleming, J. S., Bolt, L., Stratford, J. S., Kemp, P. M. 2004. The specific uptake size index for quantifying radiopharmaceutical uptake. *Phys Med Biol* 49(14): N227-234.

Goethals, I., Dobbeleir, A., Ham, H., Santens, P., D'Asseler, Y. 2007. Validation of a resolution-independent method for the quantification of I-123-FP-CIT SPELT scans. *Nuclear Medicine Communications* 28(10): 771-774.

Kaasinen, V., Vahlberg, T. 2017. Striatal dopamine in Parkinson disease: A meta-analysis of imaging studies. *Ann Neurol* 82(6): 873-882.

Karrer, T. M., Josef, A. K., Mata, R., Morris, E. D., Samanez-Larkin, G. R. 2017. Reduced dopamine receptors and transporters but not synthesis capacity in normal aging adults: a meta-analysis. *Neurobiol Aging* 57: 36-46.

Kupitz, D., Apostolova, I., Lange, C., Ulrich, G., Amthauer, H., Brenner, W., Buchert, R. 2014. Global scaling for semi-quantitative analysis in FP-CIT SPECT. *Nuklearmedizin* 53(6): 234-241.

Lange, C., Seese, A., Schwarzenbock, S., Steinhoff, K., Umland-Seidler, B., Krause, B. J., Brenner, W., Sabri, O., Kurth, J., Hesse, S., Buchert, R. 2014. CT-based attenuation correction in I-123-ioflupane SPECT. *PLoS One* 9(9): e108328.

Lavalaye, J., Booij, J., Reneman, L., Habraken, J. B., van Royen, E. A. 2000. Effect of age and gender on dopamine transporter imaging with [123I]FP-CIT SPET in healthy volunteers. *Eur J Nucl Med* 27(7): 867-869.

Marek, K., Chowdhury, S., Siderowf, A., Lasch, S., Coffey, C. S., Caspell-Garcia, C., Simuni, T., Jennings, D., Tanner, C. M., Trojanowski, J. Q., Shaw, L. M., Seibyl, J., Schuff, N., Singleton, A., Kieburtz, K., Toga, A. W., Mollenhauer, B., Galasko, D., Chahine, L. M., Weintraub, D., Foroud, T., Tosun-Turgut, D., Poston, K., Arnedo, V., Frasier, M., Sherer, T., Parkinson's Progression Markers, I. 2018. The Parkinson's progression markers initiative (PPMI) - establishing a PD biomarker cohort. *Ann Clin Transl Neurol* 5(12): 1460-1477.

Marek, K., Jennings, D., Lasch, S., Siderowf, A., Tanner, C., Simuni, T., Coffey, C., Kieburtz, K., Flagg, E., Chowdhuty, S., Poewe, W., Mollenhauer, B., Sherer, T., Frasier, M., Meunier, C., Rudolph, A., Casaceli, C., Seibyl, J., Mendick, S., Schuff, N., Zhang, Y., Toga, A., Crawford, K., Ansbach, A., Piovella, M., Trojanowski, J., Shaw, L., Singleton, A., Hawkins, K., Eberling, J., Brooks, D., Russell, D., Leary, L., Factor, S., Sommerfeld, B., Hogarth, P., Pighetti, E., Williams, K., Standaert, D., Guthrie, S., Hauser, R., Delgado, H., Jankovic, J., Hunter, C., Stern, M., Tran, B., Leverenz, J., Baca, M., Frank, S., Thomas, C. A., Richard, I., Deeley, C., Rees, L., Sprenger, F., Lang, E., Shill, H., Obradov, S., Fernandez, H., Winters, A., Berg, D., Gauss, K., Galasko, D., Fontaine, D., Mari, Z., Gerstenhaber, M., Brooks, D., Malloy, S., Barone, P., Longo, K., Comery, T., Ravina, B., Grachev, I., Gallagher, K., Collins, M., Widnell, K. L., Ostrowizki, S., Fontoura, P., La-Roche, H., Ho, T., Luthman, J., van der Brug, M., Reith, A. D., Taylor, P., Marker, T. P. P., Comm, E. S., Cores, S. C. 2011. The Parkinson Progression Marker Initiative (PPMI). *Progress in Neurobiology* 95(4): 629-635.

Mintun, M. A., Raichle, M. E., Kilbourn, M. R., Wooten, G. F., Welch, M. J. 1984. A quantitative model for the in vivo assessment of drug binding sites with positron emission tomography. *Ann Neurol* 15(3): 217-227.

Morbelli, S., Esposito, G., Arbizu, J., Barthel, H., Boellaard, R., Bohnen, N. I., Brooks, D. J., Darcourt, J., Dickson, J. C., Douglas, D., Drzezga, A., Dubroff, J., Ekmekcioglu, O., Garibotto, V., Herscovitch, P., Kuo, P., Lammertsma, A., Pappata, S., Penuelas, I., Seibyl, J., Semah, F., Tossici-Bolt, L., Van de Giessen, E., Van Laere, K., Varrone, A., Wanner, M., Zubal, G., Law, I. 2020. EANM practice guideline/SNMMI procedure standard for dopaminergic imaging in Parkinsonian syndromes 1.0. *Eur J Nucl Med Mol Imaging* 47(8): 1885-1912.

Soret, M., Koulibaly, P. M., Darcourt, J., Hapdey, S., Buvat, I. 2003. Quantitative accuracy of dopaminergic neurotransmission imaging with (123)I SPECT. *J Nucl Med* 44(7): 1184-1193.

Suwijn, S. R., van Boheemen, C. J., de Haan, R. J., Tissingh, G., Booij, J., de Bie, R. M. 2015. The diagnostic accuracy of dopamine transporter SPECT imaging to detect nigrostriatal cell loss in patients with Parkinson's disease or clinically uncertain parkinsonism: a systematic review. *EJNMMI Res* 5: 12.

Tatsch, K., Poepperl, G. 2012. Quantitative approaches to dopaminergic brain imaging. *Q J Nucl Med Mol Imaging* 56(1): 27-38.

Tossici-Bolt, L., Dickson, J. C., Sera, T., Booij, J., Asenbaun-Nan, S., Bagnara, M. C., Borght, T. V., Jonsson, C., de Nijs, R., Hesse, S., Koulibaly, P. M., Akdemir, U. O., Koole, M., Tatsch, K., Varrone, A. 2017. [123I]FP-CIT ENC-DAT normal database: the impact of the reconstruction and quantification methods. *EJNMMI Phys* 4(1): 8.

Tossici-Bolt, L., Dickson, J. C., Sera, T., de Nijs, R., Bagnara, M. C., Jonsson, C., Scheepers, E., Zito, F., Seese, A., Koulibaly, P. M., Kapucu, O. L., Koole, M., Raith, M., George, J., Lonsdale, M. N., Munzing, W., Tatsch, K., Varrone, A. 2011. Calibration of gamma camera systems for a multicentre European (1)(2)(3)I-FP-CIT SPECT normal database. *Eur J Nucl Med Mol Imaging* 38(8): 1529-1540.

Tossici-Bolt, L., Hoffmann, S. M., Kemp, P. M., Mehta, R. L., Fleming, J. S. 2006. Quantification of [123I]FP-CIT SPECT brain images: an accurate technique for measurement of the specific binding ratio. *Eur J Nucl Med Mol Imaging* 33(12): 1491-1499.

Youden, W. J. 1950. Index for rating diagnostic tests. *Cancer* 3(1): 32-35.

9. Eidesstattliche Erklärung

„Ich, Catharina Lange, versichere an Eides statt durch meine eigenhändige Unterschrift, dass ich die vorgelegte Dissertation mit dem Thema: *‚Optimierte semi-quantitative Analyse der Dopamintransporter-SPECT zur Unterstützung der visuellen Bildinterpretation in der Diagnostik von Parkinsonsyndromen‘/‚Optimized semi-quantitative analysis of dopamine transporter SPECT to support visual image interpretation in the diagnosis of parkinsonian syndromes‘* selbstständig und ohne nicht offengelegte Hilfe Dritter verfasst und keine anderen als die angegebenen Quellen und Hilfsmittel genutzt habe.

Alle Stellen, die wörtlich oder dem Sinne nach auf Publikationen oder Vorträgen anderer Autoren/innen beruhen, sind als solche in korrekter Zitierung kenntlich gemacht. Die Abschnitte zu Methodik (insbesondere praktische Arbeiten, Laborbestimmungen, statistische Aufarbeitung) und Resultaten (insbesondere Abbildungen, Graphiken und Tabellen) werden von mir verantwortet.

Ich versichere ferner, dass ich die in Zusammenarbeit mit anderen Personen generierten Daten, Datenauswertungen und Schlussfolgerungen korrekt gekennzeichnet und meinen eigenen Beitrag sowie die Beiträge anderer Personen korrekt kenntlich gemacht habe (siehe Anteilserklärung). Texte oder Textteile, die gemeinsam mit anderen erstellt oder verwendet wurden, habe ich korrekt kenntlich gemacht.

Meine Anteile an etwaigen Publikationen zu dieser Dissertation entsprechen denen, die in der untenstehenden gemeinsamen Erklärung mit dem Erstbetreuer, angegeben sind. Für sämtliche im Rahmen der Dissertation entstandenen Publikationen wurden die Richtlinien des ICMJE (International Committee of Medical Journal Editors; www.icmje.og) zur Autorenschaft eingehalten. Ich erkläre ferner, dass ich mich zur Einhaltung der Satzung der Charité – Universitätsmedizin Berlin zur Sicherung Guter Wissenschaftlicher Praxis verpflichte.

Weiterhin versichere ich, dass ich diese Dissertation weder in gleicher noch in ähnlicher Form bereits an einer anderen Fakultät eingereicht habe.

Die Bedeutung dieser eidesstattlichen Versicherung und die strafrechtlichen Folgen einer unwahren eidesstattlichen Versicherung (§§156, 161 des Strafgesetzbuches) sind mir bekannt und bewusst.“

_____ _____

Datum Unterschrift
Catharina Lange

10. Anteilserklärung an den erfolgten Publikationen

Catharina Lange hatte folgenden Anteil an den nachkommenden Publikationen:

Publikation 1: Catharina Lange, Jens Kurth, Anita Seese, Sarah Schwarzenböck, Karen Steinhoff, Bert Umland-Seidler, Bernd J. Krause, Winfried Brenner, Osama Sabri, Swen Hesse, Ralph Buchert. 2015. Robust, fully automatic delineation of the head contour by stereotactical normalization for attenuation correction according to Chang in dopamine transporter scintigraphy. *European Radiology*.

Beitrag im Einzelnen: Studienkonzept und -design, Datenaufbereitung und Datenanalyse, Interpretation der Ergebnisse, Manuskriptverfassung und ausführliche Revision im Rahmen des Review-Prozesses. Dabei erfolgte die Aufbereitung und Auswertung der Bilddaten (inkl. Implementierung der Bildverarbeitungsroutinen) und (statistische) Analyse des multizentrischen Datensatzes zentral und ausschließlich von mir. Aus meiner statistischen Auswertung entstanden Tabelle 1 und Abbildungen 1 bis 6.

Publikation 2: Ralph Buchert*, **Catharina Lange***, Timo S. Spehl, Ivayla Apostolova, Lars Frings, Cathrine Jonsson, Philipp T. Meyer, Sabine Hellwig. 2019. Diagnostic performance of the specific uptake size index for semi-quantitative analysis of I-123-FP-CIT SPECT: harmonized multi-center trial setting versus typical clinical single-camera setting. *EJNMMI Research*.

Beitrag im Einzelnen: Beteiligung an Datenaufbereitung und Datenanalyse, Interpretation der Ergebnisse, Manuskriptverfassung und ausführliche Revision im Rahmen des Review-Prozesses. Dabei erfolgte die Aufbereitung und Auswertung der Bilddaten (inkl. Implementierung der Bildverarbeitungsroutinen) und (statistische) Analyse des multizentrischen Datensatzes der Parkinson's Progression Markers Initiative (PPMI) Datenbank ausschließlich von mir, die Auswertung der klinischen Daten erfolgte in Zusammenarbeit mit Dr. R. Buchert. Aus meiner statistischen Auswertung entstanden Tabelle 1 und Abbildungen 1, 2, 5 und 6.

Publikation 3: Helen Schmitz-Steinkrüger*, **Catharina Lange***, Ivayla Apostolova, Holger Amthauer, Wencke Lehnert, Susanne Klutmann, Ralph Buchert. 2020. Impact of the size of the normal database on the performance of semi-quantitative analysis in dopamine transporter SPECT. *EJNMMI Physics*.

Beitrag im Einzelnen: Beteiligung an Datenaufbereitung und Datenanalyse, Interpretation der Ergebnisse, Manuskriptverfassung und ausführliche Revision im Rahmen des Review-Prozesses. Dabei erfolgte die Aufbereitung und Auswertung der Bilddaten (inkl. Implementierung der Bildverarbeitungsroutinen) und (statistische) Analyse des multizentrischen Datensatzes der PPMI Datenbank ausschließlich von mir, die Auswertung der klinischen Daten erfolgte in Zusammenarbeit mit H. Schmitz-Steinkrüger. Aus meiner statistischen Auswertung entstanden die Abbildungen 1, 2, 3, 4, 5 und 7.

_____

Unterschrift
Catharina Lange

11. Ausgewählte Publikationen

Publikation 1

Catharina Lange, Jens Kurth, Anita Seese, Sarah Schwarzenböck, Karen Steinhoff, Bert Umland-Seidler, Bernd J. Krause, Winfried Brenner, Osama Sabri, Swen Hesse, Ralph Buchert. 2015. Robust, fully automatic delineation of the head contour by stereotactical normalization for attenuation correction according to Chang in dopamine transporter scintigraphy. *European Radiology*. 25(9): 2709-2717. https://doi.org/10.1007/s00330-015-3667-6.

Auszug aus Journal Summary List 2013

Journal Data Filtered By: **Selected JCR Year: 2013** Selected Editions: SCIE Selected Categories: **"RADIOLOGY, NUCLEAR MEDICINE & MEDICAL IMAGING"** Selected Category Scheme: WoS
Gesamtanzahl: 122 Journale

Rank	Full Journal Title	Total Cites	Journal Impact Factor	Eigenfactor Score
1	JACC-Cardiovascular Imaging	3,744	6.986	0.023020
2	HUMAN BRAIN MAPPING	14,858	6.924	0.041660
3	Circulation-Cardiovascular Imaging	2,341	6.752	0.013990
4	RADIOLOGY	45,811	6.214	0.071870
5	NEUROIMAGE	69,654	6.132	0.172680
6	JOURNAL OF NUCLEAR MEDICINE	21,301	5.563	0.041800
7	EUROPEAN JOURNAL OF NUCLEAR MEDICINE AND MOLECULAR IMAGING	10,737	5.217	0.025530
8	JOURNAL OF CARDIOVASCULAR MAGNETIC RESONANCE	2,421	5.112	0.008260
9	RADIOTHERAPY AND ONCOLOGY	12,480	4.857	0.031610
10	ULTRASCHALL IN DER MEDIZIN	1,332	4.645	0.003350
11	Journal of Cardiovascular Computed Tomography	689	4.506	0.003530
12	INVESTIGATIVE RADIOLOGY	5,273	4.453	0.011470
13	**EUROPEAN RADIOLOGY**	**12,946**	**4.338**	**0.032650**
14	INTERNATIONAL JOURNAL OF RADIATION ONCOLOGY BIOLOGY PHYSICS	40,270	4.176	0.078760
15	IEEE TRANSACTIONS ON MEDICAL IMAGING	12,890	3.799	0.023290
16	SEMINARS IN RADIATION ONCOLOGY	1,782	3.768	0.004460
17	MEDICAL IMAGE ANALYSIS	3,925	3.681	0.010240
18	AMERICAN JOURNAL OF NEURORADIOLOGY	18,648	3.675	0.035920
19	NMR IN BIOMEDICINE	5,297	3.559	0.013420
20	Biomedical Optics Express	2,614	3.497	0.011320
21	MAGNETIC RESONANCE IN MEDICINE	25,454	3.398	0.038130
22	Contrast Media & Molecular Imaging	947	3.333	0.003770
23	ULTRASOUND IN OBSTETRICS & GYNECOLOGY	8,105	3.140	0.017320
…	…	…	…	…
122	Journal de Radiologie Diagnostique et Interventionnelle	5	0.020	0.000000

https://doi.org/10.1007/s00330-015-3667-6

https://doi.org/10.1007/s00330-015-3667-6

https://doi.org/10.1007/s00330-015-3667-6

https://doi.org/10.1007/s00330-015-3667-6

https://doi.org/10.1007/s00330-015-3667-6

https://doi.org/10.1007/s00330-015-3667-6

https://doi.org/10.1007/s00330-015-3667-6

https://doi.org/10.1007/s00330-015-3667-6

https://doi.org/10.1007/s00330-015-3667-6

Publikation 2

Ralph Buchert*, **Catharina Lange***, Timo. S. Spehl, Ivayla Apostolova, Lars Frings, Cathrine Jonsson, Philipp T. Meyer, Sabine Hellwig. 2019. Diagnostic performance of the specific uptake size index for semi-quantitative analysis of I-123-FP-CIT SPECT: harmonized multi-center research setting versus typical clinical single-camera setting. *EJNMMI Research*. 9(1): 37. https://doi.org/10.1186/s13550-019-0506-9.

Auszug aus Journal Summary List 2017

Journal Data Filtered By: **Selected JCR Year: 2017** Selected Editions: SCIE Selected Categories: **"RADIOLOGY, NUCLEAR MEDICINE & MEDICAL IMAGING"** Selected Category Scheme: WoS
Gesamtanzahl: 129 Journale

Rank	Full Journal Title	Total Cites	Journal Impact Factor	Eigenfactor Score
1	JACC-Cardiovascular Imaging	8,104	10.247	0.026350
2	European Heart Journal-Cardiovascular Imaging	4,630	8.336	0.020630
3	EUROPEAN JOURNAL OF NUCLEAR MEDICINE AND MOLECULAR IMAGING	14,983	7.704	0.024850
4	RADIOLOGY	54,109	7.469	0.063660
5	JOURNAL OF NUCLEAR MEDICINE	27,102	7.439	0.037530
6	CLINICAL NUCLEAR MEDICINE	4,756	6.309	0.006950
7	INVESTIGATIVE RADIOLOGY	6,486	6.224	0.012400
8	Circulation-Cardiovascular Imaging	5,438	6.221	0.020150
9	IEEE TRANSACTIONS ON MEDICAL IMAGING	17,837	6.131	0.024170
10	ULTRASOUND IN OBSTETRICS & GYNECOLOGY	12,420	5.654	0.018800
11	INTERNATIONAL JOURNAL OF RADIATION ONCOLOGY BIOLOGY PHYSICS	46,595	5.554	0.055010
12	JOURNAL OF CARDIOVASCULAR MAGNETIC RESONANCE	4,918	5.457	0.013520
13	NEUROIMAGE	92,719	5.426	0.152460
14	MEDICAL IMAGE ANALYSIS	6,383	5.356	0.011890
15	RADIOTHERAPY AND ONCOLOGY	17,184	4.942	0.027820
16	HUMAN BRAIN MAPPING	20,334	4.927	0.042780
17	SEMINARS IN NUCLEAR MEDICINE	2,285	4.558	0.002990
18	ULTRASCHALL IN DER MEDIZIN	2,201	4.389	0.004310
19	MAGNETIC RESONANCE IN MEDICINE	31,440	4.082	0.034090
20	EUROPEAN RADIOLOGY	18,615	4.027	0.034090
20	SEMINARS IN RADIATION ONCOLOGY	2,480	4.027	0.003620
22	JOURNAL OF NUCLEAR CARDIOLOGY	3,508	4.011	0.004130
23	AMERICAN JOURNAL OF NEURORADIOLOGY	22,667	3.653	0.029820
24	MOLECULAR IMAGING AND BIOLOGY	2,415	3.626	0.005480
25	JOURNAL OF MAGNETIC RESONANCE IMAGING	16,398	3.612	0.027400
26	Biomedical Optics Express	8,120	3.482	0.022730
27	INTERNATIONAL JOURNAL OF HYPERTHERMIA	3,350	3.440	0.004040

28	Journal of the American College of Radiology	3,231	3.393	0.007360
29	RADIOGRAPHICS	11,207	3.249	0.008990
30	AMERICAN JOURNAL OF ROENTGENOLOGY	33,453	3.125	0.031050
31	Journal of Cardiovascular Computed Tomography	1,608	3.095	0.004280
32	KOREAN JOURNAL OF RADIOLOGY	2,331	3.072	0.004670
33	NMR IN BIOMEDICINE	7,537	3.031	0.014130
34	CANCER IMAGING	1,150	3.016	0.002250
35	Contrast Media & Molecular Imaging	1,215	2.934	0.002500
36	MEDICAL PHYSICS	25,701	2.884	0.035180
37	Radiation Oncology	5,157	2.862	0.013540
38	EUROPEAN JOURNAL OF RADIOLOGY	12,571	2.843	0.025400
39	Clinical Neuroradiology	630	2.790	0.002090
40	JOURNAL OF VASCULAR AND INTERVENTIONAL RADIOLOGY	9,021	2.758	0.012460
41	JOURNAL OF NEURORADIOLOGY	949	2.706	0.001620
42	PHYSICS IN MEDICINE AND BIOLOGY	24,912	2.665	0.032130
43	ULTRASOUND IN MEDICINE AND BIOLOGY	10,316	2.645	0.013440
44	**EJNMMI Research**	**1,110**	**2.630**	**0.004030**
45	MAGNETIC RESONANCE IMAGING	7,194	2.564	0.011670
46	RADIATION RESEARCH	8,468	2.530	0.006760
47	STRAHLENTHERAPIE UND ONKOLOGIE	2,820	2.459	0.004600
48	ABDOMINAL IMAGING	3,203	2.443	0.005940
49	COMPUTERIZED MEDICAL IMAGING AND GRAPHICS	2,190	2.435	0.002730
49	Dose-Response	824	2.435	0.001320
51	ULTRASONICS	6,518	2.377	0.009140
52	QUARTERLY JOURNAL OF NUCLEAR MEDICINE AND MOLECULAR IMAGING	1,032	2.368	0.001460
53	JOURNAL OF BIOMEDICAL OPTICS	13,503	2.367	0.019530
54	NEURORADIOLOGY	5,420	2.346	0.007640
55	ULTRASONIC IMAGING	1,076	2.300	0.000690
56	CLINICAL RADIOLOGY	6,234	2.282	0.008470
57	Physica Medica-European Journal of Medical Physics	1,915	2.240	0.005110
58	Quantitative Imaging in Medicine and Surgery	861	2.231	0.002500
59	Brachytherapy	1,991	2.227	0.004240
60	CARDIOVASCULAR AND INTERVENTIONAL RADIOLOGY	5,429	2.210	0.009520
61	NUCLEAR MEDICINE AND BIOLOGY	3,880	2.203	0.004770
62	Journal of Contemporary Brachytherapy	556	2.146	0.001210
63	Diagnostic and Interventional Imaging	1,127	2.115	0.003020
64	ACADEMIC RADIOLOGY	5,399	2.110	0.009200
65	INTERNATIONAL JOURNAL OF CARDIOVASCULAR IMAGING	2,951	2.036	0.008210
…	…	…	…	…
129	JBR-BTR	239	0.195	0.000360

EJNMMI Research

ORIGINAL RESEARCH Open Access

Diagnostic performance of the specific uptake size index for semi-quantitative analysis of I-123-FP-CIT SPECT: harmonized multi-center research setting versus typical clinical single-camera setting

Ralph Buchert[1*†], Catharina Lange[2*†], Timo S. Spehl[3], Ivayla Apostolova[1], Lars Frings[3], Cathrine Jonsson[4], Philipp T. Meyer[3] and Sabine Hellwig[3,5]

Abstract

Introduction: The specific uptake size index (SUSI) of striatal FP-CIT uptake is independent of spatial resolution in the SPECT image, in contrast to the specific binding ratio (SBR). This suggests that the SUSI is particularly appropriate for multi-site/multi-camera settings in which camera-specific effects increase inter-subject variability of spatial resolution. However, the SUSI is sensitive to inter-subject variability of striatum size. Furthermore, it might be more sensitive to errors of the estimate of non-displaceable FP-CIT binding. This study compared SUSI and SBR in the multi-site/multi-camera (MULTI) setting of a prospective multi-center study and in a mono-site/mono-camera (MONO) setting representative of clinical routine.

Methods: The MULTI setting included patients with Parkinson's disease (PD, $n = 438$) and healthy controls ($n = 207$) from the Parkinson Progression Marker Initiative. The MONO setting included 122 patients from routine clinical patient care in whom FP-CIT SPECT had been performed with the same double-head SPECT system according to the same acquisition and reconstruction protocol. Patients were categorized as "neurodegenerative" ($n = 84$) or "non-neurodegenerative" ($n = 38$) based on follow-up data. FP-CIT SPECTs were stereotactically normalized to MNI space. SUSI and SBR were computed for caudate, putamen, and whole striatum using unilateral ROIs predefined in MNI space. SUSI analysis was repeated in native patient space in the MONO setting. The area (AUC) under the ROC curve for identification of PD/"neurodegenerative" cases was used as performance measure.

(Continued on next page)

* Correspondence: r.buchert@uke.de; catharina.lange@charite.de
†Ralph Buchert and Catharina Lange contributed equally to this work.
[1]Department for Diagnostic and Interventional Radiology and Nuclear Medicine, University Hospital Hamburg-Eppendorf, Martinistr. 52, 20246 Hamburg, Germany
[2]Department of Nuclear Medicine, Charité - Universitätsmedizin Berlin, corporate member of Freie Universität Berlin, Humboldt-Universität zu Berlin, and Berlin Institute of Health, Augustenburger Platz 1, 13353 Berlin, Germany
Full list of author information is available at the end of the article

(Continued from previous page)
Results: In both settings, the highest AUC was achieved by the putamen (minimum over both hemispheres), independent of the semi-quantitative method (SUSI or SBR). The putaminal SUSI provided slightly better performance with ROI analysis in MNI space compared to patient space (AUC = 0.969 vs. 0.961, $p = 0.129$). The SUSI (computed in MNI space) performed slightly better than the SBR in the MULTI setting (AUC = 0.993 vs. 0.991, $p = 0.207$) and slightly worse in the MONO setting (AUC = 0.969 vs. AUC = 0.976, $p = 0.259$). There was a trend toward larger AUC difference between SUSI and SBR in the MULTI setting compared to the MONO setting ($p = 0.073$). Variability of voxel intensity in the reference region was larger in misclassified cases compared to correctly classified cases for both SUSI and SBR (MULTI setting: $p = 0.007$ and $p = 0.012$, respectively).

Conclusions: The SUSI is particularly useful in MULTI settings. SPECT images should be stereotactically normalized prior to SUSI analysis. The putaminal SUSI provides better diagnostic performance than the SUSI of the whole striatum. Errors of the estimate of non-displaceable count density in the reference region can cause misclassification by both SUSI and SBR, particularly in borderline cases. These cases might be identified by visual checking FP-CIT uptake in the reference region for particularly high variability.

Keywords: Dopamine transporter, SPECT, FP-CIT, Semi-quantitative analysis, Specific uptake size index, Specific binding ratio

Introduction

Single-photon emission computed tomography (SPECT) with the I-123 labeled dopamine transporter (DAT) ligand FP-CIT is widely used for detection (or exclusion) of nigrostriatal degeneration in patients with clinically uncertain parkinsonian syndrome (PS) [1]. Semi-quantitative analysis of striatal FP-CIT uptake has the potential to support visual interpretation of the SPECT images [2, 3].

Semi-quantitative analysis in radionuclide imaging often aims at estimating the binding potential (BP), first defined by Mintun and co-workers as BP = Bmax / KD, where Bmax is the density of available binding sites (here DAT) and 1/KD is the affinity of the tracer (here FP-CIT) for the binding site [4]. The binding potential is a measure of the capacity of the region of interest (ROI) for specific binding of the tracer, that is, binding to the binding site of interest. More generally, a binding potential can be defined as the equilibrium concentration of specific binding to some other reference concentration [5]. The most widely used binding potential is the non-displaceable binding potential BPnd based on the concentration of the non-displaceable (by blocking of the binding site) tracer in the ROI as reference, i.e.,

$$\mathrm{BPnd} = \mathrm{Cs}/\mathrm{Cnd}, \quad (1)$$

where Cs and Cnd are the equilibrium concentration of specifically bound and non-displaceable tracer in the ROI, respectively. Determination of BPnd requires dynamic imaging and arterial blood sampling for full tracer kinetic modeling. This is not feasible in clinical routine so that a number of methods have been developed to estimate BPnd from a single static scan during equilibrium (for FP-CIT approximately given between 3 and 6 h after i.v. injection [6]). The most widely used among these methods is the specific binding ratio (SBR) defined by the formula [7]

$$\mathrm{SBR} = (\mathrm{C}-\mathrm{CR})/\mathrm{CR}, \quad (2)$$

where C is the total count concentration in the striatal ROI, and CR is the total count concentration in a reference region (almost) void of DAT. The SBR according to formula (2) is based on the assumption that CR approximates the count concentration originating from non-displaceable FP-CIT binding in the striatal ROI (the difference C − CR then approximates the specific count density originating from FP-CIT bound to DAT in the striatal ROI). The striatal ROI for computation of the SBR usually anatomically delineates the striatum or the striatal subregion of interest such as caudate nucleus or putamen [8, 9]. A major limitation of the SBR according to formula (2) is the strong underestimation of the striatal FP-CIT concentration C in the SPECT images due to partial volume effects caused by limited spatial resolution of SPECT. The recovery of actual striatal FP-CIT concentration in SPECT images typically is only about 50% if no correction for partial volume and other degrading effects is performed [10–12]. In addition to strong underestimation of the SBR, partial volume effects cause additional variability. This is due to the fact that the magnitude of the partial volume effect strongly depends on the size and shape of the striatum and the spatial resolution in the reconstructed SPECT image. Spatial resolution varies between SPECT cameras depending on both, hardware and acquisition/reconstruction protocol. The additional variability of the SBR associated with the use of different SPECT cameras negatively impacts the utility of the SBR, particularly in multi-site and in single-site/multi-camera settings or when normal values and cut-offs obtained from healthy subjects at one site are to be used at other sites [13, 14].

Only in an ideal situation in which all main causes of inaccuracy and imprecision of SPECT (attenuation, scatter, partial volume effects, statistical noise) were properly dealt with, the true SBR value would be obtained with any SPECT camera and reduction of inter-camera variability would naturally follow from accuracy.

The specific uptake size index (SUSI) has been proposed to improve accuracy of semi-quantitative analysis in FP-CIT SPECT in practice [7, 15, 16]. It has been thoroughly validated in phantom studies where true count densities are known [15, 17]. The SUSI eliminates partial volume effects by replacing *count density* in the striatal ROI by a measure of *total counts* in the ROI. More precisely, the SUSI is defined as

$$\mathrm{SUSI} = (\mathrm{T} - \mathrm{CR} \times \mathrm{V})/\mathrm{CR}, \quad (3)$$

where T is the total number of counts originating from a large striatal ROI, V is the volume of the striatal ROI, and CR is the count concentration in the reference region.

The striatal ROI for the computation of the SUSI is chosen sufficiently large around the striatum to guarantee that all counts originating from the striatum are detected within this ROI. Assuming that image reconstruction is "activity conserving" (that is, counts are neither lost nor artificially produced by the reconstruction, although limited spatial resolution can cause counts originating from the striatum to be localized outside of the striatum), summing the activity over all voxels within the large striatum ROI collects all counts originating from the striatum. This holds true independently of the spatial resolution in the reconstructed SPECT image as long as the ROI is large enough to encompass all counts originating from the striatum. Thus, the SUSI is independent of spatial resolution [15]. The SUSI approach can be seen as a method for partial volume correction of the SBR. This is due to the fact that SBR = SUSI / Vs, where Vs is the actual volume of the striatum, as is easily derived from Eqs. (2) and (3) [15].

The SUSI has been used successfully for the quantitative characterization of age effects on DAT availability in healthy subjects from the European normal control database of FP-CIT SPECT (ENC-DAT) [18]. A total of 13 sites using ten different SPECT camera models contributed to the ENC-DAT study.

The SUSI is typically computed in the original SPECT images in patient space after manual reorientation [7, 15, 16]. A limitation of the SUSI computed in patient space is that it also depends on the size of the striatum, not via partial volume effects as the SBR, but via the total amount of specifically bound FP-CIT that increases with increasing size of the striatum (assuming constant DAT concentration). Thus, inter-subject variability of striatum size causes additional variability of the SUSI that might limit its power to detect nigrostriatal degeneration. The impact of inter-subject variability of striatum size on the SUSI might be eliminated by concentration-preserving stereotactical normalization of the SPECT images into an anatomical standard space prior to ROI analysis. Inter-subject variability of partial volume effects cannot be eliminated this way.

A recent study suggested the SUSI to be more sensitive than the SBR to errors of the estimate of non-displaceable count density in the striatum by the count density CR in the reference region [19]. In both methods, SBR and SUSI, the reference region is used to correct the striatal signal for non-displaceable "background" in the striatum ROI that dilutes the effect of nigrostriatal degeneration in these measures if not corrected for. It is evident that the background contribution increases when the ROI size increases beyond the anatomical boundaries of the striatum. Thus, the relative magnitude of the correction for non-displaceable background increases with increasing ROI size. As a consequence, the computed measure of specific striatal binding (SBR or SUSI) might be more sensitive to errors (including statistical noise) of the estimate of non-displaceable FP-CIT binding the larger the striatal ROI.

Aim of the present study was to compare the SUSI and the SBR with respect to detection of nigrostriatal degeneration in (i) a sample of patients with PS in whom FP-CIT SPECT has been performed with the same SPECT camera using the same acquisition protocol with radius of rotation within very tight limits [20] and the same reconstruction protocol (mono-site/mono-camera (MONO) setting) and (ii) in the multi-site/multi-camera (MULTI) setting of the Parkinson Progression Markers Initiative (PPMI) [21]. Inter-subject variability of spatial resolution in the SPECT images most likely was larger in the MULTI setting compared to the MONO setting (due to camera-specific variability of spatial resolution in the MULTI setting). The primary hypothesis put to test was that the diagnostic performance of the SUSI relative to the SBR is better in the MULTI setting compared to the MONO setting (due to its stability with respect to varying spatial resolution in the SPECT images), particularly when the SUSI is computed after stereotactical normalization (in order to eliminate inter-subject variability of striatum size) rather than in raw images in patient space [7]. The secondary hypothesis put to test was that the variability of the count density in the reference region impacts the diagnostic performance of both SUSI and SBR, and that the effect is larger for the SUSI than for the SBR.

Materials and methods

Mono-site/mono-camera setting

One hundred twenty-two patients in whom FP-CIT SPECT had been performed for detection (or exclusion) of nigrostriatal degeneration as part of routine clinical work-up were recruited retrospectively from the patient database of the Department of Nuclear Medicine of the

University Medical Center Freiburg. The patients were categorized into two groups: "neurodegenerative PS" and "non-neurodegenerative PS." The neurodegenerative group (n = 84, 39 females, 67.3 ± 10.0 years) comprised (i) the Lewy body disease spectrum (n = 60) including Parkinson's disease (PD, n = 41), PD dementia (PDD, n = 5), and dementia with Lewy bodies (DLB, n = 14), and (ii) atypical parkinsonian syndromes (APS, n = 24) including multiple systems atrophy (MSA-P and MSA-P/C, n = 7), progressive supranuclear palsy (PSP, n = 13), and corticobasal degeneration (CBD, n = 4). The non-neurodegenerative group (n = 38, 15 females, 70.0 ± 8.0 years) comprised (i) essential tremor (n = 2), (ii) vascular parkinsonism (VaP, n = 7), (iii) drug-induced parkinsonism (n = 11), (iv) psychogenic parkinsonism (n = 1), (v) possible Alzheimer's disease (AD, n = 11), and (vi) normal pressure hydrocephalus (NPH, n = 6). The clinical diagnoses were established by a movement disorder specialist based on current consensus criteria and review of all relevant medical charts and clinical follow-up data (mean follow-up 26.8 ± 14.5 months). Patients with other than the listed diagnosis were excluded.

FP-CIT SPECT had been performed according to common guidelines [22, 23]. The same double-head SPECT system (Siemens E.CAM) and the same acquisition protocol had been used in all patients (thyroid uptake blocked with sodium perchlorate, 3 h uptake period after intravenous bolus injection of 193 ± 8 MBq FP-CIT; low-energy high-resolution parallel-hole collimators, 60 projections of 30 s duration with each head along a scan arc of 180° (i.e. 3° angular sampling), radius of rotation = 13.5 ± 0.3 cm, energy window 144–168 keV, acquisition matrix 128 × 128, zoom factor 1.23). In order to ensure consistent image reconstruction in all patients, projection data were exported from the archive and retrospectively reconstructed by three-dimensional ordered subset expectation maximization (OSEM) with resolution recovery using the Flash3D algorithm of the scanner software. The following parameter settings were used as previously proposed for FP-CIT SPECT specifically with the E.CAM camera to provide a good compromise between delineation of striatal substructures for visual inspection, recovery of striatal tracer uptake, and noise of non-displaceable tracer uptake in the reference region for semi-quantitative analysis [24]: 8 iterations, 8 subsets, postfiltering with a Gaussian kernel with 8 mm full-width-at-half-maximum (FWHM). Uniform post reconstruction attenuation correction was performed according to Chang (first order, broad-beam attenuation coefficient μ = 0.12/cm); no scatter correction was performed. Voxel size was 3.9 × 3.9 × 3.9 mm^3.

Multi-site/multi-camera setting

Data were obtained from the Parkinson's Progression Markers Initiative (PPMI) database (https://www.ppmi-info.org/access-data-specimens/download-data/) [21]. Up-to-date information on the PPMI is available at www.ppmi-info.org. The PPMI is a longitudinal, multi-center study that aims to assess the progression of clinical features, imaging, and biologic markers in patients with (idiopathic) PD and healthy control (HC) subjects. All PD patients were in an early stage of the disease (diagnosis of PD within the last 2 years prior to screening). Details of the eligibility criteria are given at http://www.ppmi-info.org/wp-content/uploads/2014/01/PPMI-AM7-Protocol.pdf.

All FP-CIT scans available from the PPMI database on 22nd November 2017 were downloaded in DICOM format, independent of subgroup and visit (n = 1710). The analyses of the present study included the first FP-CIT SPECT of all HC subjects and all PD patients, that is, the analyses included also FP-CIT SPECT at an "unscheduled" visit if FP-CIT SPECT at the screening visit was not available. Furthermore, the analyses included not only "regular" HC subjects and "regular" PD patients but also subjects who (i) declined participation in the PPMI study after the screening visit but before inclusion in the study (n = 20), or (ii) withdrew agreement after inclusion in the study (n = 78), or (iii) were excluded from participation in the study due to a reason not related to FP-CIT SPECT (n = 23). This resulted in 656 FP-CIT scans. Visual inspection resulted in exclusion of 11 of these scans: three HC scans were excluded because of clearly reduced striatal FP-CIT uptake (PPMI-ID 3221, 3478, 4095); eight PD scans were excluded because of clearly normal FP-CIT uptake in the striatum (3027, 3289, 3290, 3534, 3618, 3623, 3660, 3863). This resulted in the inclusion of a total of 645 FP-CIT SPECTs: 438 of PD patients and 207 of HC subjects.

FP-CIT SPECT data had been acquired at 24 different centers using different SPECT camera models. All centers had been qualified for participation in the study by an image center qualification process including a technical set up visit to optimize the acquisition and reconstruction protocol for the specific SPECT system to be used in the study [21]. The target dose of FP-CIT was 185 MBq (allowed range 110–185 MBq) and SPECT acquisition was to be started 4 ± 0.5 h after i.v. administration of FP-CIT (PPMI imaging protocol at http://www.ppmi-info.org/study-design/research-documents-and-sops/). Raw projection data had been transferred to the PPMI imaging core lab for central image reconstruction using an OSEM algorithm on a HERMES workstation (Hermes Medical Solutions, Stockholm, Sweden) [25]. PMOD (PMOD Technologies, Zurich, Switzerland) had been used for attenuation correction. Ellipses were drawn on the images and 0th order Chang attenuation correction was applied using a site-specific μ empirically derived from phantom data. Standard 3D Gaussian post-smoothing (6.0 mm FWHM) was applied. Only

preprocessed images that have been stereotactically normalized into the anatomical space of the Montreal Neurological Institute (MNI) were available for download. The images were in DICOM format with 91 × 109 × 91 cubic voxels of 2 mm edge length.

Semi-quantitative analyses

All semi-quantitative analyses were performed fully automatically using a MATLAB script.

SBR was computed according to formula (2) with ROI analysis in MNI space. For this purpose, individual FP-CIT SPECTs were transformed (affine, that is, without warping) into MNI space using the Statistical Parametric Mapping software package (version SPM12) and a custom-made FP-CIT template (Fig. 1). Unilateral ROIs for caudate, putamen, and entire striatum (= union of caudate and putamen ROI) predefined in MNI space by the automatic anatomic labeling (AAL) atlas [26] available in the PickAtlas of the Wake Forest University were used (Fig. 1a) [27]. In addition, custom-made unilateral ROIs for anterior and posterior putamen manually predefined in MNI space were tested (Fig. 1b). Count concentration within a ROI was characterized by the average intensity over all voxels within the ROIs. The 75th percentile of the count density in a reference region comprising the whole brain without striata, thalamus, and brain stem was used as estimate of non-displaceable count density (Fig. 1d) [28].

The SUSI was computed according to formula (3) with ROI analysis in MNI space. It was computed separately for unilateral caudate and unilateral putamen using large three-dimensional unilateral ROIs predefined in MNI space (Fig. 1c). The union of large caudate and large putamen ROI was used to compute the SUSI of the entire unilateral striatum. In the MONO setting, SUSI analysis was repeated in native patient space. For this purpose, the FP-CIT template was stereotactically normalized into patient space (affine transformation). The resulting transformation was used to map the ROIs from MNI space to the patient's FP-CIT SPECT.

Statistical analyses

SUSI and SBR were tested for identification of "neurodegenerative PS" in the MONO setting and for identification of PD patients in the MULTI setting using the minimum over both hemispheres for both semi-quantitative measures. The area (AUC) under the receiver operating characteristic (ROC) curve was employed as performance measure. Total accuracy, sensitivity, and specificity were computed with the cut-off fixed by Youden's criterion [29].

In order to test for potential impact of individual putamen size on the diagnostic performance of the putaminal SUSI computed in patient space, the volume of the AAL putamen ROI after transformation into patient space was used as measure of individual putamen size (mean of both hemispheres). Putamen size was compared between true positive, true negative, false positive, and false negative cases as classified by the SUSI computed in patient space. Univariate analysis of variance was used for this purpose.

In order to test the secondary hypothesis, that is, the impact of the uncertainty of the estimate of non-displaceable count density by the 75th percentile of voxel intensities in the reference region on the diagnostic performance of SUSI and SBR, the interquartile range (IQR) of voxel intensities in the reference region relative to the 75th percentile of voxel intensities in the reference region was used as uncertainty measure (relative IQR). First, relative IQR was compared between correctly classified scans (true positive or true negative) and incorrectly classified scans (false positive or false negative) using unpaired *t* tests. This was done separately for SUSI and SBR. Second, SUSI and

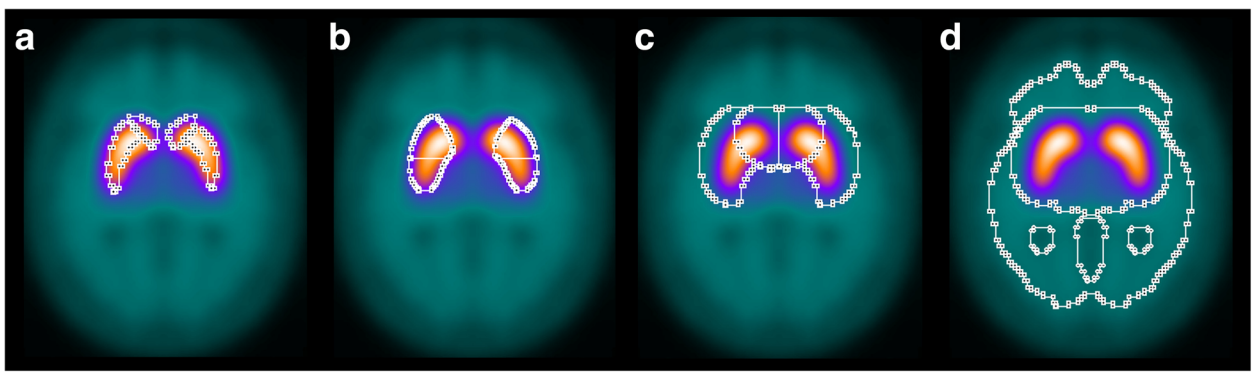

Fig. 1 Anatomical caudate and putamen ROIs from the AAL atlas (**a**), custom-made anatomical ROIs of anterior and posterior putamen (**b**), large ROIs of caudate and putamen (**c**), and reference region (**d**). All ROIs are three-dimensional. The ROIs are overlaid to the custom-made FP-CIT template used as target for stereotactical normalization. The anatomical ROIs in (**a**) and (**b**) were used for computation of the SBR. The large ROIs in (**c**) were used for computation of the SUSI. The custom-made FP-CIT template was obtained by averaging the stereotactically normalized images of 94 visually normal FP-CIT SPECT scans

SBR were compared with respect to the difference of the relative IQR between correctly classified scans and incorrectly classified scans using univariate analysis of variance of relative IQR with both, correctness of the SUSI-based classification and correctness of the SBR-based classification as fixed factors. Cut-offs fixed by Youden's criterion were used to categorize scans as correctly or incorrectly classified.

In quantitative terms, the primary hypothesis of the study (the diagnostic performance of the SUSI relative to the SBR is better in the MULTI setting than in the MONO setting) states that $(AUC_{SUSI} - AUC_{SBR})$ (MULTI) > $(AUC_{SUSI} - AUC_{SBR})$ (MONO), where AUC_{SUSI} is the AUC of the putaminal SUSI and AUC_{SBR} is the AUC of the putaminal SBR. Bootstrapping with 100,000-fold resampling was used to estimate the distribution of $(AUC_{SUSI} - AUC_{SBR})$, separately for the MULTI and the MONO setting. Then, the distribution of $(AUC_{SUSI} - AUC_{SBR})$ was compared between the MULTI and the MONO setting by generating 10,000 random pairs of $(AUC_{SUSI} - AUC_{SBR})$ (MULTI) and $(AUC_{SUSI} - AUC_{SBR})$ (MONO) from their respective distributions and counting the number of random pairs that fulfilled the alternative hypothesis $(AUC_{SUSI} - AUC_{SBR})$ (MULTI) ≤ $(AUC_{SUSI} - AUC_{SBR})$ (MONO).

Results

Fully automatic affine transformation of FP-CIT SPECT from patient space into the anatomical MNI template space or vice versa worked properly in all cases according to visual inspection. Reliable spatial transformation is required for automatic semi-quantitative analysis with standard ROIs predefined in template space.

Mono-site/mono-camera setting

SUSI and SBR showed better diagnostic performance with the putamen as region of interest compared to caudate and whole striatum (Table 1). The AUC provided by the putaminal measures was largest for the SBR of the posterior putamen (AUC = 0.981) followed by SBR of the whole putamen (AUC = 0.976). The putaminal SUSI showed slightly worse performance, particularly when computed in patient space (AUC = 0.961, DeLong test $p = 0.036$ compared to SBR of the whole putamen; Table 1, Fig. 2a). Stereotactical normalization prior to ROI analysis improved the performance of the putaminal SUSI from AUC = 0.961 to AUC = 0.969, but the difference did not reach statistical significance ($p = 0.129$, Table 1). Classification of patients (as "neurodegenerative PS" or "non-neurodegenerative PS") was incorrect in 7 (5.7%), 12 (9.8%), and 8 (6.6%) of the 122 patients when based on putaminal SBR, putaminal SUSI computed in patient space, or putaminal SUSI computed in MNI space, respectively (Table 1).

Classification based on putaminal SUSI computed in patient space or putaminal SBR was discrepant in seven patients (5.7%). All these discrepant cases had "neurodegenerative PS" and presented with borderline findings in FP-CIT SPECT (Fig. 3). Classification based on

Table 1 Area (AUC) under the ROC curve, cut-off (based on Youden's criterion), and resulting total accuracy, sensitivity, and specificity for identification of neurodegenerative etiology of parkinsonism (mono-site/mono-camera setting) or PD (multi-site/multi-camera setting). (Cau = caudate, Put = putamen, Str = striatum, ant = anterior, post = posterior)

		SBR					SUSI in MNI space			SUSI in patient space		
		Cau	Put	ant Put	post Put	Str	Cau	Put	Str	Cau	Put	Str
Mono-camera	AUC (95% CI)	0.636[bbb,ccc] (0.526–0.746)	0.976[c] (0.954–0.999)	0.935[b] (0.891–0.980)	0.981[c] (0.960–1.000)	0.925 (0.877–0.973)	0.764[aaa] (0.673–0.855)	0.969 (0.943–0.996)	0.927 (0.881–0.974)	0.765[aaa] (0.675–0.855)	0.961[a] (0.930–0.993)	0.924 (0.874–0.974)
	Cut-off	1.829	2.383	1.866	1.776	2.051	16.418	16.974	34.902	12.913	8.371	23.653
	Accuracy	0.672	0.943	0.885	0.943	0.877	0.705	0.934	0.877	0.770	0.902	0.877
	Sensitivity	0.762	0.940	0.857	0.917	0.881	0.643	0.929	0.869	0.821	0.881	0.881
	Specificity	0.474	0.947	0.947	1.000	0.868	0.842	0.947	0.895	0.658	0.947	0.868
Multi-camera	AUC (95% CI)	0.884[bbb] (0.856–0.911)	0.991 (0.987–0.996)	0.966[bbb] (0.954–0.978)	0.998[b] (0.996–1.000)	0.979 (0.971–0.988)	0.920[aaa] (0.898–0.942)	0.993 (0.989–0.998)	0.978 (0.969–0.987)	–	–	–
	Cut-off	1.781	2.068	1.776	1.597	1.960	21.229	14.799	39.171	–	–	–
	Accuracy	0.780	0.953	0.898	0.980	0.930	0.839	0.964	0.933	–	–	–
	Sensitivity	0.719	0.943	0.872	0.973	0.916	0.822	0.961	0.945	–	–	–
	Specificity	0.908	0.976	0.952	0.995	0.961	0.874	0.971	0.908	–	–	–

Statistical testing was restricted to caudate versus caudate, putamen versus putamen, and striatum versus striatum
[a/aa/aaa]DeLong test $p < 0.05/0.01/0.005$ compared to SBR
[b/bb/bbb]DeLong test $p < 0.05/0.01/0.005$ compared to SUSI in MNI space
[c/cc/ccc]DeLong test $p < 0.05/0.01/0.005$ compared to SUSI in patient space

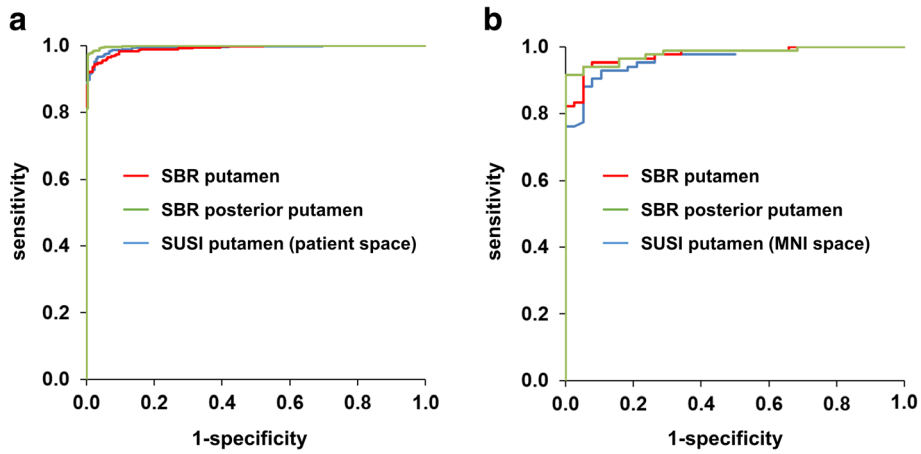

Fig. 2 ROC curves for identification of neurodegenerative etiology of parkinsonism (mono-site/mono-camera setting, **a**) or PD (multi-site/multi-camera setting, **b**)

putaminal SUSI computed in patient space was correct (true positive) and SBR-based classification was incorrect (false negative) in one of these patients. Classification based on putaminal SUSI computed in patient space was incorrect (false negative) and SBR-based classification was correct (true positive) in the remaining six patients.

Putamen volume was smaller in the two false positive cases compared to the 36 true negative cases based on putaminal SUSI in patient space; it was larger in the ten false negative cases compared to the 74 true positive cases (Fig. 4). However, neither of the two differences reached statistical significance according to analysis of variance with standard of truth ("neurodegenerative PS" versus "non-neurodegenerative PS," $p = 0.314$) and correctness of patient space SUSI (true positive or true negative versus false positive or false negative, $p = 0.372$) as fixed factors (standard of truth * correctness interaction $p = 0.170$).

The relative IQR of voxel intensities in the reference region was not different between the 12 patients with incorrect classification based on patient space SUSI

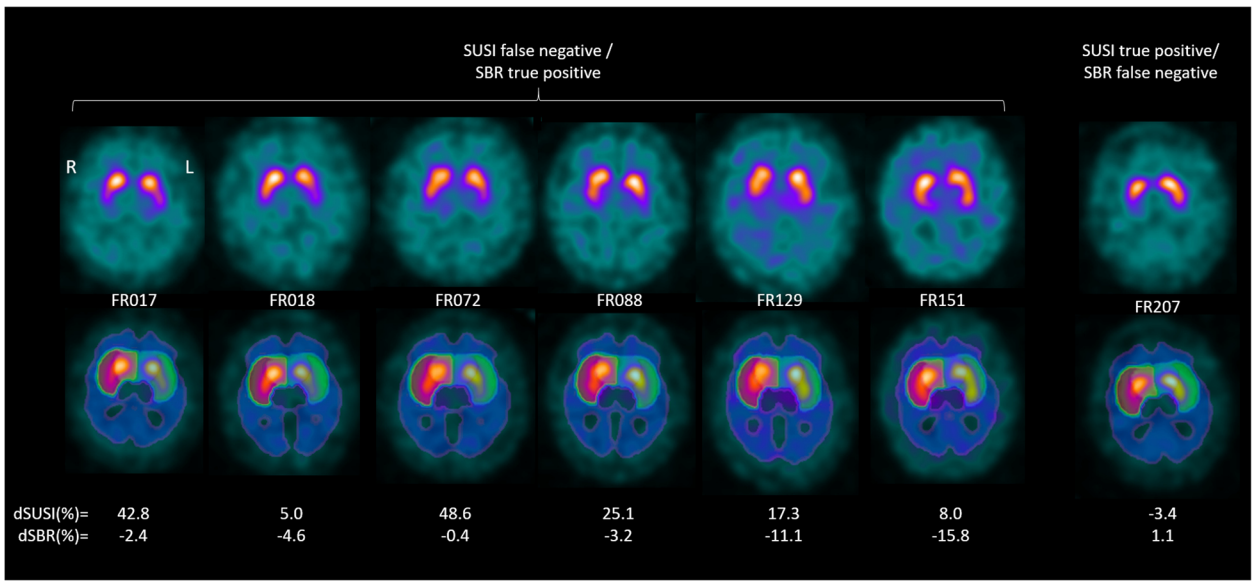

Fig. 3 FP-CIT SPECT images from the mono-site/mono-camera setting with discrepant classification as "neurodegenerative PS" or "non-neurodegenerative PS" based on the putaminal SUSI computed in patient space versus classification based on the putaminal SBR. The upper row shows transversal slices through the striatum in patient space. The lower row shows the same transversal slice with the transformed mask of caudate, putamen and the reference region overlaid. dSUSI = 100*(individual SUSI – SUSI cutoff) / SUSI cutoff, dSBR = 100*(individual SBR – SBR cutoff) / SBR cutoff

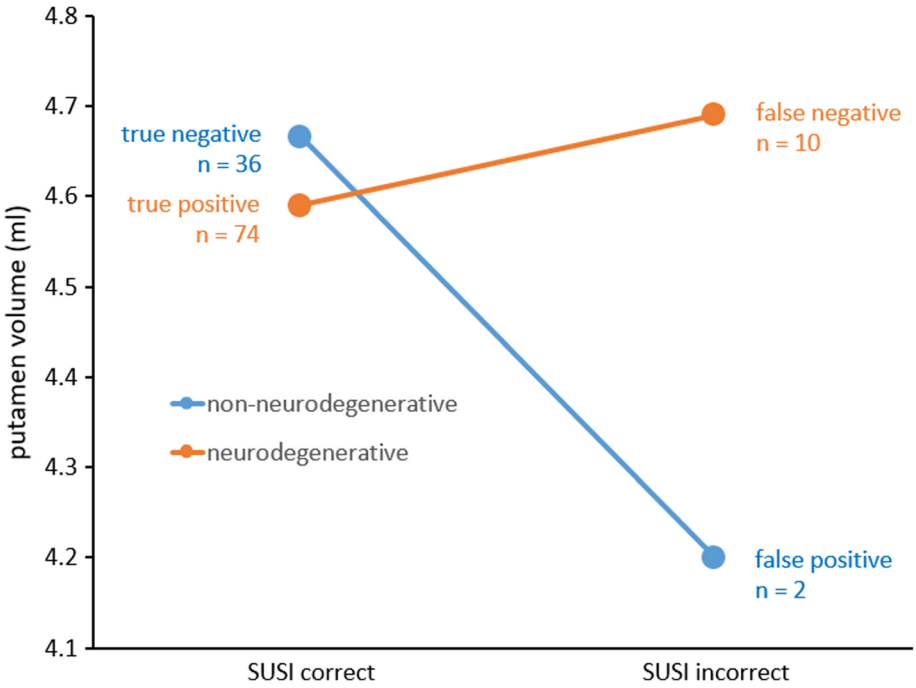

Fig. 4 Comparison of individual putamen volume between true positive and false negative cases and between true negative and false positive cases as classified by the SUSI computed in patient space. None of the differences reached statistical significance

compared to the remaining 110 patients (0.164 ± 0.012 versus 0.173 ± 0.024, *t* test $p = 0.199$).

Harmonized multi-site/multi-camera setting

In the multi-site/multi-camera setting, the SUSI was computed in MNI space only, because the PPMI provides only preprocessed FP-CIT SPECT images in MNI space, the original FP-CIT images in patient space are not available. Thus, all SUSI results in the multi-site/multi-camera setting refer to the SUSI computed in MNI space.

In the harmonized MULTI setting, too, the putamen achieved the highest performance with both SUSI and SBR (Table 1). The AUC of the SUSI increased to AUC = 0.993 when the putamen was used as region of interest from AUC = 0.978 for the whole striatum ($p < 0.001$).

The AUC provided by the putaminal measure was largest for the SBR of the posterior putamen (AUC = 0.998), followed by the SUSI (AUC = 0.993) and the SBR of the whole putamen (AUC = 0.991) (Fig. 2b). The AUC difference between SUSI and SBR of the whole putamen did not reach statistical significance ($p = 0.207$). Classification of subjects (as PD or HC) was incorrect in 30 (4.7%) and 23 (3.6%) of the 645 subjects when based on putaminal SBR or putaminal SUSI, respectively (Table 1).

The relative IQR of voxel intensities in the reference region was higher in the 23 subjects with incorrect SUSI-based classification compared to the remaining 622 subjects with correct SUSI-based classification (0.15713 ± 0.03098 versus 0.14390 ± 0.02259, *t* test $p = 0.007$). The same was true for the 30 subjects with incorrect SBR-based classification compared to the remaining 615 subjects (0.15474 ± 0.02612 versus 0.14387 ± 0.02278, *t* test $p = 0.012$).

Classification based on putaminal SUSI or on putaminal SBR was discrepant in 23 of the 645 patients (3.6%). The relative IQR of voxel intensities in the reference region was higher in the 23 subjects with discrepant classification compared to the remaining 622 subjects with concordant classification (0.154 ± 0.028 versus 0.144 ± 0.023, *t* test $p = 0.044$). SUSI-based classification was correct and SBR-based classification was incorrect in two HC subjects and 13 PD patients. SUSI-based classification was incorrect and SBR-based classification was correct in three HC subjects and 5 PD patients. The difference of relative IQR between incorrectly classified scans and correctly classified scans based on the SUSI was larger for scans with correct SBR-based classification (0.157 ± 0.037, $n = 8$, versus 0.144 ± 0.023, $n = 607$) compared to scans with incorrect SBR-based classification (0.157 ± 0.029, $n = 15$, versus 0.152 ± 0.024, $n = 15$) (Fig. 5). However, the difference was not significant according to univariate analysis of variance of relative IQR with correctness of the SUSI-based classification and the correctness of the SBR-based classification as fixed factors (SUSI correctness * SBR correctness interaction $p = 0.482$).

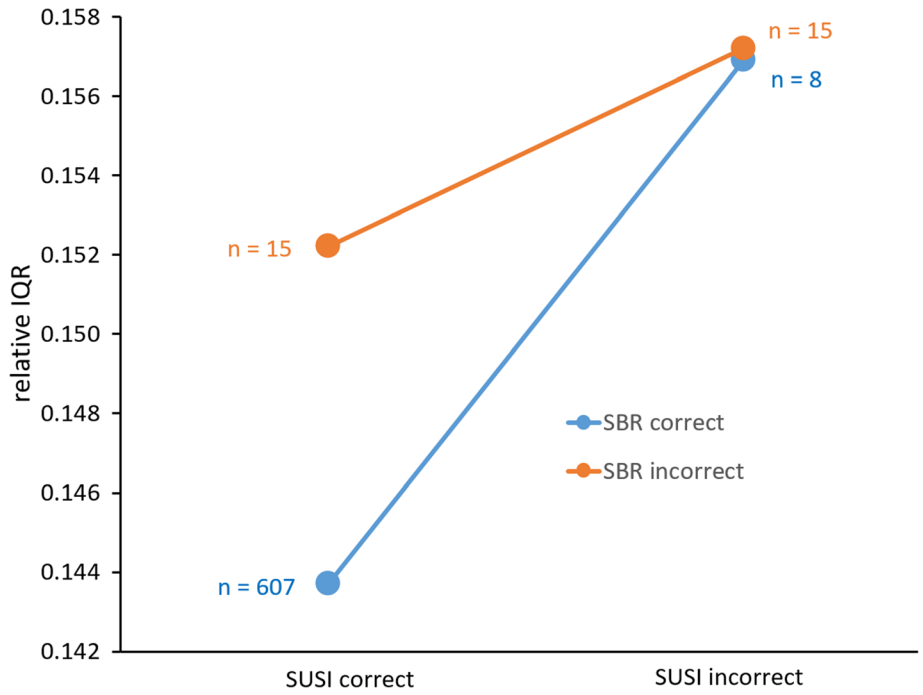

Fig. 5 Interquartile range (IQR) relative to the 75th percentile of the voxel intensity in the reference region according to correctness of SUSI-based and SBR-based classification of the PPMI FP-CIT images as PD or HC ("correct" = true positive or true negative, "incorrect" = false positive or false negative). The relative IQR is as measure of the uncertainty of the estimate of the non-displaceable count density by the 75th percentile of the voxel intensity in the reference region

SUSI versus SBR in harmonized multi-site versus mono-camera setting

The putaminal SUSI performed slightly worse than the putaminal SBR in the MONO setting (AUC = 0.969 versus 0.976, $p = 0.259$) and slightly better in the MULTI setting (AUC = 0.993 versus 0.991, $p = 0.207$).

The distribution of the difference ($AUC_{SUSI} - AUC_{SBR}$) in the MULTI setting and in the MONO setting estimated by bootstrapping is shown in Fig. 6. Mean ($AUC_{SUSI} - AUC_{SBR}$) was 0.002 (95% CI -0.001–0.005) in the MULTI setting and -0.007 (-0.021–0.004) in the MONO setting. The sign test revealed a trend toward larger ($AUC_{SUSI} - AUC_{SBR}$) in the MULTI setting compared to the MONO setting ($p = 0.073$).

Discussion

SUSI and SBR showed better classification performance with the putamen as region of interest compared to the whole striatum. The difference was highly significant for both SUSI and SBR (e.g., multi-site/multi-camera setting: putaminal SUSI = 0.993, striatal SUSI = 0.978, $p < 0.001$, Table 1). The fraction of misclassified cases was almost twice as large for the SUSI of the whole striatum compared to the putaminal SUSI (6.7% versus 3.6% in the MULTI setting, Table 1). Thus, the SUSI should be used with the putamen as striatal region of interest. This might appear in conflict with the rationale of the SUSI at first sight, because there is some loss of putaminal counts and some contamination by counts from the caudate at the boundary between putamen and caudate ROI. This probably explains that all previous studies used the SUSI with the whole striatum as region of interest [7, 15, 16, 18, 19]. Furthermore, the putaminal SUSI depends on the definition of the putamen ROI, in contrast to the striatal SUSI that is rather independent of the striatum ROI as long as it is large enough [15]. However, the SBR has the same limitations: the SBR of the (whole) putamen depends on the putamen ROI, and it is affected by spill-out and spill-in at the boundary between putamen and caudate ROI. These limitations, therefore, should not prevent use of the putaminal SUSI, considering the relevant improvement in diagnostic accuracy it provides compared to the conventional SUSI of the whole striatum. The large putamen ROI used for SUSI analysis in the present study excluded part of the anterior putamen in order to reduce contamination of the putaminal SUSI by counts from the caudate (Fig. 1c). As a result, the contribution of the posterior putamen was pronounced in the putaminal SUSI. This probably contributed to the excellent performance of the putaminal SUSI in the multi-site/multi-camera setting.

In the MONO setting, putaminal SUSI computed in patient space performed slightly worse than the SUSI computed in MNI space (AUC = 0.961 versus 0.969, $p = 0.129$, total accuracy = 90.2% versus 93.4%, Table 1).

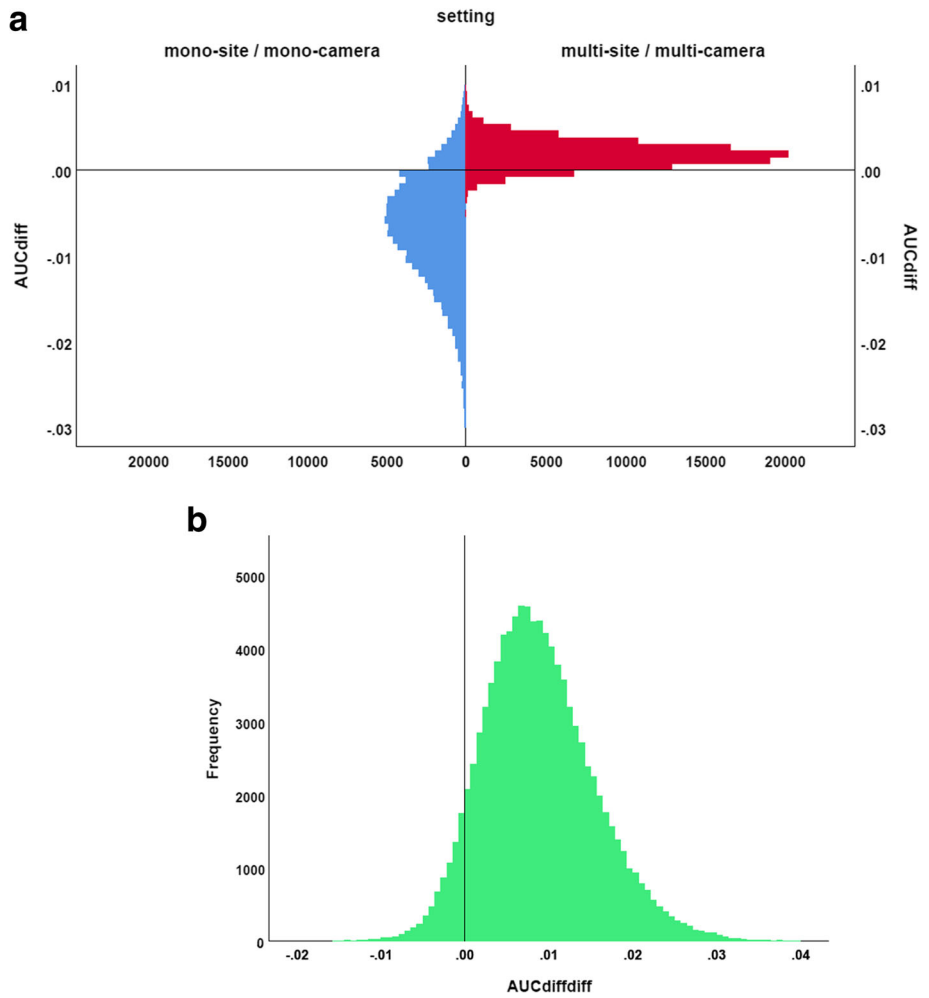

Fig. 6 Distribution of the performance difference $AUC_{diff} = (AUC_{SUSI} - AUC_{SBR})$ between putaminal SUSI and putaminal SBR in the mono-site/mono-camera (MONO) setting and in the multi-site/multi-camera (MULTI) setting (**a**), and distribution of the double difference $AUC_{diffdiff} = AUC_{diff}$ (MULTI) – AUC_{diff} (MONO) (**b**). All distributions were estimated by bootstrapping with 100,000-fold resampling

Putamen volume was smaller in the two false positive cases compared to the 36 true negative cases based on putaminal SUSI in patient space; it was larger in the ten false negative cases compared to the 74 true positive cases (Fig. 4). This is in line with the fact that the putaminal SUSI increases with increasing putamen size so that the SUSI tends to overestimate putaminal DAT concentration in patients with large putamen and to underestimate putaminal DAT density in patients with small putamen. This can be avoided by scaling the putaminal SUSI to individual putamen size estimated from individual high resolution MRI which, however, is not always available in clinical routine. Alternatively, inter-subject variability of putamen size can be reduced by concentration-preserving stereotactical normalization, that is, stereotactical normalization without modulation to account for the amount of local expansion/contraction that typically is used in MRI-based morphometry to guarantee that regional brain volume is the same in anatomical standard space as in the original image in patient space. Based on the findings of this study, we recommend stereotactical normalization prior to SUSI analysis, although the effects of inter-subject variability of putamen size on diagnostic performance of the SUSI computed in patient space did not reach the level of statistical significance (possibly due to the rather small number of incorrectly classified cases).

Concerning the primary hypothesis put to test in this study (the classification performance of the SUSI relative to the SBR is better in the MULTI setting than in the MONO setting), the putaminal SUSI (computed in MNI space) performed slightly worse than the putaminal SBR in the MONO setting (AUC = 0.969 versus 0.976) and slightly better in the MULTI setting (AUC = 0.993 versus 0.991). This is in line with the primary hypothesis, although neither the difference in the MONO setting nor

the difference in the MULTI setting reached statistical significance ($p = 0.259$ and 0.207, respectively). However, direct statistical comparison of the AUC difference between the SUSI and the SBR between the MULTI setting and the MONO setting showed a trend toward larger AUC difference in the MULTI setting compared to the MONO setting ($p = 0.073$, Fig. 6), supporting the primary hypothesis. Thus, we recommend the use of the SUSI in multi-site settings and in mono-site settings with more than one SPECT camera.

The fact that the SUSI did not outperform the SBR more clearly in the MULTI setting might be explained by two factors. First, very successful harmonization of SPECT image quality (including spatial resolution) in the PPMI by careful adaption of the acquisition protocol for each single camera and central image reconstruction at a core imaging center. Second, the relative IQR of the voxel intensity in the reference region was significantly larger in cases that were incorrectly classified by the putaminal SUSI compared to those that were correctly classified. The same was observed for the putaminal SBR. This demonstrates that the diagnostic performance of both, SUSI and SBR, is affected by uncertainty of the estimate of non-displaceable striatal FP-CIT count density by the count density in the reference region. The difference of the relative IQR between cases that were incorrectly classified by the putaminal SUSI and those that were correctly classified by the putaminal SUSI was larger in cases correctly classified by the putamen SBR compared to those incorrectly classified by the putamen SBR (Fig. 5). This is in line with the hypothesis that the impact of uncertainty in the estimate of non-displaceable count density is larger for the SUSI than for the SBR. However, the difference did not reach statistical significance. The small number of incorrectly classified cases might have contributed to the lack of significance.

Goethals and co-workers compared the SUSI computed in patient space and SBR computed in template space for detection of nigrostriatal degeneration in a mono-camera setting very similar to the mono-camera setting in the present study [16]. The AUC under the ROC curve for identification of neurodegenerative PS was highest for the SUSI of the whole striatum (minimum over left and right hemisphere, AUC = 0.859, 95% CI 0.766–0.952). The highest AUC achieved among several variants of the SBR was for the minimum over bilateral caudate and bilateral putamen SBR (AUC = 0.830, 95% CI 0.727–0.932). The minimum of putaminal SBR over both hemispheres was not considered in this study. The different ranking of SUSI and SBR in the study by Goethals and co-workers (striatal SUSI better than subregional SBR) compared to the present study (putaminal SBR better than striatal SUSI) most likely is due to methodological differences in the computation of the SBR.

The following limitations of the present study should be noted. First, the classification performance of SUSI and SBR in FP-CIT SPECT not only depends on the setting (multi-site/multi-camera versus mono-site/mono-camera). Classification performance of both semi-quantitative measures also depends on the subjects referred to FP-CIT SPECT.

The PPMI PD sample differs from the group of patients with neurodegenerative PS in the clinical mono-site/mono-camera sample in several respects, particularly by inclusion of patients with atypical neurodegenerative PS (MSA, PSP, CBD) in the clinical mono-site/mono-camera sample and the exclusion of subjects without evidence of dopaminergic deficit (SWEDD) from the PPMI PD sample [25]. There is also a relevant difference between the PPMI group of healthy control subjects and the non-neurodegenerative subgroup of the clinical mono-site/mono-camera sample: the latter included etiologies (e.g., vascular parkinsonism) that are associated with variable reduction of striatal DAT availability in a considerable fraction of patients. The differences between the PPMI multi-site/multi-camera research sample and the clinical mono-site/mono-camera sample most likely explain the fact that all tested semi-quantitative measures performed better in the PPMI sample than in the clinical sample despite the additional variability due to camera-specific effects in the PPMI sample.

Second, the excellent performance of both SUSI and SBR in the PPMI sample limits the power to detect performance differences (ceiling effect). Good diagnostic performance of FP-CIT SPECT independent of the analysis method in general makes it difficult to demonstrate differences in the diagnostic performance between methods and to reliably identify factors that might affect performance [2].

Third, classification performance of semi-quantitative measures also depends on the SPECT cameras, the acquisition protocol (including radius of rotation and delay of acquisition after tracer administration), the reconstruction algorithm, and, in the multi-site/multi-camera setting, the extent of harmonization of acquisition protocol and reconstruction algorithm. These factors not only affect the absolute classification performance of both SUSI and SBR, they also might affect the performance difference between SUSI and SBR. This may affect the generalizability of the results of the present study. In particular, it is to be expected that the SUSI more clearly outperforms the SBR in multi-site/multi-camera settings with lower degree of harmonization than in the PPMI.

Conclusion

The specific uptake size index (SUSI) of striatal FP-CIT uptake is particularly appropriate for semi-quantitative analysis in multi-site/multi-camera settings in which

camera-specific effects increase inter-subject variability of spatial resolution. SPECT images should be stereotactically normalized prior to SUSI analysis in order to reduce the impact of inter-subject variability of striatum size. The SUSI of the putamen provides better diagnostic performance than the SUSI of the whole striatum. In mono-camera settings without camera-specific inter-subject variability of spatial resolution, the specific binding ratio (SBR) provides similar performance as the SUSI. Errors of the estimate of non-displaceable count density can cause misclassification by both, SUSI and SBR, particularly in borderline cases. We recommend to check for high uncertainty associated with high variability of voxel intensity in the reference ROI in addition to verification of proper placement of the ROI.

Abbreviations

AAL: Automatic anatomic labeling; AD: Alzheimer's disease; APS: Atypical parkinsonian syndromes; AUC: Area under the ROC curve; BP: Binding potential; CBD: Corticobasal degeneration; CI: Confidence interval; DAT: Dopamine transporter; DLB: Dementia with Lewy bodies; FP-CIT: [I-123] N-ω-fluoropropyl-2β-carbomethoxy-3β-(4-iodophenyl)nortropane; FWHM: Full-width-at-half-maximum; HC: Healthy control; IQR: Interquartile range; MNI: Montreal Neurological Institute; MONO: Mono-site/mono-camera; MSA: Multiple systems atrophy; MULTI: Multi-site/multi-camera; NPH: Normal pressure hydrocephalus; OSEM: Ordered subset expectation maximization; PD: Parkinson's disease; PDD: Parkinson's disease dementia; PPMI: Parkinson's Progression Marker Initiative; PS: Parkinsonian syndrome; PSP: Progressive supranuclear palsy; ROC: Receiver operating characteristic; ROI: Region of interest; SBR: Specific binding ratio; SPECT: Single-photon emission computed tomography; SPM: Statistical Parametric Mapping; SUSI: Specific uptake size index; VaP: Vascular parkinsonism

Acknowledgements

PPMI—a public-private partnership—is funded by the Michael J. Fox Foundation for Parkinson's Research and funding partners including Abbvie, Avid Radiopharmaceuticals, Biogen, BioLegend, Bristol-Myers Squibb, GE Healthcare, Genentech, GlaxoSmithKline, Lilly, Lundbeck, Merck, Meso Scale Discovery, Pfizer, Piramal, Roche, Sanofi Genzyme, Servier, Takeda, Teva, UCB. For up-to-date information about all of the PPMI funding partners, visit www.ppmi-info.org/fundingpartners.

The authors acknowledge support from the Open Access Publication Fund of Charité – Universitätsmedizin Berlin and German Research Foundation (DFG).

Funding

None.

Availability of data and materials

The datasets supporting the conclusions of this article can be made available on request.

Authors' contributions

RB: study concept and design, data analysis, interpretation of study results, and manuscript drafting. CL: data analysis, interpretation of study results, and manuscript drafting. TSS: data acquisition and substantial revision of manuscript. IA: interpretation of study results and substantial revision of manuscript. LF: data acquisition and substantial revision of manuscript. CJ: interpretation of study results and substantial revision of manuscript. PTM: study concept and design, data acquisition, interpretation of study results, and substantial revision of manuscript. SH: study concept and design, data acquisition, interpretation of study results, and substantial revision of manuscript. All authors read and approved the final manuscript.

Ethics approval and consent to participate

Waiver of ethics approval for this retrospective analysis was obtained from the ethics committee of the University Medical Center Freiburg. All patients had given written informed consent for scientific analysis of their data.

Consent for publication

Not applicable.

Competing interests

The authors declare that they have no competing interests.

Publisher's Note

Author details

[1]Department for Diagnostic and Interventional Radiology and Nuclear Medicine, University Hospital Hamburg-Eppendorf, Martinistr. 52, 20246 Hamburg, Germany. [2]Department of Nuclear Medicine, Charité - Universitätsmedizin Berlin, corporate member of Freie Universität Berlin, Humboldt-Universität zu Berlin, and Berlin Institute of Health, Augustenburger Platz 1, 13353 Berlin, Germany. [3]Department of Nuclear Medicine, Medical Center - University of Freiburg, Faculty of Medicine, University of Freiburg, Freiburg, Germany. [4]Medical Radiation Physics and Nuclear Medicine, Imaging and Physiology, Karolinska University Hospital, Stockholm, Sweden. [5]Department of Psychiatry and Psychotherapy, Medical Center - University of Freiburg, Faculty of Medicine, University of Freiburg, Freiburg, Germany.

Received: 25 January 2019 Accepted: 15 April 2019
Published online: 07 May 2019

References

1. Tatsch K, Poepperl G. Nigrostriatal dopamine terminal imaging with dopamine transporter SPECT: an update. J Nucl Med. 2013;54:1331–8. https://doi.org/10.2967/jnumed.112.105379.
2. Booij J, Dubroff J, Pryma D, Yu JQ, Agarwal R, Lakhani P, et al. Diagnostic performance of the visual reading of 123I-ioflupane SPECT images when assessed with or without quantification in patients with movement disorders or dementia. J Nucl Med. 2017;58:1821–6. https://doi.org/10.2967/jnumed.116.189266.
3. Soderlund TA, Dickson JC, Prvulovich E, Ben-Haim S, Kemp P, Booij J, et al. Value of semiquantitative analysis for clinical reporting of 123I-2-beta-carbomethoxy-3beta-(4-iodophenyl)-N-(3-fluoropropyl)nortropane SPECT studies. J Nucl Med, Society of Nuclear Medicine. 2013;54:714–22. https://doi.org/10.2967/jnumed.112.110106.
4. Mintun MA, Raichle ME, Kilbourn MR, Wooten GF, Welch MJ. A quantitative model for the in vivo assessment of drug binding sites with positron emission tomography. Ann Neurol. 1984;15:217–27. https://doi.org/10.1002/ana.410150302.
5. Innis RB, Cunningham VJ, Delforge J, Fujita M, Gjedde A, Gunn RN, et al. Consensus nomenclature for in vivo imaging of reversibly binding radioligands. J Cereb Blood Flow Metab. 2007;27:1533–9. https://doi.org/10.1038/sj.jcbfm.9600493.
6. Booij J, Hemelaar TG, Speelman JD, de Bruin K, Janssen AG, van Royen EA. One-day protocol for imaging of the nigrostriatal dopaminergic pathway in Parkinson's disease by [123I]FPCIT SPECT. J Nucl Med, Society of Nuclear Medicine. 1999;40:753–61.
7. Tossici-Bolt L, Hoffmann SM, Kemp PM, Mehta RL, Fleming JS. Quantification of [123I]FP-CIT SPECT brain images: an accurate technique for measurement of the specific binding ratio. Eur J Nucl Med Mol Imaging. 2006;33:1491–9. https://doi.org/10.1007/s00259-006-0155-x.
8. Badiavas K, Molyvda E, Iakovou I, Tsolaki M, Psarrakos K, Karatzas N. SPECT imaging evaluation in movement disorders: far beyond visual assessment. Eur J Nucl Med Mol Imaging. 2011;38:764–73. https://doi.org/10.1007/s00259-010-1664-1.
9. Tatsch K, Poepperl G. Quantitative approaches to dopaminergic brain imaging. Q J Nucl Med Mol Imaging. 2012;56:27–38.
10. Lange C, Seese A, Schwarzenbock S, Steinhoff K, Umland-Seidler B, Krause BJ, et al. CT-based attenuation correction in I-123-ioflupane SPECT. PLoS One. 2014;9:e108328. https://doi.org/10.1371/journal.pone.0108328.

11. Crespo C, Gallego J, Cot A, Falcon C, Bullich S, Pareto D, et al. Quantification of dopaminergic neurotransmission SPECT studies with 123I-labelled radioligands. A comparison between different imaging systems and data acquisition protocols using Monte Carlo simulation. Eur J Nucl Med Mol Imaging. 2008;35:1334–42. https://doi.org/10.1007/s00259-007-0711-z.
12. Meyer PT, Sattler B, Lincke T, Seese A, Sabri O. Investigating dopaminergic neurotransmission with 123I-FP-CIT SPECT: comparability of modern SPECT systems. J Nucl Med, Society of Nuclear Medicine. 2003;44:839–45.
13. Tossici-Bolt L, Dickson JC, Sera T, Booij J, Asenbaun-Nan S, Bagnara MC, et al. [123I]FP-CIT ENC-DAT normal database: the impact of the reconstruction and quantification methods. EJNMMI Phys. 2017;4:8. https://doi.org/10.1186/s40658-017-0175-6.
14. Dickson JC, Tossici-Bolt L, Sera T, Booij J, Ziebell M, Morbelli S, et al. The impact of reconstruction and scanner characterisation on the diagnostic capability of a normal database for [123I]FP-CIT SPECT imaging. EJNMMI Res. 2017;7:10. https://doi.org/10.1186/s13550-016-0253-0.
15. Fleming JS, Bolt L, Stratford JS, Kemp PM. The specific uptake size index for quantifying radiopharmaceutical uptake. Phys Med Biol. 2004;49:N227–34.
16. Goethals I, Dobbeleir A, Ham H, Santens P, D'Asseler Y. Validation of a resolution-independent method for the quantification of 123I-FP-CIT SPECT scans. Nucl Med Commun. 2007;28:771–4. https://doi.org/10.1097/MNM.0b013e32829152c9.
17. Tossici-Bolt L, Dickson JC, Sera T, de Nijs R, Bagnara MC, Jonsson C, et al. Calibration of gamma camera systems for a multicentre European (1)(2)(3)I-FP-CIT SPECT normal database. Eur J Nucl Med Mol Imaging. 2011;38:1529–40. https://doi.org/10.1007/s00259-011-1801-5.
18. Varrone A, Dickson JC, Tossici-Bolt L, Sera T, Asenbaum S, Booij J, et al. European multicentre database of healthy controls for [123I]FP-CIT SPECT (ENC-DAT): age-related effects, gender differences and evaluation of different methods of analysis. Eur J Nucl Med Mol Imaging. 2013;40:213–27. https://doi.org/10.1007/s00259-012-2276-8.
19. Buchert R, Kluge A, Tossici-Bolt L, Dickson J, Bronzel M, Lange C, et al. Reduction in camera-specific variability in [(123)I]FP-CIT SPECT outcome measures by image reconstruction optimized for multisite settings: impact on age-dependence of the specific binding ratio in the ENC-DAT database of healthy controls. Eur J Nucl Med Mol Imaging. 2016;43:1323–36. https://doi.org/10.1007/s00259-016-3309-5.
20. Koch W, Bartenstein P, la Fougere C. Radius dependence of FP-CIT quantification: a Monte Carlo-based simulation study. Ann Nucl Med. 2014;28:103–11. https://doi.org/10.1007/s12149-013-0789-2.
21. Parkinson Progression Marker I. The Parkinson Progression Marker initiative (PPMI). Prog Neurobiol. 2011;95:629–35. https://doi.org/10.1016/j.pneurobio.2011.09.005.
22. Darcourt J, Booij J, Tatsch K, Varrone A, Vander Borght T, Kapucu OL, et al. EANM procedure guidelines for brain neurotransmission SPECT using (123)I-labelled dopamine transporter ligands, version 2. Eur J Nucl Med Mol Imaging. 2010;37:443–50. https://doi.org/10.1007/s00259-009-1267-x.
23. Djang DS, Janssen MJ, Bohnen N, Booij J, Henderson TA, Herholz K, et al. SNM practice guideline for dopamine transporter imaging with 123I-ioflupane SPECT 1.0. J Nucl Med. 2012;53:154–63. https://doi.org/10.2967/jnumed.111.100784.
24. Winz OH, Hellwig S, Mix M, Weber WA, Mottaghy FM, Schafer WM, et al. Image quality and data quantification in dopamine transporter SPECT: advantage of 3-dimensional OSEM reconstruction? Clin Nucl Med. 2012;37:866–71. https://doi.org/10.1097/RLU.0b013e318251e1b3.
25. Marek K, Chowdhury S, Siderowf A, Lasch S, Coffey CS, Caspell-Garcia C, et al. The Parkinson's progression markers initiative (PPMI)—establishing a PD biomarker cohort. Ann Clin Transl Neurol. 2018;5:1460–77. https://doi.org/10.1002/acn3.644.
26. Tzourio-Mazoyer N, Landeau B, Papathanassiou D, Crivello F, Etard O, Delcroix N, et al. Automated anatomical labeling of activations in SPM using a macroscopic anatomical parcellation of the MNI MRI single-subject brain. Neuroimage. 2002;15:273–89. https://doi.org/10.1006/nimg.2001.0978.
27. Maldjian JA, Laurienti PJ, Kraft RA, Burdette JH. An automated method for neuroanatomic and cytoarchitectonic atlas-based interrogation of fMRI data sets. Neuroimage. 2003;19:1233–9.
28. Kupitz D, Apostolova I, Lange C, Ulrich G, Amthauer H, Brenner W, et al. Global scaling for semi-quantitative analysis in FP-CIT SPECT. Nuklearmedizin. 2014;53:234–41. https://doi.org/10.3413/Nukmed-0659-14-04.
29. Youden WJ. Index for rating diagnostic tests. Cancer. 1950;3:32–5.

Publikation 3

Helen Schmitz-Steinkrüger*, **Catharina Lange***, Ivayla Apostolova, Holger Amthauer, Wencke Lehnert, Susanne Klutmann, Ralph Buchert. 2020. Impact of the size of the normal database on the performance of the specific binding ratio in dopamine transporter SPECT. *EJNMMI Physics*. 7(1): 34. https://doi.org/10.1186/s40658-020-00304-z.

Auszug aus Journal Summary List 2018

Journal Data Filtered By: **Selected JCR Year: 2018** Selected Editions: SCIE Selected Categories: **"RADIOLOGY, NUCLEAR MEDICINE & MEDICAL IMAGING"** Selected Category Scheme: WoS
Gesamtanzahl: 129 Journale

Rank	Full Journal Title	Total Cites	Journal Impact Factor	Eigenfactor Score
1	JACC-Cardiovascular Imaging	8,801	10.975	0.026170
2	MEDICAL IMAGE ANALYSIS	7,694	8.880	0.013360
3	IEEE TRANSACTIONS ON MEDICAL IMAGING	19,545	7.816	0.024980
4	RADIOLOGY	54,641	7.608	0.061270
5	JOURNAL OF NUCLEAR MEDICINE	27,551	7.308	0.037980
6	EUROPEAN JOURNAL OF NUCLEAR MEDICINE AND MOLECULAR IMAGING	15,406	7.182	0.024740
7	CLINICAL NUCLEAR MEDICINE	4,922	6.703	0.007670
8	INTERNATIONAL JOURNAL OF RADIATION ONCOLOGY BIOLOGY PHYSICS	45,833	6.203	0.046920
9	INVESTIGATIVE RADIOLOGY	6,563	6.091	0.011140
10	Circulation-Cardiovascular Imaging	5,456	5.813	0.018470
11	NEUROIMAGE	99,720	5.812	0.132680
12	ULTRASOUND IN OBSTETRICS & GYNECOLOGY	12,336	5.595	0.020120
13	European Heart Journal-Cardiovascular Imaging	5,498	5.260	0.021640
14	RADIOTHERAPY AND ONCOLOGY	17,873	5.252	0.027480
15	Photoacoustics	512	5.250	0.001330
16	JOURNAL OF CARDIOVASCULAR MAGNETIC RESONANCE	5,113	5.070	0.014000
17	ULTRASCHALL IN DER MEDIZIN	2,238	4.613	0.003700
18	HUMAN BRAIN MAPPING	22,040	4.554	0.043220
19	JOURNAL OF NUCLEAR CARDIOLOGY	3,711	4.112	0.004480
20	EUROPEAN RADIOLOGY	19,597	3.962	0.033840
21	RADIOGRAPHICS	11,768	3.923	0.009160
22	Biomedical Optics Express	9,547	3.910	0.021740
23	MAGNETIC RESONANCE IN MEDICINE	32,648	3.858	0.034970
24	SEMINARS IN NUCLEAR MEDICINE	2,245	3.798	0.002710
25	Journal of the American College of Radiology	4,191	3.785	0.009760
26	JOURNAL OF MAGNETIC RESONANCE IMAGING	17,147	3.732	0.027780
27	KOREAN JOURNAL OF RADIOLOGY	2,687	3.730	0.004800
28	INTERNATIONAL JOURNAL OF HYPERTHERMIA	3,552	3.589	0.004020

29	**EJNMMI Physics**	**394**	**3.475**	**0.001350**
30	NMR IN BIOMEDICINE	7,511	3.414	0.014790
31	MOLECULAR IMAGING AND BIOLOGY	2,543	3.341	0.005360
32	Journal of Cardiovascular Computed Tomography	1,711	3.316	0.004430
33	COMPUTERIZED MEDICAL IMAGING AND GRAPHICS	2,464	3.298	0.002990
34	AMERICAN JOURNAL OF NEURORADIOLOGY	23,231	3.256	0.028000
35	MEDICAL PHYSICS	26,715	3.177	0.030860
36	AMERICAN JOURNAL OF ROENTGENOLOGY	33,633	3.161	0.028520
37	CANCER IMAGING	1,406	3.153	0.002220
38	Quantitative Imaging in Medicine and Surgery	1,072	3.074	0.002420
39	PHYSICS IN MEDICINE AND BIOLOGY	27,458	3.030	0.031950
40	EJNMMI Research	1,408	3.000	0.004320
41	EUROPEAN JOURNAL OF RADIOLOGY	12,871	2.948	0.019470
42	Radiation Oncology	5,669	2.895	0.012980
43	MAGNETIC RESONANCE MATERIALS IN PHYSICS BIOLOGY AND MEDICINE	1,600	2.836	0.003630
44	JOURNAL OF VASCULAR AND INTERVENTIONAL RADIOLOGY	8,813	2.828	0.011270
45	Clinical Neuroradiology	798	2.800	0.002250
46	Practical Radiation Oncology	1,563	2.794	0.005060
47	RADIATION RESEARCH	8,561	2.779	0.006480
48	SEMINARS IN RADIATION ONCOLOGY	2,395	2.741	0.003600
49	STRAHLENTHERAPIE UND ONKOLOGIE	2,949	2.717	0.004490
50	ULTRASONICS	7,026	2.598	0.009090
51	JOURNAL OF DIGITAL IMAGING	2,191	2.572	0.003680
52	JOURNAL OF BIOMEDICAL OPTICS	13,787	2.555	0.016930
53	Physica Medica-European Journal of Medical Physics	2,641	2.532	0.006260
54	NEURORADIOLOGY	5,656	2.504	0.007010
55	NUCLEAR MEDICINE AND BIOLOGY	3,858	2.492	0.004230
56	ULTRASONIC IMAGING	1,117	2.490	0.000860
57	Diagnostic and Interventional Imaging	1,359	2.486	0.003400
58	JOURNAL OF NEURORADIOLOGY	985	2.467	0.001440
59	Dose-Response	997	2.451	0.001460
60	Zeitschrift fur Medizinische Physik	558	2.322	0.001360
61	ACADEMIC RADIOLOGY	5,625	2.267	0.008230
62	INTERNATIONAL JOURNAL OF RADIATION BIOLOGY	4,537	2.266	0.003740
63	ULTRASOUND IN MEDICINE AND BIOLOGY	10,769	2.205	0.012780
64	International Journal of Computer Assisted Radiology and Surgery	2,416	2.155	0.005160
65	Abdominal Radiology	1,420	2.147	0.003820
66	MAGNETIC RESONANCE IMAGING	7,321	2.112	0.009310
…	…	…	…	…
129	RADIOLOGE	529	0.413	0.000390

EJNMMI Physics

ORIGINAL RESEARCH Open Access

Impact of the size of the normal database on the performance of the specific binding ratio in dopamine transporter SPECT

Helen Schmitz-Steinkrüger[1†], Catharina Lange[2*†], Ivayla Apostolova[1], Holger Amthauer[2], Wencke Lehnert[1], Susanne Klutmann[1] and Ralph Buchert[1*]

* Correspondence: catharina.lange@charite.de; r.buchert@uke.de
†Helen Schmitz-Steinkrüger and Catharina Lange contributed equally to this work.
[2]Department of Nuclear Medicine, Charité - Universitätsmedizin Berlin, Corporate Member of Freie Universität Berlin, Humboldt-Universität zu Berlin, and Berlin Institute of Health, Berlin, Germany
[1]Department for Diagnostic and Interventional Radiology and Nuclear Medicine, University Hospital Hamburg-Eppendorf, Hamburg, Germany

Abstract

Background: This study investigated the impact of the size of the normal database on the classification performance of the specific binding ratio (SBR) in dopamine transporter (DAT) SPECT with [^{123}I]FP-CIT in different settings.

Methods: The first subject sample comprised 645 subjects from the Parkinson's Progression Marker Initiative (PPMI), 207 healthy controls (HC), and 438 Parkinson's disease (PD) patients. The second sample comprised 372 patients from clinical routine patient care, 186 with non-neurodegenerative parkinsonian syndrome (PS) and 186 with neurodegenerative PS. Single-photon emission computed tomography (SPECT) images of the clinical sample were reconstructed with two different reconstruction algorithms (filtered backprojection, iterative ordered subsets expectation maximization (OSEM) reconstruction with resolution recovery). The putaminal specific binding ratio (SBR) was computed using an anatomical region of interest (ROI) predefined in standard (MNI) space in the Automated Anatomic Labeling (AAL) atlas or using hottest voxels (HV) analysis in large predefined ROIs. SBR values were transformed to z-scores using mean and standard deviation of the SBR in a normal database of varying sizes ($n = 5, 10, 15, \ldots, 50$) randomly selected from the HC subjects (PPMI sample) or the patients with non-neurodegenerative PS (clinical sample). Accuracy, sensitivity, and specificity for identifying patients with PD or neurodegenerative PS were determined as performance measures using a predefined fixed cutoff on the z-score. This was repeated for 10,000 randomly selected normal databases, separately for each size of the normal database. Mean and 5th percentile of the performance measures over the 10,000 realizations were computed. Accuracy, sensitivity, and specificity when using the whole set of HC or non-neurodegenerative PS subjects as normal database were used as benchmark.

(Continued on next page)

(Continued from previous page)

Results: Mean loss of accuracy of the putamen SBR z-score was below 1% when the normal database included at least 15 subjects, independent of subject sample (PPMI or clinical), reconstruction method (filtered backprojection or OSEM), and ROI method (AAL or HV). However, the variability of the accuracy of the putamen SBR z-score decreased monotonically with increasing size of normal database and was still considerable at size 15. In order to achieve less than 5% "maximum" loss of accuracy (defined by the 5th percentile) in all settings required at least 25 to 30 subjects in the normal database. Reduction of mean and "maximum" loss of accuracy of the putamen SBR z-score by further increasing the size of the normal database was very small beyond size 40.

Conclusions: The results of this study suggest that 25 to 30 is the minimum size of the normal database to reliably achieve good performance of semi-quantitative analysis in dopamine transporter (DAT) SPECT, independent of the algorithm used for image reconstruction and the ROI method used to estimate the putaminal SBR.

Keywords: Dopamine transporter, SPECT, FP-CIT, Specific binding ratio, Normal database

Introduction

Single-photon emission computed tomography (SPECT) with N-ω-fluoropropyl-2β-carbomethoxy-3β-(4-I-123-iodophenyl)nortropane (FP-CIT) is widely used for the detection (or exclusion) of nigrostriatal degeneration in clinically uncertain parkinsonian syndromes (PS) [1–4]. Visual reading of the FP-CIT SPECT images can be complemented by semi-quantitative analysis using the specific binding ratio (SBR) to characterize FP-CIT binding to the dopamine transporter (DAT) in the striatum and striatal subregions [5–10].

SBR analysis is sensitive to site- and/or camera-specific variability of SPECT image characteristics caused by differences in acquisition and reconstruction protocols, which limits sharing of normal databases and SBR cutoff values between sites and/or cameras [5, 11–18]. In prospective studies, this problem can be addressed by harmonization of acquisition protocols and centralized image reconstruction in an imaging core lab [15–17, 19]. This is difficult to realize in everyday clinical patient care so that the use of a camera-specific normal database often is the most straightforward solution in clinical routine. This is facilitated by the fact that generation of a camera-specific normal database does not necessarily require prospective scanning of healthy subjects. FP-CIT SPECT images from patients with clinically uncertain PS that have been interpreted normal in clinical routine might be used retrospectively for the normal database.

This raises the question about the impact of the size of the normal database on the performance of semi-quantitative analysis. Of particular interest is the minimum size of the normal database required for good performance of SBR analysis.

More complex methods including convolutional neural networks have been proposed for automatic classification of FP-CIT SPECT [18, 20, 21]. However, conventional SBR analysis is still widely used because it is easy to understand (no black box) and achieves high accuracy provided that an appropriate normal database is used. Furthermore, more complex methods such as convolutional neural networks usually require considerably larger databases for training and validation than univariate SBR analysis. Thus, SBR analysis most likely will continue to play a role in FP-CIT SPECT in the future.

The aim of the present study, therefore, was to analyze the impact of the size of the normal database on the performance of SBR analysis of FP-CIT SPECT in different settings, that is, for two different patient samples, two different reconstruction algorithms, and two different region-of-interest (ROI) methods to estimate the SBR.

Materials and methods

Parkinson's Progression Markers Initiative (PPMI) sample

The first sample of FP-CIT SPECT images used in this study was obtained from the PPMI (http://www.ppmi-info.org/data) [19]. It comprised the baseline FP-CIT scans of 645 FP-subjects, 207 healthy control (HC) subjects and 438 Parkinson's disease (PD) patients. Up-to-date information on the PPMI is given at http://www.ppmi-info.org. The PPMI is a longitudinal, multi-center study that aims to assess the progression of clinical features, imaging, and biologic markers in patients with PD and HC subjects. Details of the PPMI eligibility criteria are given at http://www.ppmi-info.org/wp-content/uploads/2014/01/PPMI-AM7-Protocol.pdf. Details of the PPMI FP-CIT SPECT protocol are given at http://www.ppmi-info.org/study-design/research-documents-and-sops/ [19]. Raw projection data had been transferred to the PPMI imaging core lab for central image reconstruction using an iterative ordered subsets expectation maximization (OSEM) algorithm with eight iterations and eight subsets and no filtering on a Hermes workstation [22]. Post-reconstruction attenuation correction according to Chang [23] had been performed using a site-specific attenuation coefficient derived from phantom measurements performed during site initiation for the PPMI [24]. A three-dimensional Gaussian filter with 6-mm full width at half maximum had been applied after attenuation correction [24]. No scatter correction had been performed [22].

Clinical sample

Three-hundred-and-seventy-two patients from routine clinical patient care were recruited retrospectively from the database of the University Medical Center Hamburg-Eppendorf. The patients were categorized into "neurodegenerative PS" and "non-neurodegenerative PS". The neurodegenerative group (n = 186, 45.7% females, 65.9 ± 10.4 years) comprised the Lewy body disease spectrum including PD, PD dementia and dementia with Lewy bodies, and atypical Parkinsonian syndromes including multiple systems atrophy, progressive supranuclear palsy, and corticobasal degeneration. The non-neurodegenerative group (n = 186, 52.2% females, 65.5 ± 12.5 years) comprised essential tremor, drug-induced parkinsonism, several types of dystonia, psychogenic parkinsonism, and various other diagnoses not associated with nigrostriatal degeneration. The clinical diagnoses as standard of truth were taken from the written report of a movement disorder specialist in the patient's file at least 12 months after FP-CIT SPECT in all 186 patients with neurodegenerative PS (mean follow-up 41 ± 22 months, range 12–95 months) and in 44 of the patients with non-neurodegenerative PS (mean follow-up 38 ± 22 months, 13–97 months). The remaining patients with non-neurodegenerative PS had less than 12 months follow-up and were included to increase sample size and to avoid imbalance with respect to group size (neurodegenerative versus non-neurodegenerative).

FP-CIT SPECT had been performed according to common guidelines [25] with a double-head SPECT system (Siemens Symbia T2 or Siemens E.CAM). In order to

ensure consistent image reconstruction in all patients, projection data were retrieved from the archive and reconstructed retrospectively. Two different reconstruction algorithms were used in all patients. First, SPECT images were reconstructed using filtered backprojection implemented in the SPECT system software (Butterworth filter of the 5th order with cutoff 0.6 cycles/pixel). Uniform post reconstruction attenuation correction was performed according to Chang's method ($\mu = 0.12$/cm) [23]; scatter correction was not performed. Second, SPECT images were reconstructed using the OSEM algorithm with resolution recovery implemented in the HybridRecon-Neurology tool of the Hermes SMART workstation v1.6 with parameter settings recommended for FP-CIT SPECT by Hermes (effective number of iterations 80, postfiltering with three-dimensional Gaussian kernel of 7-mm full width at half maximum, uniform attenuation correction with narrow-beam attenuation coefficient 0.146/cm, simulation-based scatter correction, resolution recovery with a Gaussian model).

Representative FP-CIT SPECT images from the different settings are shown in Fig. 1.

Semi-quantitative SBR analysis

Individual SPECT images were normalized (affine) to a custom-made FP-CIT template in the anatomical space of the Montreal Neurological Institute (MNI) using the Statistical Parametric Mapping software package (version SPM12) [26]. Voxel intensities were scaled voxel-wise to the 75th percentile of the voxel intensity in a reference region

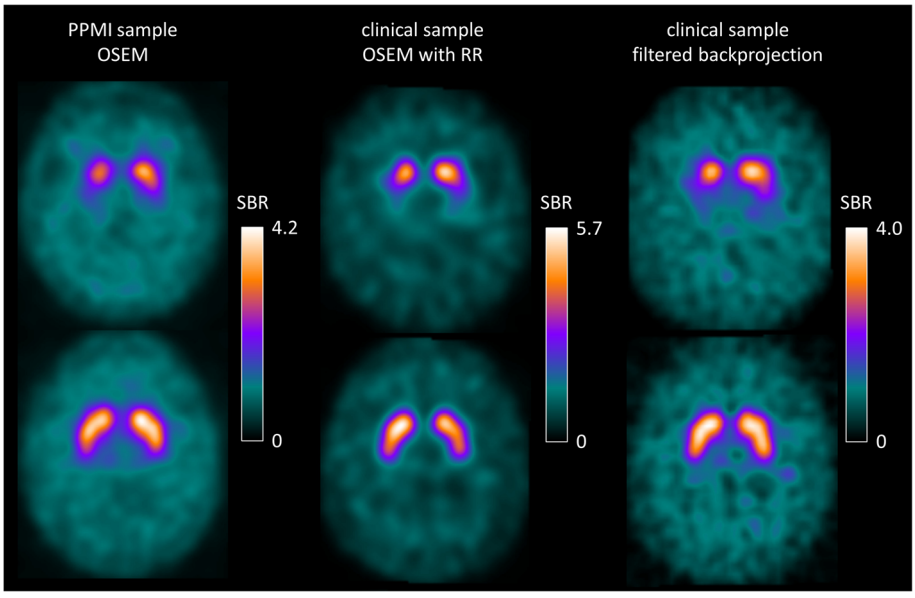

Fig. 1 Representative FP-CIT SPECT images. The left column shows a patient with Parkinson's disease (top) and a healthy control subject (bottom) from the PPMI sample. The middle and right columns show the same patient with neurodegenerative PS (top) and the same patient with non-neurodegenerative PS (bottom) from the clinical sample reconstructed with iterative reconstruction (ordered subsets expectation maximization, OSEM) with resolution recovery (RR; middle column) or with filtered backprojection (right column). Shown are 4-mm-thick transaxial slices in MNI space with voxel intensities scaled to the individual 75th percentile of the voxel intensity in the reference region. The upper threshold of the colour table was adjusted separately for each of the three settings

comprising the whole brain except the striata, thalamus, brain stem, and ventricles [27, 28].

The conventional unilateral putamen SBR was computed by applying anatomical ROIs predefined in MNI space by the Automatic Anatomical Labeling atlas (AAL) [29]. The mean value of the scaled voxel intensity in the AAL ROI was used to calculate the conventional SBR (= mean scaled voxel intensity in the ROI – 1).

In addition, hottest voxels (HV) analysis was performed using large unilateral ROIs predefined in MNI space [30]. The ROIs for HV analysis were much bigger than the actual putamen volume in order to guarantee that all counts originating from the putamen were included. The number of hottest voxels to be averaged for the unilateral putamen was fixed to a volume of 10 ml. The hottest voxel SBR (HV-SBR) was calculated as mean scaled voxel intensity in the 10-ml hottest ROI voxels – 1.

SBR analysis was restricted to the putamen, and the minimum of the unilateral putamen SBR of left and right hemispheres was used in all further analyses. The rationale for this was that the effect size of the reduction in PD in general is larger in the bilateral putamen compared to the bilateral caudate, and larger in the contralateral putamen compared to the ipsilateral putamen [31]. Other conventional semi-quantitative parameters such as putamen-to-caudate ratio and left-right asymmetry were not considered because they did not provide additional information beyond the putamen SBR (Appendix).

Statistical analysis

Normal databases of sizes $n = 5, 10, 15,\ldots, 50$ were obtained by randomly selecting the appropriate number of HC subjects (in case of the PPMI sample) or patients with non-neurodegenerative PS (in case of the clinical sample). Mean and standard deviation of the SBR in the resulting normal database was used to transform individual SBR values to z-scores using the following formula: z-score = (individual SBR – mean SBR in normal database) / standard deviation of SBR in normal database. Overall accuracy, sensitivity, and specificity of the z-score to identify patients with PD (PPMI sample) or neurodegenerative PS (clinical sample) were computed using a z-score of –2.5 as cutoff. The whole sample was used as test set in all cases, that is, the test set comprised all 645 PPMI subjects or all 372 clinical patients, independent of the (size of) the normal database. This was repeated for 10,000 randomly selected normal databases for each size of the normal database. The mean and the 5th percentile of overall accuracy, specificity, and sensitivity were computed over the 10,000 repeats. The performance of the z-score obtained with all HC subjects or all patients with non-neurodegenerative PS as normal database was used as benchmark.

Results

Box plots of the putamen SBR for the different settings are shown in Fig. 2. The absolute value of the SBR strongly depended on the reconstruction algorithm and on the method used to estimate the SBR.

Histograms of putamen SBR in HC subjects or patients with non-neurodegenerative PS showed slightly skewed distributions, mainly due to extended tails towards high SBR values (Fig. 3). The skewness of the SBR distribution was significantly different from zero in all settings. The skewness was largest in the patients with non-neurodegenerative PS of

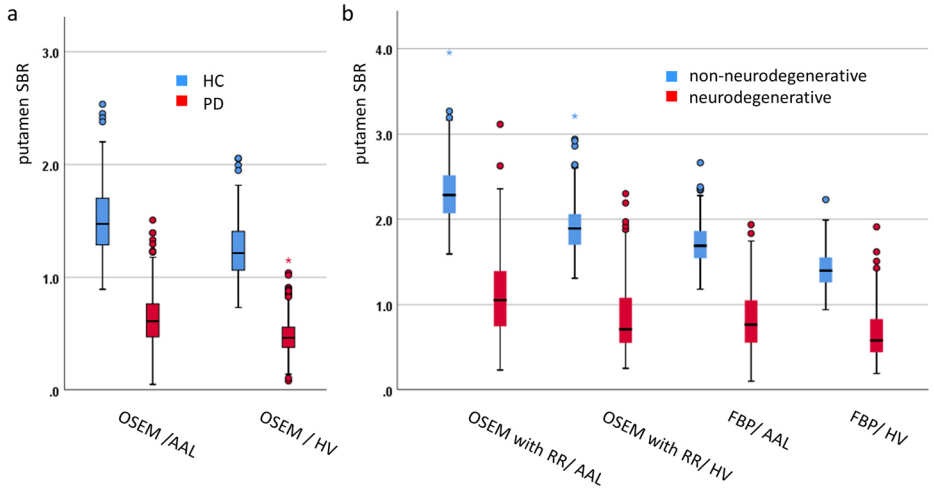

Fig. 2 Box-and-whisker-plot of putamen SBR in healthy control (HC) subjects versus patients with Parkinson's disease (PD) of the PPMI (**a**) and patients with non-neurodegenerative PS versus patients with neurodegenerative PS of the clinical sample (**b**) for different ROI methods to estimate the putamen SBR (conventional analysis with AAL ROI versus hottest voxels (HV) analysis). Different algorithms to reconstruct the SPECT images (iterative ordered subsets expectation maximization (OSEM) reconstruction with resolution recovery (RR) versus filtered backprojection (FBP)) were tested in the clinical sample only

the clinical sample with OSEM reconstruction with resolution recovery (skewness = 0.877 and 0.908 for AAL-SBR and HV-SBR, respectively). The skewness was smallest in the patients with non-neurodegenerative PS of the clinical sample with filtered backprojection (skewness = 0.560 and 0.455 for AAL-SBR and HV-SBR, respectively). In order to account for the skewness of the SBR distributions, SBR values were Ln-transformed prior to transforming them to z-scores (Fig. 3). This was done in all settings.

Figure 4 shows the impact of the size of the normal database on overall accuracy, sensitivity, and specificity of the putamen SBR z-score to identify patients with PD in the PPMI sample or patients with neurodegenerative PS in the clinical sample.

Mean relative loss of accuracy and "maximum" relative loss of accuracy of the putamen SBR z-score for differentiation between PD patients and HC subjects of the PPMI or between patients with neurodegenerative PS and patients with non-neurodegenerative PS of the clinical sample as a function of size of the normal database are given in Fig. 5.

Discussion

Mean loss of overall accuracy of the z-score of the (Ln-transformed) putamen SBR was below 1% when the normal database included at least 15 subjects, independent of the subject sample, the reconstruction method, and the ROI method (Fig. 5a). However, the variability of accuracy, sensitivity, and specificity of the putamen SBR z-score decreased monotonically with increasing size of the normal database and was still considerable at size 15 (Fig. 4). The "maximum" loss of accuracy of the putamen SBR z-score was less than 5% when the normal database included at least 25 to 30 subjects (Fig. 5b). This suggests that a normal database for SBR analysis in DAT SPECT in clinical routine should include at least 25 to 30 subjects.

Reduction of mean and "maximum" loss of accuracy of the putamen SBR z-score by further increasing the size of the normal database was very small beyond size 40 (Fig.

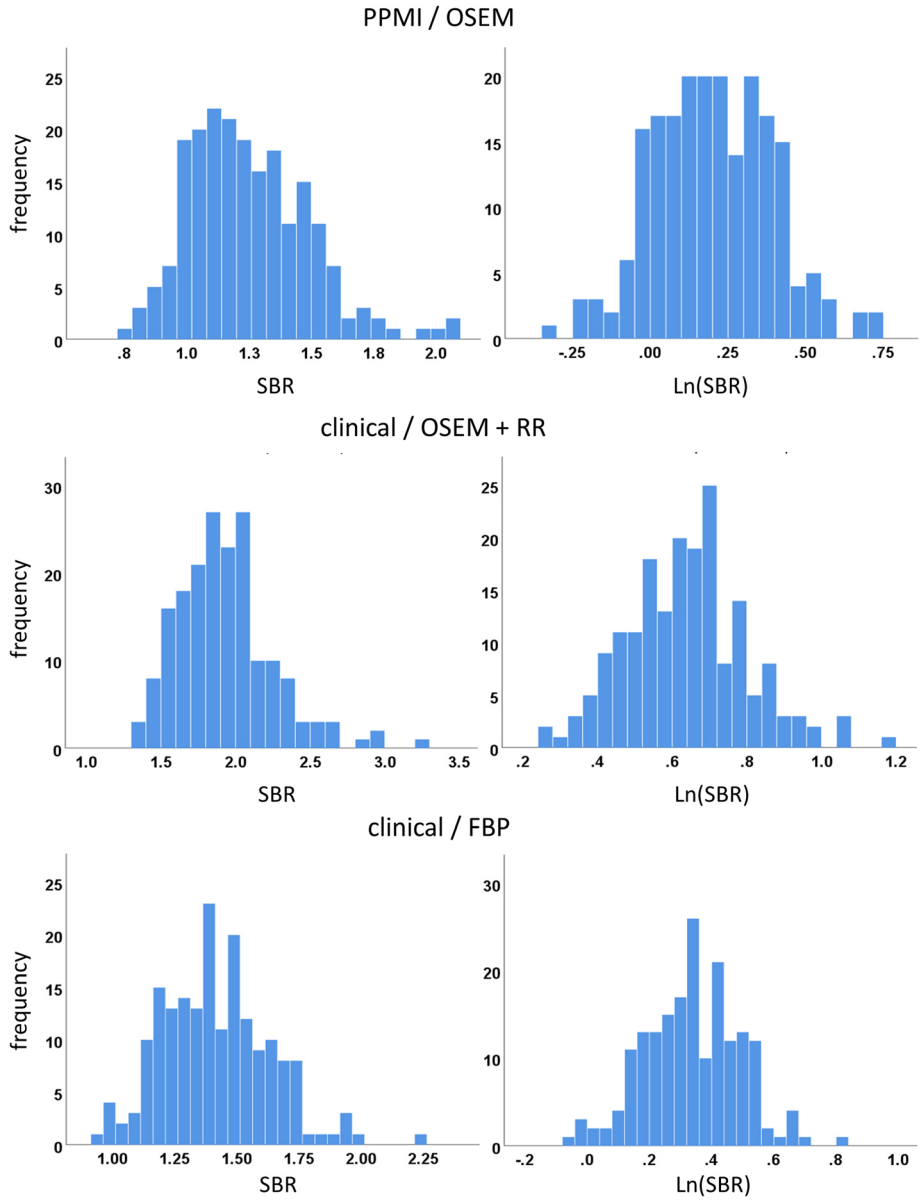

Fig. 3 Histogram of the putamen hottest voxels SBR before (left column) and after (right column) Ln-transformation in the healthy controls of the PPMI sample with ordered subsets expectation maximization (OSEM) reconstruction (top row) and in the patients with non-neurodegenerative PS of the clinical sample with OSEM reconstruction and resolution recovery (RR, middle row) or with filtered backprojection (bottom row)

5). This suggests that a normal database including 40 subjects provides close-to-optimal performance of putaminal SBR in DAT SPECT.

Sensitivity was lower than specificity in all settings (Fig. 4). This was due to the rather conservative cutoff of −2.5 on the z-score for classification of FP-CIT SPECT images. Sensitivity can be increased by using a less conservative cutoff which, however, will result in the reduction of specificity. In the absence of disease-modifying treatment for neurodegenerative PS, the trade-off between sensitivity and specificity is usually balanced in favor of high specificity in clinical routine. The use of a rather conservative cutoff in this study is in line with this.

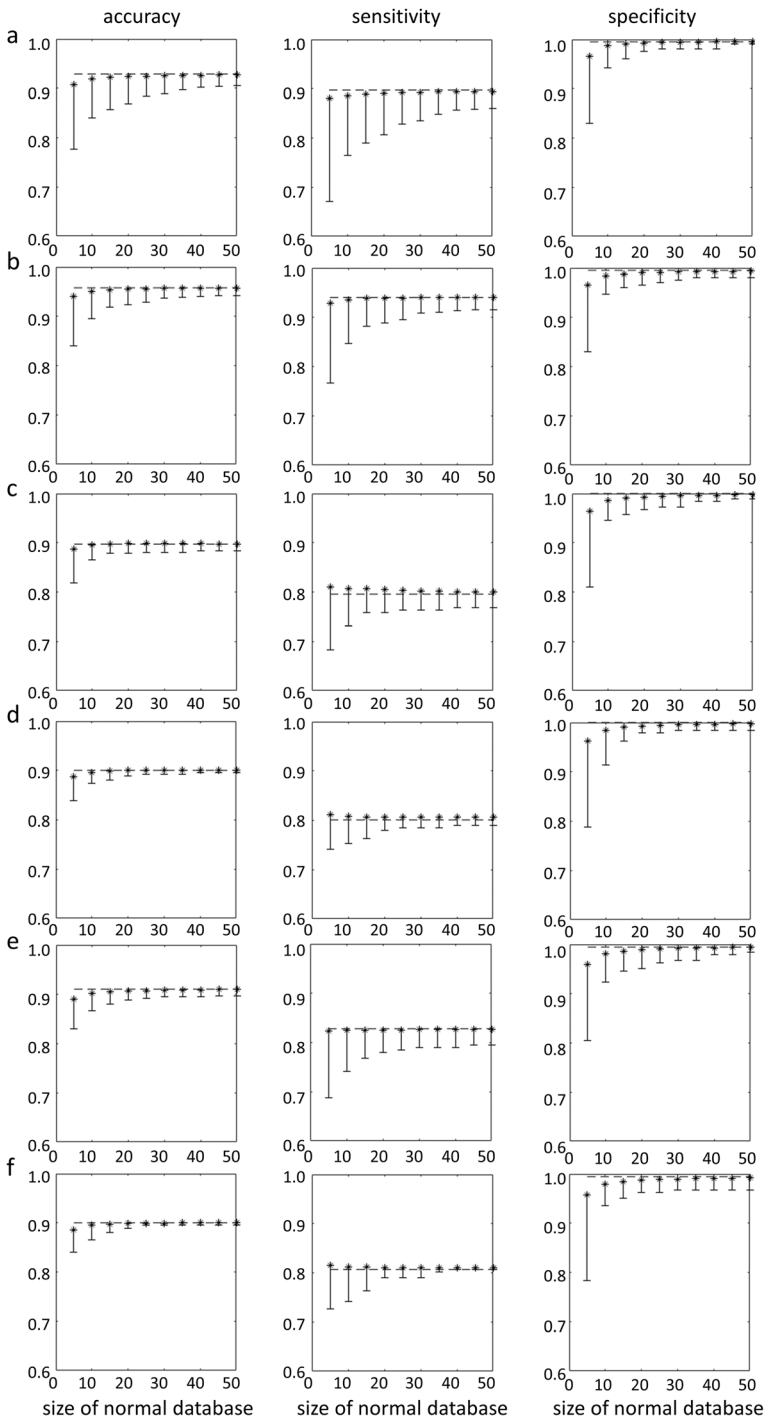

Fig. 4 (See legend on next page.)

(See figure on previous page.)
Fig. 4 Mean accuracy (left column), sensitivity (middle column), and specificity (right column) of the putamen SBR z-score for identification of PD patients or patients with neurodegenerative PS as a function of the size of the normal database used to estimate mean and standard deviation of normal putamen SBR for transforming SBR values into z-scores (**a** PPMI sample, OSEM, AAL-SBR; **b** PPMI sample, OSEM, HV-SBR; **c** clinical sample, OSEM with resolution recovery, AAL-SBR; **d** clinical sample, OSEM with resolution recovery, HV-SBR; **e** clinical sample, filtered backprojection, AAL-SBR; **f** clinical sample, filtered backprojection, HV-SBR). SBR values were Ln-transformed prior to transforming them into z-scores in all settings. The error bars indicate the difference between mean accuracy, sensitivity, or specificity and the 5th percentile over the 10,000 randomly sampled normal databases. The dashed line represents the performance of the z-score of the putamen SBR when all HC subjects ($n = 207$) or all patients with non-neurodegenerative PS ($n = 186$) were used to estimate mean and standard deviation of normal putamen SBR for transforming SBR values into z-scores as benchmark

Lower overall accuracy of the putamen SBR in the clinical sample relative to the PPMI sample was mainly driven by reduced sensitivity in the clinical sample (Fig. 4). Visual inspection of the false-negative clinical SPECT images confirmed the SBR-based classification in most cases. Thus, most of the false-negative cases in the clinical sample were subjects without evidence of dopaminergic deficit (SWEDD). Several studies suggest that the majority of SWEDD patients do not have a neurodegenerative PS [32, 33]. Reduced sensitivity of the putamen SBR in the clinical sample therefore most likely was due to clinical overdiagnosis of neurodegenerative PS at clinical follow-up used as standard of truth in this study [34]. The PPMI sample did not include SWEDD subjects, as the PPMI handles SWEDD as a separate category, different from healthy controls and PD patients (s. PPMI study protocol at http://www.ppmi-info.org/wp-content/uploads/2018/02/PPMI-AM-13-Protocol.pdf). The lack of SWEDD patients in the PPMI sample explains the lower sensitivity of the putamen SBR z-score in the clinical sample at least to some extent. Thus, the findings in the

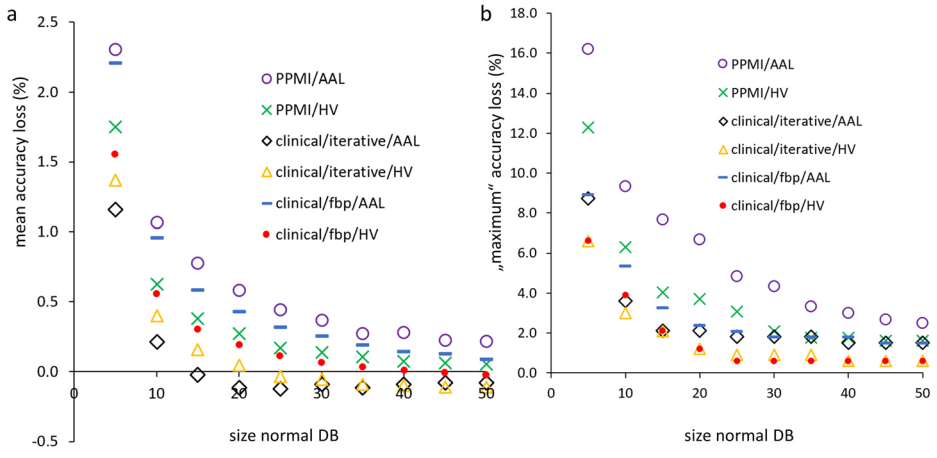

Fig. 5 Mean relative loss of accuracy (**a**) and "maximum" relative loss of accuracy (**b**) of the putamen SBR z-score for differentiation between PD patients and HC subjects of the PPMI or between patients with neurodegenerative PS and patients with non-neurodegenerative PS of the clinical sample as a function of size of the normal database (DB) used to estimate mean and standard deviation of normal putamen SBR for transforming SBR values into z-scores. SBR values were Ln-transformed prior to transforming them into z-scores in all settings. The relative loss of accuracy was computed with respect to the benchmark accuracy (normal database comprising all HC subjects or all patients with non-neurodegenerative PS), that is, relative accuracy loss (%) = 100 * (benchmark accuracy – accuracy) / benchmark accuracy. The maximum accuracy loss corresponds to the 5th percentile of the accuracy estimates over the 10,000 random samples to generate the normal database.

clinical sample support the use of a normal database comprised of patients with a non-neurodegenerative parkinsonian syndrome. This is practically relevant because prospective scanning of healthy subjects constitutes a major obstacle at many sites, particularly in smaller hospitals and private practices.

The findings with respect to the impact of the size of the normal database on classification performance were rather independent of the setting, that is, the findings were very similar for both subject samples (PPMI, clinical), all reconstruction algorithms (OSEM with and without resolution recovery, filtered backprojection), and both ROI methods to estimate the SBR (conventional ROI analysis, hottest voxels analysis). Given that the settings considered here are quite different (Figs. 1, 2, 3), the robustness of the results with respect to the setting suggests that these findings hold more generally in the spectrum of settings encountered in clinical routine.

A secondary finding of this study was the skewness of the distribution of the putaminal SBR in normal DAT SPECT scans that could be reduced by Ln-transformation of the SBR values (Fig. 3). Ln-transformation prior to transformation to z-scores improved the classification performance of the putamen SBR (Fig. 6). The improvement of overall accuracy was mainly driven by improved sensitivity (Fig. 6), most likely due to avoiding overestimation of the standard deviation of normal SBR from skewed distributions. The effect of the Ln-transformation was larger for the 5th percentile than for the average performance over the 10,000 random realizations of the normal database, suggesting that the main benefit from Ln-transformation was stabilization of classification performance by reducing the impact of potential outliers in the normal database. In line with this, the decline of the "maximum" performance loss with increasing size of the normal database was faster with Ln-transformation than without. As a consequence, without Ln-transformation, a larger normal database might be required to reliably achieve the same level of performance of the putamen SBR z-score than with Ln-transformation. In general, estimates of mean and standard deviation of normal putamen SBR derived from the normal database are the more sensitive to outliers the smaller the database. Thus, careful control of the DAT SPECT images to be included in the normal database is particularly important in case of a small database.

This study focused on DAT SPECT with FP-CIT. In order to discuss potential generalizability of the findings, one might hypothesize that univariable binary classification of FP-CIT SPECT, that is, differentiation between neurodegenerative and non-neurodegenerative PS using the putaminal SBR, can be considered a two-sample t-test with the single subject to be classified comprising one group and the normal database comprising the other group. Furthermore, the statistical power of testing a given feature for a mean difference between two groups of different size (n_1, n_2) is approximately equal to the power of comparing it between two groups of equal size n_{eff} with $n_{\mathrm{eff}} = 2 * n_1 * n_2 / (n_1 + n_2)$ [35]. Assuming this equation to be approximately valid also for the extreme case of single subject comparison against a normal database [36], that is, $n_1 = 1$ and $n_2 = n$ = size of the normal database, it is $n_{\mathrm{eff}} = 2 * n / (n + 1)$. The plot of this relation (Fig. 7) shows that n_{eff} effectively starts to reach its plateau at about $n = 10$ to $n = 15$. We hypothesize, therefore, that adequate mean accuracy of univariable binary classification in general requires a normal database of at least 10 to 15 subjects. The present finding of less than 1% mean loss of accuracy of the putamen SBR z-score when the normal database included at least 15 subjects is in line with this. Yet, the

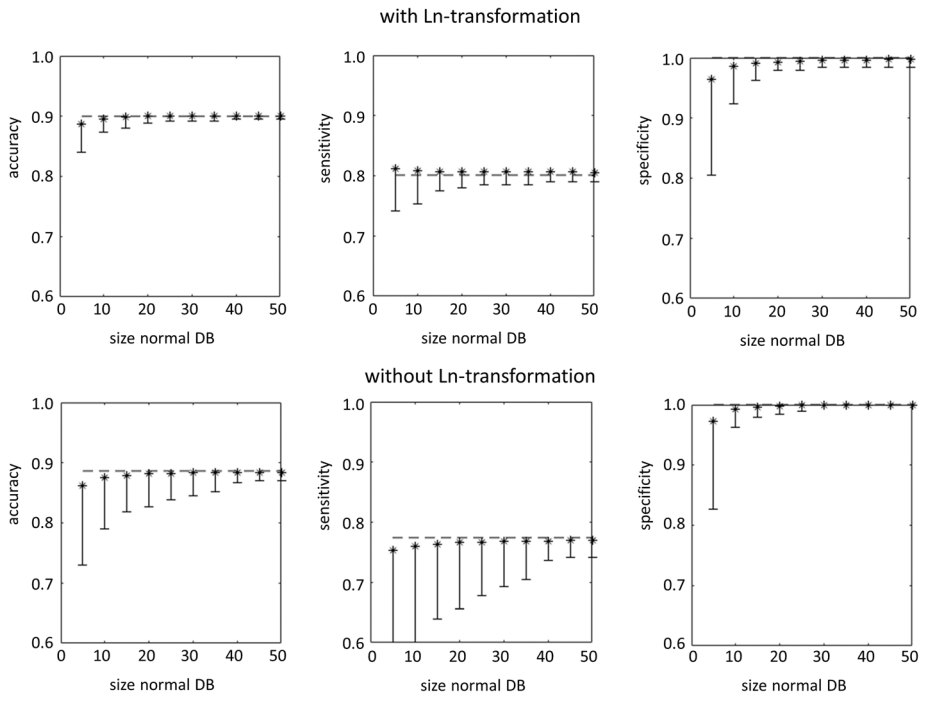

Fig. 6 Mean accuracy (left column), sensitivity (middle column), and specificity (right column) of the hottest voxels putamen SBR for identification of the patients with neurodegenerative PS in the clinical sample with iterative OSEM reconstruction and resolution recovery (= setting with largest skewness of the SBR distribution). The top row shows the performance with Ln-transformation, the bottom row without Ln-transformation. The error bars indicate the difference between mean accuracy, sensitivity, or specificity and the 5th percentile over the 10,000 randomly sampled normal databases. The dashed line represents the performance of the z-score of the putamen SBR when all patients with non-neurodegenerative PS ($n = 186$) were used to estimate mean and standard deviation of normal putamen SBR for transforming SBR values into z-scores as benchmark

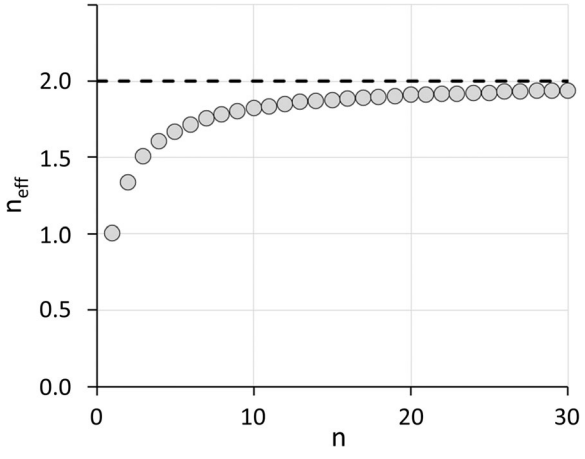

Fig. 7 Effective sample size n_{eff} versus size n of the normal database. The dashed line indicates the limit of n_{eff} approached at very large n

variability of the accuracy between different realizations of the normal database can still vary considerably at this normal database size (comp. Fig. 5b). The number of additional subjects in the normal database required to achieve adequate stability of the classification performance between different realizations of the normal database depends on the between-subjects variability of the feature used for classification as well as on the mean difference of the feature between disease-positive patients and the normal database (effect size). The number of additional normal subjects required to achieve stable performance between different realizations of the normal database, therefore, is expected to depend on the application. In case of putamen SBR-based classification of FP-CIT SPECT, the number of additional normal subjects required was 10 to 15 (resulting in a total of 25 to 30 subjects in the normal database).

The following limitations of this study should be noted. First, the comparison of filtered backprojection versus iterative OSEM reconstruction was restricted to the clinical sample. The PPMI provides only FP-CIT SPECT images reconstructed with OSEM for download. Raw FP-CIT SPECT projection data for retrospective reconstruction to test other reconstruction algorithms are not available. Furthermore, the OSEM parameters differed between the PPMI sample and the clinical sample. In particular, OSEM reconstruction was performed with resolution recovery in the clinical sample and without in the PPMI sample. The rationale for this was to increase the heterogeneity among the tested settings. Second, the whole sample was used as test set in all cases. The rationale for this was to use the same test set for all sizes of the normal database in order to avoid bias by varying sizes of the test set. As a consequence, the healthy controls (PPMI sample) or the patients with non-neurodegenerative PS (clinical sample) randomly selected for the normal database were also included in the test set. This might have resulted in overly optimistic performance estimates. However, the effect is expected to be small, because the subjects in the normal database represented only a small fraction (< 13.5%) of the test set in all cases. Third, the normal database of the clinical sample was generated retrospectively from patients who had received FP-CIT SPECT for the etiological diagnosis of a clinically uncertain PS in routine patient care. The clinical diagnosis of a non-neurodegenerative etiology (not associated with nigrostriatal degeneration) as standard of truth was based on the written report of a movement disorder specialist in the patient's file after FP-CIT SPECT. The movement disorder specialist was not blinded for the FP-CIT SPECT findings. This might have caused some bias in favor of FP-CIT SPECT resulting in overly optimistic performance estimates of the putamen SBR in the clinical sample. The potential bias is not expected to affect the evaluation of the impact of the size of the normal database on the performance of the putamen SBR. Fourth, this study used conversion to z-scores and a fixed, predefined cutoff on the z-score for SBR-based classification of FP-CIT SPECT. Other methods to define a cutoff such as receiver operating characteristic (ROC) analysis require a database of patients with nigrostriatal degeneration in addition to a normal database. The impact of the sizes of the two databases (without and with nigrostriatal degeneration) on SBR classification performance using cutoffs derived from ROC analysis might be addressed in future studies. Fifth, neither age nor gender were taken into account in this study, although there is strong evidence for age related decline of striatal DAT availability [37] and moderate evidence for higher striatal DAT availability in females compared to males [38–40]. However, so far no studies have been published that clearly demonstrate

that age- and/or gender-correction of the putaminal FP-CIT SBR improves its diagnostic performance [41]. Finally, normal databases of FP-CIT SPECT from healthy control subjects were used for the PPMI settings, whereas normal databases composed of visually normal FP-CIT SPECT from patients with non-neurodegenerative PS were used for the clinical settings. Nevertheless, the present study did not allow testing the impact of the type of the normal database (healthy control subjects versus patients with Parkinsonism but visually normal FP-CIT SPECT) on the performance of semi-quantitative analysis in FP-CIT SPECT. This would require two normal databases for the same setting, one comprised of healthy controls, the other comprised of patients with non-neurodegenerative PS.

Conclusion

In conclusion, the results of this study suggest that 25 to 30 is the minimum size of the normal database to reliably achieve good performance of semi-quantitative analysis in DAT SPECT, independent of the algorithm used for image reconstruction and the ROI method used to estimate the putaminal SBR. Increasing the size of the normal database beyond 40 provides only very small further improvement.

Appendix: Other conventional semi-quantitative parameters did not provide additional information beyond putaminal DAT availability

The following other conventional semi-quantitative parameters were tested for identification of patients with neurodegenerative PS in the clinical sample (with filtered back-projection) using receiver operating characteristic (ROC) analysis: minimum of left and right caudate SBR, minimum of left and right putamen-to-caudate SBR ratio, left-right asymmetry of putamen SBR (= 200 * abs (left – right) / (left + right)), and left-right asymmetry of caudate SBR. The clinical sample was used for this purpose in order to avoid the ceiling effect in the PPMI sample (due to very good performance of the putaminal SBR alone in the PPMI sample).

The area under the ROC curve was significantly smaller for each of the other conventional semi-quantitative parameters than for the (minimum of left and right) putamen SBR (0.953 ± 0.011): 0.932 ± 0.012 (DeLong $p = 0.017$), 0.886 ± 0.018 ($p < 0.001$), 0.824 ± 0.023 ($p < 0.001$), and 0.730 ± 0.027 ($p < 0.001$) for caudate SBR, putamen-to-caudate SBR ratio, left-right asymmetry of putamen SBR, and left-right asymmetry of caudate SBR, respectively.

Discriminant analysis was performed in order to test whether one or more of the other parameters might provide additional diagnostic information beyond the putamen SBR.

Stepwise discriminant analysis (Wilks' method, entry $p = 0.05$, removal $p = 0.10$) did not include any of the other parameters ($p = 0.699$, 0.596, 0.226, and 0.341 for caudate SBR, putamen-to-caudate SBR ratio, left-right asymmetry of putamen SBR, and left-right asymmetry of caudate SBR, respectively). When the analysis was forced to include all other parameters, the resulting discriminant function was as follows:

Discriminant function = – 3.741 + 3.200 * putamen SBR + 0.105 * caudate SBR + 0.622 * putamen-to-caudate ratio – 0.590 * putamen asymmetry / 100 – 0.309 * caudate asymmetry / 100

ROC analysis of the discriminant function revealed exactly the same area under the ROC curve as for the putamen SBR alone. Thus, there was no evidence that the other conventional semi-quantitative parameters provide additional information beyond the

putaminal SBR that might improve the performance of semi-quantitative analysis of FP-CIT SPECT in the clinical sample.

This does not rule out that the other conventional semi-quantitative parameters might provide additional information beyond the putaminal SBR in other patient samples, for example, in samples with more borderline cases or a larger fraction of atypical neurodegenerative PS (multiple system atrophy, progressive supranuclear palsy, corticobasal degeneration), or in the differentiation between dementia with Lewy bodies and Alzheimer's disease [42].

Abbreviations

AAL: Automatic Anatomic Labeling; DAT: Dopamine transporter; FBP: Filtered backprojection; FP-CIT: N-ω-fluoropropyl-2β-carbomethoxy-3β-(4-I-123-iodophenyl)nortropane; HC: Healthy controls; HV: Hottest voxels; Ln: Log natural; MNI: Montreal Neurological Institute; OSEM: Ordered subsets expectation maximization; PD: Parkinson's disease; PPMI: Parkinson's Progression Marker Initiative; PS: Parkinsonian syndrome; ROI: Region of interest; RR: Resolution recovery; SBR: Specific binding ratio; SPECT: Single-photon emission computed tomography; SPM12: Statistical Parametric Mapping software package, version 12

Acknowledgements

PPMI—a public-private partnership—is funded by the Michael J. Fox Foundation for Parkinson's Research and funding partners including Abbvie, Avid Radiopharmaceuticals, Biogen, BioLegend, Bristol-Myers Squibb, GE Healthcare, Genentech, GlaxoSmithKline, Lilly, Lundbeck, Merck, Meso Scale Discovery, Pfizer, Piramal, Roche, Sanofi Genzyme, Servier, Takeda, Teva, and UCB. For up-to-date information about all of the PPMI funding partners, visit http://www.ppmi-info.org/fundingpartners. The authors acknowledge support from the Open Access Publication Fund of Charité – Universitätsmedizin Berlin and German Research Foundation (DFG).

Authors' contributions

HSS did the data analysis, interpretation of study results, and manuscript drafting. CL did the data analysis, interpretation of study results, and manuscript drafting. IA did the data acquisition, interpretation of study results, and substantial revision of manuscript. HA did the interpretation of study results and substantial revision of manuscript. WL did the interpretation of study results and substantial revision of manuscript. SK did the data acquisition, interpretation of study results, and substantial revision of manuscript. RB did the study concept and design, data acquisition, data analysis, interpretation of study results, and manuscript drafting. The authors read and approved the final manuscript.

Funding

None

Availability of data and materials

The datasets supporting the conclusions of this article can be made available on request.

Ethics approval and consent to participate

Waiver of informed consent for the retrospective analysis of the clinical sample was obtained from the ethics review board of the general medical council of the state of Hamburg, Germany. All procedures performed in this study were in accordance with the ethical standards of the ethics review board of the general medical council of the state of Hamburg, Germany, and with the 1964 Helsinki declaration and its later amendments.

Consent for publication

There is no actual or potential conflict of interest for any of the authors.

Competing interests

The authors declare that they have no competing interests.

Received: 26 February 2020 Accepted: 5 May 2020
Published online: 20 May 2020

References

1. Booij J, Speelman JD, Horstink MW, Wolters EC. The clinical benefit of imaging striatal dopamine transporters with [^{123}I]FP-CIT SPET in differentiating patients with presynaptic parkinsonism from those with other forms of parkinsonism. Eur J Nucl Med. 2001;28:266–72.
2. Darcourt J, Booij J, Tatsch K, Varrone A, Vander Borght T, Kapucu OL, et al. EANM procedure guidelines for brain neurotransmission SPECT using (123)I-labelled dopamine transporter ligands, version 2. Eur J Nucl Med Mol Imaging. 2010;37:443–50. https://doi.org/10.1007/s00259-009-1267-x.
3. Tatsch K, Poepperl G. Nigrostriatal dopamine terminal imaging with dopamine transporter SPECT: an update. J Nucl Med. 2013;54:1331–8. https://doi.org/10.2967/jnumed.112.105379.
4. Van Laere K, Everaert L, Annemans L, Gonce M, Vandenberghe W, Vander BT. The cost effectiveness of ^{123}I-FP-CIT SPECT imaging in patients with an uncertain clinical diagnosis of parkinsonism. European journal of nuclear medicine and molecular imaging. 2008;35:1367–76. https://doi.org/10.1007/s00259-008-0777-2.

5. Tossici-Bolt L, Dickson JC, Sera T, Booij J, Asenbaun-Nan S, Bagnara MC, et al. [^{123}I]FP-CIT ENC-DAT normal database: the impact of the reconstruction and quantification methods. EJNMMI Phys. 2017;4:8. doi:10.1186/s40658-017-0175-6.
6. Soderlund TA, Dickson JC, Prvulovich E, Ben-Haim S, Kemp P, Booij J, et al. Value of semiquantitative analysis for clinical reporting of ^{123}I-2-beta-carbomethoxy-3beta-(4-iodophenyl)-N-(3-fluoropropyl)nortropane SPECT studies. J Nucl Med. 2013;54:714–22. https://doi.org/10.2967/jnumed.112.110106.
7. Badiavas K, Molyvda E, Iakovou I, Tsolaki M, Psarrakos K, Karatzas N. SPECT imaging evaluation in movement disorders: far beyond visual assessment. Eur J Nucl Med Mol Imaging. 2011;38:764–73. https://doi.org/10.1007/s00259-010-1664-1.
8. Tatsch K, Poepperl G. Quantitative approaches to dopaminergic brain imaging. Q J Nucl Med Mol Imaging. 2012;56:27–38.
9. Oliveira FPM, Faria DB, Costa DC, Castelo-Branco M, Tavares J. Extraction, selection and comparison of features for an effective automated computer-aided diagnosis of Parkinson's disease based on [^{123}I]FP-CIT SPECT images. European journal of nuclear medicine and molecular imaging. 2018;45:1052–62. https://doi.org/10.1007/s00259-017-3918-7.
10. Nobili F, Naseri M, De Carli F, Asenbaum S, Booij J, Darcourt J, et al. Automatic semi-quantification of [^{123}I]FP-CIT SPECT scans in healthy volunteers using BasGăn version 2: results from the ENC-DAT database. European journal of nuclear medicine and molecular imaging. 2013;40:565–73. https://doi.org/10.1007/s00259-012-2304-8.
11. Dickson JC, Tossici-Bolt L, Sera T, Booij J, Ziebell M, Morbelli S, et al. The impact of reconstruction and scanner characterisation on the diagnostic capability of a normal database for [^{123}I]FP-CIT SPECT imaging. EJNMMI Res. 2017;7:10. https://doi.org/10.1186/s13550-016-0253-0.
12. Fujita M, Varrone A, Kim KM, Watabe H, Zoghbi SS, Baldwin RM, et al. Effect of scatter correction in the measurement of striatal and extrastriatal dopamine D_2 receptors using [^{123}I]epidepride SPECT. Journal of Nuclear Medicine. 2001;42:217p-p.
13. Lange C, Seese A, Schwarzenbock S, Steinhoff K, Umland-Seidler B, Krause BJ, et al. CT-based attenuation correction in I-123-ioflupane SPECT. PLoS One. 2014;9:e108328. https://doi.org/10.1371/journal.pone.0108328.
14. Meyer PT, Sattler B, Lincke T, Seese A, Sabri O. Investigating dopaminergic neurotransmission with ^{123}I-FP-CIT SPECT: comparability of modern SPECT systems. Journal of Nuclear Medicine. 2003;44:839–45.
15. Tossici-Bolt L, Dickson JC, Sera T, de Nijs R, Bagnara MC, Jonsson C, et al. Calibration of gamma camera systems for a multicentre European ^{123}I-FP-CIT SPECT normal database. Eur J Nucl Med Mol Imaging. 2011;38:1529–40. https://doi.org/10.1007/s00259-011-1801-5.
16. Varrone A, Dickson JC, Tossici-Bolt L, Sera T, Asenbaum S, Booij J, et al. European multicentre database of healthy controls for [^{123}I]FP-CIT SPECT (ENC-DAT): age-related effects, gender differences and evaluation of different methods of analysis. Eur J Nucl Med Mol Imaging. 2013;40:213–27. https://doi.org/10.1007/s00259-012-2276-8.
17. Buchert R, Kluge A, Tossici-Bolt L, Dickson J, Bronzel M, Lange C, et al. Reduction in camera-specific variability in [^{123}I]FP-CIT SPECT outcome measures by image reconstruction optimized for multisite settings: impact on age-dependence of the specific binding ratio in the ENC-DAT database of healthy controls. Eur J Nucl Med Mol Imaging. 2016;43:1323–36. https://doi.org/10.1007/s00259-016-3309-5.
18. Wenzel M, Milletari F, Kruger J, Lange C, Schenk M, Apostolova I, et al. Automatic classification of dopamine transporter SPECT: deep convolutional neural networks can be trained to be robust with respect to variable image characteristics. Eur J Nucl Med Mol Imaging. 2019. https://doi.org/10.1007/s00259-019-04502-5.
19. Parkinson Progression Marker I. The Parkinson Progression Marker Initiative (PPMI). Prog Neurobiol. 2011;95:629-35. doi:10.1016/j.pneurobio.2011.09.005.
20. Choi H, Ha S, Im HJ, Paek SH, Lee DS. Refining diagnosis of Parkinson's disease with deep learning-based interpretation of dopamine transporter imaging. Neuroimage Clin. 2017;16:586–94. https://doi.org/10.1016/j.nicl.2017.09.010.
21. Kim DH, Wit H, Thurston M. Artificial intelligence in the diagnosis of Parkinson's disease from ioflupane-123 single-photon emission computed tomography dopamine transporter scans using transfer learning. Nucl Med Commun. 2018;39:887–93. https://doi.org/10.1097/MNM.0000000000000890.
22. Taylor JC, Romanowski C, Lorenz E, Lo C, Bandmann O, Fenner J. Computer-aided diagnosis for (^{123}I)FP-CIT imaging: impact on clinical reporting. EJNMMI Res. 2018;8:36. https://doi.org/10.1186/s13550-018-0393-5.
23. Chang LT. Method for attenuation correction in radionuclide computed tomography. IEEE T Nucl Sci. 1978;25:638-43. doi:Doi 10.1109/Tns.1978.4329385.
24. Marek K, Chowdhury S, Siderowf A, Lasch S, Coffey CS, Caspell-Garcia C, et al. The Parkinson's progression markers initiative (PPMI) - establishing a PD biomarker cohort. Ann Clin Transl Neurol. 2018;5:1460–77. https://doi.org/10.1002/acn3.644.
25. Djang DS, Janssen MJ, Bohnen N, Booij J, Henderson TA, Herholz K, et al. SNM practice guideline for dopamine transporter imaging with ^{123}I-ioflupane SPECT 1.0. J Nucl Med. 2012;53:154–163. doi:https://doi.org/10.2967/jnumed.111.100784.
26. Acton PD, Friston KJ. Statistical parametric mapping in functional neuroimaging: Beyond PET and fMRI activation studies. European journal of nuclear medicine. 1998;25(7):663–7.
27. Kupitz D, Apostolova I, Lange C, Ulrich G, Amthauer H, Brenner W, et al. Global scaling for semi-quantitative analysis in FP-CIT SPECT. Nuklearmed-Nucl Med. 2014;53:234–41. https://doi.org/10.3413/Nukmed-0659-14-04.
28. Koch W, Unterrainer M, Xiong G, Bartenstein P, Diemling M, Varrone A, et al. Extrastriatal binding of [^{123}I]FP-CIT in the thalamus and pons: gender and age dependencies assessed in a European multicentre database of healthy controls. European journal of nuclear medicine and molecular imaging. 2014;41:1938–46. https://doi.org/10.1007/s00259-014-2785-8.
29. Tzourio-Mazoyer N, Landeau B, Papathanassiou D, Crivello F, Etard O, Delcroix N, et al. Automated anatomical labeling of activations in SPM using a macroscopic anatomical parcellation of the MNI MRI single-subject brain. Neuroimage. 2002;15:273–89. https://doi.org/10.1006/nimg.2001.0978.
30. Buchert R, Lange C, Spehl TS, Apostolova I, Frings L, Jonsson C, et al. Diagnostic performance of the specific uptake size index for semi-quantitative analysis of I-123-FP-CIT SPECT: harmonized multi-center research setting versus typical clinical single-camera setting. EJNMMI Res. 2019;9:37. https://doi.org/10.1186/s13550-019-0506-9.
31. Kaasinen V, Vahlberg T. Striatal dopamine in Parkinson disease: a meta-analysis of imaging studies. Ann Neurol. 2017;82:873–82. https://doi.org/10.1002/ana.25103.
32. Erro R, Schneider SA, Stamelou M, Quinn NP, Bhatia KP. What do patients with scans without evidence of dopaminergic deficit (SWEDD) have? New evidence and continuing controversies. J Neurol Neurosur Ps. 2016;87:319–23. https://doi.org/10.1136/jnnp-2014-310256.
33. Nicastro N, Garibotto V, Badoud S, Burkhard PR. Scan without evidence of dopaminergic deficit: a 10-year retrospective study. Parkinsonism Relat D. 2016;31:53–8. https://doi.org/10.1016/j.parkreldis.2016.07.002.

34. Marshall VL, Reininger CB, Marquardt M, Patterson J, Hadley DM, Oertel WH, et al. Parkinson's disease is overdiagnosed clinically at baseline in diagnostically uncertain cases: a 3-year European multicenter study with repeat [^{123}I]FP-CIT SPECT. Movement Disord. 2009;24:500–8. https://doi.org/10.1002/mds.22108.
35. Armitage P, Berry G. Statistical methods in medical research. Oxford: Blackwell Science; 1998.
36. Buchert R. On the effect of sample size of the normal database on statistical power of single subject analysis. Nuclear Medicine Communications. 2008;29:837-. doi:DOI 10.1097/MNM.0b013e3283023f8d.
37. Karrer TM, Josef AK, Mata R, Morris ED, Samanez-Larkin GR. Reduced dopamine receptors and transporters but not synthesis capacity in normal aging adults: a meta-analysis. Neurobiol Aging. 2017;57:36–46. https://doi.org/10.1016/j.neurobiolaging.2017.05.006.
38. Best SE, Sarrel PM, Malison RT, Laruelle M, Zoghbi SS, Baldwin RM, et al. Striatal dopamine transporter availability with [^{123}I]beta-CIT SPECT is unrelated to gender or menstrual cycle. Psychopharmacology (Berl). 2005;183:181-9. doi:10.1007/s00213-005-0158-5.
39. Lavalaye J, Booij J, Reneman L, Habraken JB, van Royen EA. Effect of age and gender on dopamine transporter imaging with [^{123}I]FP-CIT SPET in healthy volunteers. Eur J Nucl Med. 2000;27:867–9. https://doi.org/10.1007/s002590000279.
40. Wong KK, Muller ML, Kuwabara H, Studenski SA, Bohnen NI. Gender differences in nigrostriatal dopaminergic innervation are present at young-to-middle but not at older age in normal adults. J Clin Neurosci. 2012;19:183–4. https://doi.org/10.1016/j.jocn.2011.05.013.
41. Albert NL, Unterrainer M, Diemling M, Xiong GM, Bartenstein P, Koch W, et al. Implementation of the European multicentre database of healthy controls for [^{123}I]FP-CIT SPECT increases diagnostic accuracy in patients with clinically uncertain parkinsonian syndromes. Eur J Nucl Med Mol I. 2016;43:1315–22. https://doi.org/10.1007/s00259-015-3304-2.
42. Lloyd JJ, Petrides G, Donaghy PC, Colloby SJ, Attems J, O'Brien JT, et al. A new visual rating scale for Ioflupane imaging in Lewy body disease. Neuroimage Clin. 2018;20:823–9. https://doi.org/10.1016/j.nicl.2018.09.012.

Publisher's Note

12. Lebenslauf

Mein Lebenslauf wird aus datenschutzrechtlichen Gründen in der elektronischen Version meiner Arbeit nicht veröffentlicht.

Mein Lebenslauf wird aus datenschutzrechtlichen Gründen in der elektronischen Version meiner Arbeit nicht veröffentlicht.

Mein Lebenslauf wird aus datenschutzrechtlichen Gründen in der elektronischen Version meiner Arbeit nicht veröffentlicht.

13. Komplette Publikationsliste

ORCID: https://orcid.org/0000-0002-6745-8441

Lange, C., Mäurer, A., Suppa, P., Apostolova, I., Steffen, I. G., Grothe, M. J., Buchert, R. Predictive power of brain FDG PET with respect to further cognitive decline, change to assisted living, and survival in acutely hospitalized geriatric patients with newly manifested cognitive impairment. *In Preparation*.

Levin, F., Ferreira, D., **Lange, C.**, Dyrba, M., Westman, E., Buchert, R., Teipel, S., Grothe, M. J. Characterization of FDG-PET subtypes of Alzheimer's disease-related neurodegeneration: association with differential biomarker profiles and clinical trajectories. *In Submission*.

Schmitz-Steinkrüger, H., **Lange, C.**, Apostolova, I., Mathies, F. L., Frings, L., Klutmann, S., Hellwig, S., Meyer, P. T., Buchert, R. Impact of age and sex correction on the diagnostic performance of the specific binding ratio in dopamine transporter SPECT. *In Submission*.

Lia, S., Daamen, M., Scheef, L., Gaertner, F. C., Buchert, R., Buchmann, M., Buerger, K., Cataki, C., Dobisch, L., Drzezga, A., Ertl-Wagner, B., Essler, M., Fliessbach, K., Haynes, J. D., Incesoy, E. I., Kilimann, I., Krause, B. J., **Lange, C.**, Laske, C., Priller, J., Ramirez, A., Reimold, M., Rominger, A., Roy, N., Scheffler, K., Schmitt, A., Schneider, A., Spottke, A., Spruth, E. J., Teipel, S., Tscheuschler, M., Wagner, M., Wolfsgruber, S., Düzel, E., Jessen, F., Peters, O., Boecker, H. The DELCODE Study Group. Abnormal Regional and Global Connectivity Measures in Subjective Cognitive Decline Depending on Cerebral Amyloid Status. *In Revision*.

Gaubert, M.*, **Lange, C.***, Garnier-Crussard, A., Köbe, T., Bougacha, S., Gonneaud, J., De Flores, R., Tomadesso, C., Mézenge, F., Landeau, B., de la Sayette, V., Chételat, G., Wirth, M. Association between multimodal Alzheimer's disease biomarkers and white matter hyperintensities: a voxel-based study. *In Revision*.

Hallab, A., **Lange, C.**, Apostolova, I., Özden, C., Gonzalez-Escamilla, G., Klutmann, S., Brenner, W., Grothe, M. J., Buchert, R. Impairment of everyday spatial navigation abilities in mild cognitive impairment is associated with reduced grey matter volume specifically in the medial part of the entorhinal cortex. *In Revision*.

Nikulin, P., Hofheinz, F., Maus, J., Li, Y., Bütof, R., **Lange, C.**, Furth, C., Zschaeck, S., Kreißl, M. C., Kotzerke, J., van den Hoff, J. A convolutional neural network for fully automated blood SUV determination to facilitate SUR computation in oncological FDG-PET. *Eur J Nucl Med Mol Imaging*. *Accepted for publication*. (Impact Factor: 7,182)

Mathies, F. L., **Lange, C.**, Mäurer, A., Apostolova, I., Klutmann, S., Buchert, R. Brain FDG PET for etiological diagnosis of clinically uncertain cognitive impairment during delirium in remission. *J Alzheimers Dis*. *Accepted for publication*. (Impact Factor: 3,455)

Schmitz-Steinkrüger, H.*, **Lange, C.***, Apostolova, I., Amthauer, H., Lehnert, W., Klutmann, S., Buchert, R. 2020. Impact of the size of the normal database on the performance of the specific binding ratio in dopamine transporter SPECT. *EJNMMI Phys* 7(1): 34. (Impact Factor: 3,475)

Scheibe, F., Neumann, W. J., **Lange, C.**, Scheel, M., Furth, C., Kohnlein, M., Mergenthaler, P., Schultze-Amberger, J., Triebkorn, P., Ritter, P., Kuhn, A. A., Meisel, A. 2020. Movement disorders after hypoxic brain injury following cardiac arrest in adults. *Eur J Neurol* Online ahead of print. (Impact Factor: 4,391)

Özden, C., Frings, L., Apostolova, I., **Lange, C.**, Klutmann, S., Adam, G., Bannas, P., Meyer, P. T., Grothe, M. J., Buchert, R. 2020. FDG Uptake in the Basal Forebrain as Measured by Digital High-Resolution PET Is a Promising Marker of Basal Forebrain Degeneration in the Lewy Body Disease Spectrum: A Pilot Study. *Clin Nucl Med* 45(4):261-266. (Impact Factor: 6,703)

Apostolova, I., **Lange, C.**, Frings, L., Klutmann, S., Meyer, P. T., Buchert, R. 2020. Nigrostriatal Degeneration in the Cognitive Part of the Striatum in Parkinson Disease Is Associated With Frontomedial Hypometabolism. *Clin Nucl Med* 45(2): 95-99. (Impact Factor: 6,309)

Buchert, R.*, **Lange, C.***, Spehl, T. S., Apostolova, I., Frings, L., Jonsson, C., Meyer, P. T., Hellwig, S. 2019. Diagnostic performance of the specific uptake size index for semi-quantitative analysis of I-123-FP-CIT SPECT: harmonized multi-center research setting versus typical clinical single-camera setting. *EJNMMI Res* 9(1): 37. (Impact Factor: 2,630)

Wenzel, M., Milletari, F., Kruger, J., **Lange, C.**, Schenk, M., Apostolova, I., Klutmann, S., Ehrenburg, M., Buchert, R. 2019. Automatic classification of dopamine transporter SPECT: deep convolutional neural networks can be trained to be robust with respect to variable image characteristics. *Eur J Nucl Med Mol Imaging* 46(13):2800-2811. (Impact Factor: 7,704)

Wirth, M.*, **Lange, C.***, Huijbers, W.*, Alzheimer's Disease Neuroimaging, I. 2019. Plasma cortisol is associated with cerebral hypometabolism across the Alzheimer's disease spectrum. *Neurobiol Aging* 84: 80-89. (Impact Factor: 4,747)

Wirth, M., Schwarz, C., Benson, G., Horn, N., Buchert, R., **Lange, C.**, Kobe, T., Hetzer, S., Maglione, M., Michael, E., Marschenz, S., Mai, K., Kopp, U., Schmitz, D., Grittner, U., Sigrist, S. J., Stekovic, S., Madeo, F., Floel, A. 2019. Effects of spermidine supplementation on cognition and biomarkers in older adults with subjective cognitive decline (SmartAge)-study protocol for a randomized controlled trial. *Alzheimers Res Ther* 11(1): 36. (Impact Factor: 5,515)

Buchert, R., **Lange, C.**, Suppa, P., Apostolova, I., Spies, L., Teipel, S., Dubois, B., Hampel, H., Grothe, M. J. 2018. Magnetic resonance imaging-based hippocampus volume for prediction of dementia in mild cognitive impairment: Why does the measurement method matter so little? *Alzheimers Dement* 14(7): 976-978. (Impact Factor: 9,343)

Lange, C., Suppa, P., Pietrzyk, U., Makowski, M. R., Spies, L., Peters, O., Buchert, R., Alzheimer's Disease Neuroimaging, I. 2018. Prediction of Alzheimer's Dementia in Patients with Amnestic Mild Cognitive Impairment in Clinical Routine: Incremental Value of Biomarkers of Neurodegeneration and Brain Amyloidosis Added Stepwise to Cognitive Status. *J Alzheimers Dis* 61(1): 373-388. (Impact Factor: 4,237)

Huang, K., Lukas, M., Steffen, I. G., **Lange, C.**, Huang, E. L., Dorau, V., Brenner, W., Beindorff, N. 2018. Normal Values of Renal Function measured with 99mTechnetium

Mercaptoacetyltriglycine SPECT in Mice with Respect to Age, Sex and Circadian Rhythm. *Nuklearmedizin* 57(6): 224-233. (Impact Factor: 1,087)

Apostolova, I., **Lange, C.**, Suppa, P., Spies, L., Klutmann, S., Adam, G., Grothe, M. J., Buchert, R., Alzheimer's Disease Neuroimaging, I. 2018. Impact of plasma glucose level on the pattern of brain FDG uptake and the predictive power of FDG PET in mild cognitive impairment. *Eur J Nucl Med Mol Imaging* 45(8): 1417-1422. (Impact Factor: 7,277)

Benson, G., Hildebrandt, A., **Lange, C.**, Schwarz, C., Kobe, T., Sommer, W., Floel, A., Wirth, M. 2018. Functional connectivity in cognitive control networks mitigates the impact of white matter lesions in the elderly. *Alzheimers Res Ther* 10(1): 109. (Impact Factor: 6,688)

Apostolova, I.*, **Lange, C.***, Maurer, A., Suppa, P., Spies, L., Grothe, M. J., Nierhaus, T., Fiebach, J. B., Steinhagen-Thiessen, E., Buchert, R., Alzheimer's Disease Neuroimaging, I. 2018. Hypermetabolism in the hippocampal formation of cognitively impaired patients indicates detrimental maladaptation. *Neurobiol Aging* 65: 41-50. (Impact Factor: 5,447)

Beindorff, N., Bartelheimer, A., Huang, K., Lukas, M., **Lange, C.**, Huang, E. L., Aschenbach, J. R., Eary, J. F., Steffen, I. G., Brenner, W. 2018. Normal Values of Thyroid Uptake of 99mTechnetium Pertechnetate SPECT in Mice with Respect to Age, Sex, and Circadian Rhythm. *Nuklearmedizin* 57(5): 181-189. (Impact Factor: 1,087)

Acker, G., **Lange, C.**, Schatka, I., Pfeifer, A., Czabanka, M. A., Vajkoczy, P., Buchert, R. 2018. Brain Perfusion Imaging Under Acetazolamide Challenge for Detection of Impaired Cerebrovascular Reserve Capacity: Positive Findings with (15)O-Water PET in Patients with Negative (99m)Tc-HMPAO SPECT Findings. *J Nucl Med* 59(2): 294-298. (Impact Factor: 5,849)

Apostolova, I., Taleb, D. S., Lipp, A., Galazky, I., Kupitz, D., **Lange, C.**, Makowski, M. R., Brenner, W., Amthauer, H., Plotkin, M., Buchert, R. 2017. Utility of Follow-up Dopamine Transporter SPECT With 123I-FP-CIT in the Diagnostic Workup of Patients With Clinically Uncertain Parkinsonian Syndrome. *Clin Nucl Med* 42(8): 589-594. (Impact Factor: 4,278)

Lange, C., Suppa, P., Maurer, A., Ritter, K., Pietrzyk, U., Steinhagen-Thiessen, E., Fiebach, J. B., Spies, L., Buchert, R. 2017. Mental speed is associated with the shape irregularity of white matter MRI hyperintensity load. *Brain Imaging Behav* 11(6): 1720-1730. (Impact Factor: 5,398)

Gonzalez-Escamilla, G., **Lange, C.**, Teipel, S., Buchert, R., Grothe, M. J., Alzheimer's Disease Neuroimaging, I. 2017. PETPVE12: an SPM toolbox for Partial Volume Effects correction in brain PET - Application to amyloid imaging with AV45-PET. *Neuroimage* 147: 669-677. (Impact Factor: 6,605)

Cavedo, E., Suppa, P., **Lange, C.**, Opfer, R., Lista, S., Galluzzi, S., Schwarz, A. J., Spies, L., Buchert, R., Hampel, H., Alzheimer's Disease Neuroimaging, I., Alzheimer Precision Medicine, I. 2017. Fully Automatic MRI-Based Hippocampus Volumetry Using FSL-FIRST: Intra-Scanner Test-Retest Stability, Inter-Field Strength Variability, and Performance as Enrichment Biomarker for Clinical Trials Using Prodromal Target Populations at Risk for Alzheimer's Disease. *J Alzheimers Dis* 60(1): 151-164. (Impact Factor: 4,237)

Apostolova, I., **Lange, C.**, Roberts, A., Igel, H. J., Maurer, A., Liese, S., Estrella, M., Prasad, V., Stechl, E., Lammler, G., Steinhagen-Thiessen, E., Buchert, R. 2017. Challenges in Screening and Recruitment for a Neuroimaging Study in Cognitively Impaired Geriatric Inpatients. *J Alzheimers Dis* 56(1): 197-204. (Impact Factor: 4,659)

Lange, C., Suppa, P., Frings, L., Brenner, W., Spies, L., Buchert, R. 2016. Optimization of Statistical Single Subject Analysis of Brain FDG PET for the Prognosis of Mild Cognitive Impairment-to-Alzheimer's Disease Conversion. *J Alzheimers Dis* 49(4): 945-959. (Impact Factor: 3,988)

Apostolova, I., **Lange, C.**, Spies, L., Ritter, K., Maurer, A., Seybold, J., Fiebach, J. B., Steinhagen-Thiessen, E., Buchert, R. 2016. Preserved brain metabolic activity at the age of 96 years. *Int Psychogeriatr* 28(9): 1575-1577. (Impact Factor: 2,169)

Ritter, K., **Lange, C.**, Weygandt, M., Maurer, A., Roberts, A., Estrella, M., Suppa, P., Spies, L., Prasad, V., Steffen, I., Apostolova, I., Bittner, D., Govercin, M., Brenner, W., Mende, C., Peters, O., Seybold, J., Fiebach, J. B., Steinhagen-Thiessen, E., Hampel, H., Haynes, J. D., Buchert, R. 2016. Combination of Structural MRI and FDG-PET of the Brain Improves Diagnostic Accuracy in Newly Manifested Cognitive Impairment in Geriatric Inpatients. *J Alzheimers Dis* 54(4): 1319-1331. (Impact Factor: 4,659)

Suppa, P., Hampel, H., Kepp, T., **Lange, C.**, Spies, L., Fiebach, J. B., Dubois, B., Buchert, R., Alzheimer's Disease Neuroimaging, I. 2016. Performance of Hippocampus Volumetry with FSL-FIRST for Prediction of Alzheimer's Disease Dementia in at Risk Subjects with Amnestic Mild Cognitive Impairment. *J Alzheimers Dis* 51(3): 867-873. (Impact Factor: 3,988)

Buchert, R., Hutton, C., **Lange, C.**, Hoppe, P., Makowski, M., Bamousa, T., Platsch, G., Brenner, W., Declerck, J. 2016. Semiquantitative slab view display for visual evaluation of 123I-FP-CIT SPECT. *Nucl Med Commun* 37(5): 509-518. (Impact Factor: 1,669)

Buchert, R., Kluge, A., Tossici-Bolt, L., Dickson, J., Bronzel, M., **Lange, C.**, Asenbaum, S., Booij, J., Atay Kapucu, L. O., Svarer, C., Koulibaly, P. M., Nobili, F., Pagani, M., Sabri, O., Sera, T., Tatsch, K., Vander Borght, T., Van Laere, K., Varrone, A., Iida, H. 2016. Reduction in camera-specific variability in [(123)I]FP-CIT SPECT outcome measures by image reconstruction optimized for multisite settings: impact on age-dependence of the specific binding ratio in the ENC-DAT database of healthy controls. *Eur J Nucl Med Mol Imaging* 43(7): 1323-1336. (Impact Factor: 5,383)

Lange, C., Kurth, J., Seese, A., Schwarzenbock, S., Steinhoff, K., Umland-Seidler, B., Krause, B. J., Brenner, W., Sabri, O., Hesse, S., Buchert, R. 2015. Robust, fully automatic delineation of the head contour by stereotactical normalization for attenuation correction according to Chang in dopamine transporter scintigraphy. *Eur Radiol* 25(9): 2709-2717. (Impact Factor: 4,338)

Lange, C., Seese, A., Schwarzenbock, S., Steinhoff, K., Umland-Seidler, B., Krause, B. J., Brenner, W., Sabri, O., Kurth, J., Hesse, S., Buchert, R. 2014. CT-based attenuation correction in I-123-ioflupane SPECT. *PLoS One* 9(9): e108328. (Impact Factor: 4,302)

Lange, C., Apostolova, I., Lukas, M., Huang, K. P., Hofheinz, F., Gregor-Mamoudou, B., Brenner, W., Buchert, R. 2014. Performance evaluation of stationary and semi-stationary acquisition with a non-stationary small animal multi-pinhole SPECT system. *Mol Imaging Biol* 16(3): 311-316. (Impact Factor: 3,095)

Kupitz, D., Apostolova, I., **Lange, C.**, Ulrich, G., Amthauer, H., Brenner, W., Buchert, R. 2014. Global scaling for semi-quantitative analysis in FP-CIT SPECT. *Nuklearmedizin* 53(6): 234-241. (Impact Factor: 1,322)

14. Danksagung

Zu Beginn möchte ich meinen Betreuern Herrn Prof. Dr. med. Holger Amthauer und Frau Dr. med. Imke Schatka (Klinik für Nuklearmedizin, AB Klinische Nuklearmedizin, Charité – Universitätsmedizin Berlin) für die Ermöglichung meines Promotionsvorhabens, die engagierte Betreuung sowie für die großartige fachliche Unterstützung danken.

Ein sehr herzlicher Dank geht an meinen Mentor Herrn Dr. rer. nat. Ralph Buchert (Diagnostische und Interventionelle Radiologie und Nuklearmedizin, Universitätsklinikum Hamburg-Eppendorf), der mich bereits über viele Jahre fachlich als auch persönlich unterstützt. Seine konstruktive Kritik und gemeinsame Diskussionen sind aus meinem Alltag nicht mehr wegzudenken und ich wünsche mir, dass unsere wissenschaftliche Zusammenarbeit noch über viele Jahre aufrechterhalten bleibt. Seine leidenschaftliche Betreuung stellt eine wesentliche und verlässliche Grundlage für meine künftige wissenschaftliche Arbeit im Bereich der Neurowissenschaften dar.

Darüber hinaus gilt mein besonderer Dank für wissenschaftliche Unterstützung und konstruktive Diskussionen im Zusammenhang mit dieser Dissertationsarbeit Dr. phil. Lars Frings, Prof. Dr. med. Dr. nat. med. Philipp T. Meyer (Klinik für Nuklearmedizin, Universitätsklinikum Freiburg), Prof. Dr. med. Sabine Hellwig (Klinik für Psychiatrie und Psychotherapie, Universitätsklinikum Freiburg), PD Dr. med. Ivayla Apostolova, Helen Schmitz-Steinkrüger, Prof. Dr. med. Susanne Klutmann (Diagnostische und Interventionelle Radiologie und Nuklearmedizin, Universitätsklinikum Hamburg-Eppendorf), Prof. Dr. med. Swen Hesse, Dr. rer. nat. Anita Seese, Prof. Dr. med. Osama Sabri (Klinik und Poliklinik für Nuklearmedizin, Universitätsmedizin Leipzig), Dr.-Ing. Jens Kurth, Dr. med. Sarah Schwarzenböck und Prof. Dr. med. Bernd J. Krause (Klinik und Poliklinik für Nuklearmedizin, Universitätsmedizin Rostock).

Ein persönlicher Dank geht an meine Kolleginnen und Kollegen verschiedener Arbeitsbereiche der Charité – Universitätsmedizin Berlin. Ohne deren fachlichen Austausch sowie das herzliche Zusammensein auf und außerhalb der Arbeit wäre die Promotionszeit nur halb so schön gewesen.

Abschließend möchte ich meiner Familie und meinen Freunden für die Unterstützung, Geduld, Kraft und Liebe auf diesem bedeutungsvollen Weg danken.